N72-32761

NASA CR-112150

TECHNOLOGY DEVELOPMENT OF A BIOWASTE RESISTOJET

VOLUME II

CASE FILE COPY

by

D.G.Phillips

Prepared Under Contract NAS 1-9474 by

The Marquardt Company
Van Nuys, California

for

NATIONAL AERONAUTICS AND SPACE ADMINISRATION
LANGLEY RESEARCH CENTER

June 1972

TECHNOLOGY DEVELOPMENT
OF A
BIOWASTE RESISTOJET

VOLUME II

BY

D. G. PHILLIPS

Prepared Under Contract NAS 1-9474 by

The Marquardt Company
Van Nuys, California

For

NATIONAL AERONAUTICS AND SPACE ADMINISTRATION
LANGLEY RESEARCH CENTER

JUNE 1972

TABLE OF CONTENTS

SECTION	PAGE
LIST OF FIGURES	iv
LIST OF TABLES	vii
SUMMARY	1
INTRODUCTION	3
Potential Application	3
Program Objective	4
Resistojet Concept	4
ENVIRONMENTAL REQUIREMENTS	5
Propellant Composition	5
Performance Requirements	5
STRUCTURAL DURABILITY REQUIREMENTS	6
MATERIALS RESEARCH	7
THEORETICAL PERFORMANCE	7
ENGINE FACILITY DESCRIPTION	9
ENGINE DEVELOPMENT	11
Mark I Resistojet	11
Thruster description	11
Thruster performance	11
Water Evaporator Development	17
Mark II Resistojet	19
Design	19
Fabrication	21
Performance tests	22
Vibration tests	36
Design verification tests	36
Alternate Engine Designs	40
Mark II stress reduction	40
RD-1 resistojet	41

TABLE OF CONTENTS. - Continued

SECTION	PAGE
RD-2 resistojet	45
RD-3 resistojet	46
CONCLUSIONS AND RECOMMENDATIONS	47
REFERENCES	50

LIST OF FIGURES

FIGURE	TITLE	PAGE
1.	Evacuated Concentric Tubes Resistojet Concept	51
2.	Expected Performance of 10 MLB Resistojet	52
3.	Expected Performance of 100 MLB Resistojet	53
4.	Electric Power Requirements of 10 MLB Resistojet	54
5.	Electric Power Requirements of 100 MLB Resistojet	55
6.	Ideal Frozen Flow Specific Impulse Correlation	56
7.	Biowaste Resistojet Test Equipment	57
8.	Biowaste Resistojet Test Schematic	58
9.	Mark II Biowaste Resistojet on Thrust Dynamometer Stand	59
10.	Biowaste Resistojet Test	60
11.	Biowaste Resistojet Test	61
12.	Biowaste Resistojet Test	62
13.	Biowaste Resistojet Test - Methane Propellant	63
14.	Biowaste Resistojet Test - Transient Data	64
15.	Correlation of Experimental Specific Impulse with Propellant Molecular Weight	65
16.	Biowaste Resistojet Water Evaporator	66
17.	Biowaste Resistojet Water Evaporator	67
18.	Water Evaporator Test Temperature History	68
19.	Water Evaporator Thermal Start-up Transient	69
20.	10 MLB Resistojet - Mark II	70
21.	Mark II Biowaste Resistojet - Inner Heater Element and Nozzle	71
22.	Mark II Biowaste Resistojet Outer Heater and Cap	72
23.	Mark II Biowaste Resistojet Insulated Heater Assembly and Bellows Assembly	73
24.	Mark II Biowaste Resistojets With and Without Insulation	74
25.	E. P. L. Test Chamber Windage Effect	75

LIST OF FIGURES. - Continued

FIGURE	TITLE	PAGE
26.	E. P. L. Test Chamber Windage Effect	76
27.	Biowaste Resistojet Test	77
28.	Biowaste Resistojet Test	78
29.	Biowaste Resistojet Test	79
30.	Biowaste Resistojet Test	80
31.	Biowaste Resistojet Test	81
32.	Biowaste Resistojet Test	82
33.	Biowaste Resistojet Test	83
34.	Biowaste Resistojet Test	84
35.	Cell Pressure Effect on Mark II Biowaste Resistojet Performance	85
36.	Mark II Biowaste Resistojet - S/N 002 Thruster with Water Evaporator	86
37.	Mark II Biowaste Resistojet - S/N 002 Thruster with Water Evaporator	87
38.	Biowaste Resistojet Test	88
39.	Biowaste Resistojet Test	89
40.	Biowaste Resistojet Test	90
41.	Biowaste Resistojet Test	91
42.	Biowaste Resistojet Test	92
43.	Biowaste Resistojet Test	93
44.	Biowaste Resistojet Test	94
45.	Biowaste Resistojet Test	95
46.	Biowaste Resistojet Performance with Hydrogen	96
47.	Biowaste Resistojet Performance with Typical Propellants	97
48.	Biowaste Resistojet Performance with Typical Propellant Mixtures	98
49.	Cell Pressure Effect on Biowaste Resistojet Performance	99
50.	Mark II Biowaste Resistojet Electrical Characteristic, S/N 001 Thruster	100

LIST OF FIGURES. - Continued

FIGURE	TITLE	PAGE
51.	Vibration Test Setup	101
52.	Mark II Biowaste Resistojet After Vibration Tests	102
53.	Biowaste Resistojet- Disassembled, Mark II, S/N 001	103
54.	Biowaste Resistojet Bellows, Innercase and Radiation Shield, Mark II, S/N 001	104
55.	Biowaste Resistojet Heater Parts and Nozzle, Mark II, S/N 001	105
56.	Mark II S/N 001 Inner Heating Element and Nozzle, Longitudinal Cross Sections, Pt-20Ir	106
57.	Mark II S/N 001 Inner Heating Element, Pt-20Ir	107
58.	Mark II S/N 001 Inner Heating Element, Pt-20Ir	108
59.	Design Verification Test History	109
60.	Disassembled Mark II - S/N 002 Biowaste Resistojet	110
61.	Mark II S/N 002 Biowaste Resistojet Heater Parts and Nozzle	111
62.	Mark II S/N 002 Exit Nozzle	112
63.	Mark II S/N 002 Inner Heating Element, Pt-20Ir	113
64.	Mark II S/N 002 Outer Heating Element	114
65.	Random Vibration Spectrum Comparison	115
66.	Mark II Modified For Support of Inner Tube	116
67.	Biowaste Resistojet Component Engine	117
68.	Carbon Deposition in Component Engine After 113 Hours Operation on CH_4	118
69.	R&D Biowaste Resistojet	119
70.	Haynes Alloy No. 188 After Bell Jar Test	120
71.	Haynes Alloy No. 188 After Bell Jar Test	121
72.	Haynes Alloy No. 188 After Bell Jar Test	122

LIST OF TABLES

TABLE	TITLE	PAGE
I	Summary of High Temperature Materials Test Results	123
II	Biowaste Resistojet Performance Summary, Mark I	125
III	Mark I Versus Mark II Thruster Performance	126
IV	Estimated Performance for Threshold Carbon Deposition Mark II Resistojet	126
V	Estimated Performance for 10 MLB Biowaste Resistojet	127

TECHNOLOGY DEVELOPMENT OF A BIOWASTE RESISTOJET

By D. G. Phillips

SUMMARY

This final report summarizes the effort conducted between September 1969 and June 1972 on a biowaste resistojet program. This report summarizes only the thruster development effort. The supporting materials effort is detailed in a separate report, Reference 1.

Under this program, several variations of the concentric tube resistojet were built and tested. Because of the corrosive nature of the biowaste gases available for propellants, thruster effort was concentrated on the use of noble metals (platinum and its alloys) for the critical center tube heating element. This tube must operate at high temperatures. Initially the biowaste gases were projected to be CO_2, CH_4, H_2O or H_2 with only very small amounts of O_2 or N_2. However, during 1971, results from experimental life support tests indicated that the oxygen content would probably be in the range from 0.5 to 1.0%.

To achieve the desired high specific impulses, metal temperatures as high as 1700°K (3060°R) were considered desirable goals. The first thruster, designated Mark I, employed the alloy platinum-rhodium for the center tube. Although this material was oxidation resistant and had high strength relative to pure platinum, experimental materials tests showed that this alloy suffered from carbonyl reactions when tested on pure CO_2. These reactions resulted in a depletion of rhodium and significantly weakened the tubes. The Mark I thruster did demonstrate the use of noble metals for the concentric tube biowaste resistojet, however, and did result in a highly efficient unit.

The next series of thrusters were designated Mark II and employed platinum-iridium for the center tubes. When the selection of this material was made, the biowaste gases were not expected to contain a significant amount of oxygen. There was no carbonyl reaction problem with platinum-iridium, and this material had very high strength. Several structural improvements were also incorporated in the Mark II design and one thruster successfully completed relatively severe acceleration and vibration tests which simulated the booster launch phase. These thrusters were also tested with a large variety of simulated biowaste propellants and performance was documented.

When platinum-iridium tubes were tested with biowaste gases containing from 0.25 to 1.5% oxygen, the tubes failed in a relatively short time from oxidation reactions. As a result, it was necessary to select another tube material which neither suffered from carbonyl reactions nor from oxidation attack. The materials which possessed these qualities were pure platinum, thoriated platinum and platinum-palladium. These materials all had considerably lower strength than did either platinum-rhodium or platinum-iridium and therefore it was necessary to modify the Mark II design to permit the use of lower strength materials.

The Mark I and Mark II thrusters also had the potential problem of contact between the two inner tubes if bending of the center tube occurred. This touching could occur during repeated cycling and would result in reduced performance. The Mark II thruster was redesigned to permit the use of low strength materials for the center tube and the tendency of the tube contact was eliminated by employing ceramic spacers between the center tube and second tube. This redesigned thruster, designated RD-1, was fabricated and tested. Test results were very encouraging with high performance being obtained at high power levels with hydrogen propellant. The concept of using low strength materials for the center tube was demonstrated and this experience resulted in a further improved design designated RD-3, which is compatible with all biowaste thruster requirements.

The RD-1 thruster incorporated a pure platinum center tube but later materials tests demonstrated that 0.6% thoria dispersed in platinum is superior to pure platinum for biowaste thruster use. The thoriated platinum is superior to all the other tested materials in that it has improved long term strength properties at elevated temperatures, the thoria inhibits grain growth at high temperature, and the thoria apparently reduces oxidation and vaporization of the platinum material. The new thruster, RD-3, incorporates a center tube heating element fabricated from thoriated platinum. Component tests of the new thruster design indicate improved performance. Further testing of the thruster is planned on a follow-on DVT type program. The DVT program should result in a demonstration that the RD-3 concept using TD-Pt will meet all of the currently projected requirements for a biowaste resistojet thruster.

INTRODUCTION

Resistojets have been under development at The Marquardt Company for the past ten years. Some of this effort has been government-sponsored and some has been conducted under Independent Research and Development programs. Various applications have identified certain design concepts as optimum and generally the specific propellants define materials of construction. This final report summarizes the engine development effort conducted between September 1969 and June 1972 on a biowaste resistojet technology development program, conducted for the National Aeronautics and Space Administration, Langley Research Center, under Contract NAS 1-9474.

Potential Application

Future long duration manned space flight laboratory systems will require sophisticated stabilization control techniques to provide vehicle stability and precise attitude control. As reported in Reference 2, the biowaste resistojet system was selected for simultaneous orbit-keeping and control moment gyro desaturation for the Manned Space Station/Base Concept. Selection of the biowaste resistojet system was the result of complex system and integrated system tradeoffs. These types of application studies identify desirable resistojet characteristics, define operational requirements and sometimes impose certain restrictions or requirements upon thruster operation that require improvements or significant changes to the resistojet thruster designs that are presently available.

Some of the significant biowaste resistojet requirements may be summarized as follows:

1. The resistojet must use the available biowaste gases as propellant and use water as a supplemental propellant.

2. The resistojet should produce a high specific impulse and use the electrical power efficiently.

3. The thrusters must operate reliably over long periods of time.

4. Thruster operation will be intermittent or continuous as required.

5. The thruster system must be structurally adequate to withstand the vehicle launch environment as well as sustained operation and exposure in space.

Program Objectives

The objectives of this technology development program included the design, fabrication, and testing of electrically heated 10 millipound thrusters utilizing as propellant typical by-products of spacecraft life support systems. Since high temperature materials, resistant to these propellants and having suitable manufacturability characteristics, are required to achieve high specific impulse, high thermal efficiencies and long life, materials studies were included. This report summarizes the engine development portion of this program. Reference 1 summarizes the materials research phase of the program.

Resistojet Concept

The biowaste resistojet design utilized under this program has resulted from ten years experience at Marquardt in the development of high performance resistojets ranging in thrust from ten millipounds to one pound. The Marquardt design is based upon use of a concentric tube heat exchanger configuration which has the following advantages: (1) high thermal efficiency for low power consumption, (2) final gas temperatures close to maximum wall temperature for high specific impulse, and (3) minimized creep stresses with zero hoop-creep stress in the hottest inner element for long life.

Figure 1 shows the 10 millipound resistojet concept as developed for the MORL (Reference 3). It consisted basically of two functional parts: (1) an electric-gas heat exchanger, and (2) a nozzle for accelerating the resultant high temperature gas to produce thrust. The electrical flow was through the outer case, case end, nozzle and inner heating elements. A strut connector provided an electrical connection between the two main heating elements while concurrently allowing gas to flow through the engine. Approximately seventy-five percent of the ohmic heating took place in the inner heating elements.

The gas flowed between the inner and outer case, intercepting the radial-thermal flow and carrying much of the heat back toward the center of the device. The gas then passed through the annulus between the inner and outer heating elements where a significant amount of gas heating took place. The final gas pass was down the inner heating element (center tube), where the gas very closely approached the wall temperature. The gas was then expanded through the nozzle.

The inner heating element was the critical component that necessitated the materials research phase of this program. This tube was small in diameter, I.D. = 0.1016 cm (0.040 in.), with a thin, 0.01718 cm (0.007 in.), wall. This tube is approximately 4.24 cm in length. As is evident from Figure 1, the propellant gas flows on both sides of the center tube and therefore there is little pressure drop across the tube. The second tube is exposed to propellant gas on one side and vacuum on the other, and therefore must withstand a higher ΔP, but its temperature is lower than that of the center tube.

ENVIRONMENTAL REQUIREMENTS

Propellant Composition

Definition of the specific propellant combination for biowaste development is extremely important because of the corrosive nature of these gases at high temperature. Unfortunately, these gases cannot always be defined rigorously because of the experimental nature of, and associated development of, biowaste life support systems. Early in the program, typical biowaste propellants included CO_2, H_2O, H_2, CH_4, other hydrocarbons and trace gases such as N_2 and O_2. It was expected that several of these gases would be available as a mixture.

Contact with personnel from McDonnell Douglas, Huntington Beach, during the latter part of 1971, indicated that the most probable biowaste gases for use with resistojets would contain about 1.0% oxygen instead of just a trace amount. The estimated gas composition, based upon a 90 day life support test was:

97% CO_2
2% N_2
1% O_2

Other typical gas compositions could be mixtures of CO_2 and CH_4 with smaller amounts of N_2, O_2 and H_2O. The early materials studies and tests were concerned with biowaste gases containing only trace amounts of oxygen. As a result of the change in projected gas composition, later tests were conducted with propellants containing significant amounts of oxygen.

Performance Requirements

To achieve high performance, heater tube surface temperatures may be as high as 1700°K (3060°R) while gas temperatures will extend from 1500 to 1600°K. These high temperatures can cause reactions to occur in either the gas or the tube or both. Because of the type of gases, the inner heating element must be resistant to both oxidizing and reducing atmospheres. Elemental carbon and hydrogen may form from the hydrocarbons, therefore, heater parts must resist both carburization and hydrogen embrittlement. Nitriding may be a consideration in the case of steels when nitrogen is present. Carbon monoxide (which can form from CO_2, hydrocarbon with oxygen or water, etc.) may be present as a contaminant gas. If it occurs it can form carbonyls with many elements including iron, nickel and rhodium. The high metal temperature requirements and the corrosive nature of the gases severely limit the choice of materials.

STRUCTURAL DURABILITY REQUIREMENTS

The biowaste resistojet must withstand the vehicle launch environment as well as the sustained environment in space during operation. Because of the requirement for long life (the envisioned thruster operating life is two years) care must be exercised in the selection of the most critical elements - the heater tubes. These tubes operate at very high temperatures and must be capable of repeated cycling. Although the number of on-off cycles has not been rigorously defined, it is projected to number several thousand. From a shock and vibration standpoint, the launch (boost) phase is the most severe. The specified vibration requirement calls for a random vibration level of 0.5 g^2/cps at low frequency decreasing to 0.032 g^2/cps at 2000 cps. Other requirements are specified for shock and acceleration, all of which correspond to wet launch conditions for a manned orbiting laboratory. Biowaste thruster structural analysis and design modifications are being directed toward a more general, and stringent, requirement corresponding to a dry launch laboratory. Orbital workshop vibration spectrums being considered on some Marquardt contracts for cold gas thruster valves reach maximums of 1.0 g^2/cps. Efforts on the biowaste design were toward a goal of 1.5 g^2/cps.

The resistojet heater elements in their present concentric tube configuration require the use of a ductile material. The structural geometry in this design concept is not compatible with the brittleness and poor shock resistance of ceramic materials. The heater material selection study logically suggests the use of noble metals. A final selection is highly dependent upon the final chemistry of the propellants available from the spacecraft.

Corrosion resistance is a primary selection criteria. Other considerations include: (1) sufficient creep strength at high temperatures to withstand thermal-mechanical stresses, (2) sufficient cold mechanical strength to withstand the launch vibration and acceleration loads, and (3) fabricability. Also, an electrical resistivity which is high and which increases with temperature is desirable. A low emissivity is desirable to reduce radial heat transfer by radiation.

Maximum heater temperatures are most likely dictated by required corrosion resistance and potentially by creep strength. Creep stress in the inner heater element, due to thermal expansion, was minimized by an expansion bellows in the early designs. Vibration-acceleration induced stresses are most severe in the innermost heater element when inertia forces are along the thrust axis. An adequate modulus of elasticity and yield strength are required for these stresses. Assuming acceptance testing (hot firing) will be required before launch, yield strength must be sufficient in the annealed condition.

MATERIALS RESEARCH

While many candidate materials were considered for the biowaste resistojet, development efforts concentrated on the noble metals. The early biowaste resistojets (designated Mark I) had heater and nozzle parts made of platinum-20% rhodium. This alloy has sufficient mechanical strength and excellent oxidation resistance. However, tests conducted on sample Pt-20Rh heater tubes revealed that severe corrosion occurred in the presence of carbon dioxide. These test results are discussed in detail in Reference 1.

Platinum-iridium alloy was chosen for heater-nozzle parts in the Mark II biowaste resistojet. This alloy offers higher mechanical strength and higher resistivity than platinum-rhodium alloys; however, it is more difficult to form and machine and oxidation resistance is reduced. At the time platinum-iridium was selected for the Mark II thruster, it was projected that biowaste mixtures would not contain significant amounts of oxygen but would be primarily CO_2, CH_4, and H_2 or mixtures of these gases, therefore, the lower oxidation resistance was not critical. Since then, the projected biowaste propellants have changed and are expected to include up to about 1.0% oxygen by weight. Tests in bell jars conducted on Pt-Ir tubes revealed severe corrosion problems with a CO_2 propellant containing 0.25 to 1.5% oxygen (see Reference 1). Therefore, the Mark II designs using Pt-20 Ir for the center heater elements had to be changed.

The materials tests in the bell jars, with simulated center tubes of various materials, indicated that several lower strength materials, such as platinum-palladium alloys, pure platinum and thoriated platinum (platinum with a dispersion of thorium oxide) offered promising resistance to both oxidation and carbonyl attack. Modifications were made to the Mark II design to allow the use of these lower strength materials.

Table I summarizes the major conclusions resulting from the materials study, summarized in Reference 1. The obvious conclusion resulting from all of the material tests is that TD-Pt (thoriated platinum) with 0.6% thoria* offers the best promise of satisfying all of the required design criteria and makes it possible to develop a thruster which is compatible with all of the currently projected biowaste gases.

THEORETICAL PERFORMANCE

Theoretical performance can be computed as a function of the propellant gas temperature and an assumed optimum expansion nozzle. Specific impulse curves for the various biowaste gases are presented as a function of gas temperature and are applicable to any resistojet heater configuration using an optimum nozzle. The optimum nozzle is one with a geometry which maximizes the product of nozzle viscous, expansion and divergence efficiencies for a specific gas temperature and propellant. The specific impulse curves are presented in Figures 2 and 3 for a 10 mlb and a 100 mlb thruster.

---

*TD-Pt development was conducted at Engelhard Industries under Contract NAS1-10433

The performance given in Figures 2 and 3 correspond to optimum thrusters for each specific case (propellant and temperature). Viscous nozzle losses are predominant in the 10 mlb to 100 mlb thrust range and correlate with nozzle throat Reynolds number. Nozzle efficiency decreases with decreasing Reynolds number. Therefore, a thruster optimized for H_2O would not deliver the predicted performance on H_2 for example. Reynolds numbers for a thruster using H_2O, CO_2, and CH_4 are not too different and one thruster with optimum geometry would deliver close to (within 2% in specific impulse) optimum performance for these propellants at the same operating temperature. This same thruster operating with hydrogen at the same biowaste resistojet temperature would perform about 3% and 1% lower in specific impulse (relative to corresponding optimum values) for 10 and 100 mlb, respectively.

The electric power requirements are shown in Figures 4 and 5. They apply specifically to the concentric tube resistojet heater concept with appropriate heater efficiencies having been considered. Power required for water as a propellant includes the energy of evaporation and is therefore, for liquid water. Liquid propellants cannot be supplied to the resistojet directly. A pre-evaporator is required. The power requirements for liquid water in Figures 4 and 5 include losses for an electric pre-evaporator. A pre-evaporator suitable for operation in a zero-g environment was also developed for the 10 mlb biowaste resistojet. Thermal efficiencies in the high nineties were demonstrated for a prototype evaporator. If steam is availabe, from a waste heat evaporator for example, the electric power requirement for the resistojet is reduced significantly. For steam received at 735°R, for instance, the required electric power curve would fall about two-thirds of the way from the CO_2 to the $34CH_4/66CO_2$ curve.

Equilibrium chemistry is assumed for the Figures 4 and 5 curves, except for methane bearing propellants. Nonreacted chemistry is assumed and is appropriate for the CH_4, $80CH_4/20H_2$, and $34CH_4/66CO_2$ curves. For the biowaste resistojet temperatures, the degree of equilibrium decomposition of H_2, H_2O and CO_2 is not significant and the Figures 4 and 5 curves are, therefore, realistic. The NH_3 curves are for equilibrium chemistry which is not necessarily realistic. Ammonia does decompose at biowaste temperatures, but the degree of reaction is not certain. At the high temperature end, the NH_3 curves are considered to be close to realistic.

Current 10 mlb biowaste resistojets being developed are capable of achieving chamber gas temperatures to 3000°R. A chamber gas temperature of 2700°R is recommended, however, for long lifetime capability. Thus, expected specific impulse ranges from 160 seconds for carbon dioxide to 570 seconds for hydrogen. While methane offers better than 300 seconds specific impulse at full operating temperature, this performance cannot be practically utilized because of the carbon deposition problem. Assuming the wall threshold temperature of about 1970°R resulting in a gas temperature of 1800°R will apply to the propellants containing methane, then 230 seconds specific impulse appears possible with methane. If the resistojet is always to flow methane and be limited to about 2000°R maximum wall temperature, certainly other materials than noble metal alloys can be used. The present biowaste resistojet program is directed toward the development of a thruster for all biopropellant possibilities.

Figure 6 presents a simplified correlation of ideal frozen flow specific impulse versus propellant molecular weight at a chamber condition of 1667°K (3000°R) and 1 to 2 atmospheres pressure. Theoretically, specific impulse is proportional to the square root of the ratio of temperature to molecular weight.

$$I_{sp} \sim \sqrt{T/MW} \qquad (1)$$

This relationship follows from the limiting velocity corresponding to an infinite isentropic expansion to vacuum and the assumption of a perfect gas. The specific heat ratio is considered a constant in the above proportion.

Several typical propellants and mixtures are compared in Figure 6. Those cases not containing methane correlate rather well as shown by a solid curve fit. While specific heat ratio is not constant for these cases (open symbols), the specific heat ratio decreases consistently with increasing molecular weight. This is reflected in the systematic deviation away from an equation (1) correlation shown as a dashed line referenced to the hydrogen point. It is interesting to note that typical cases involving methane (solid symbols) do not correlate well with the open symbol cases. Reacted CH_4 falls low in specific impulse while the unreacted CH_4 mixtures fall high. This is the result of a particularly high relative (to the other gases on a molecular weight basis) specific heat. For a given temperature, unreacted methane contains more energy than other gases at the same molecular weight and, hence, delivers more specific impulse. The reacted methane point is low apparently because of the large amount of dissociation energy lost in the assumed frozen flow.

The correlation in Figure 6 is convenient for preliminary design purposes in estimating the performance of various propellant mixtures where caution is exercised with strange propellants. This correlation is also valuable in making quick checks on actual thruster performance.

ENGINE FACILITY DESCRIPTION

The Marquardt high vacuum test cell is a stainless steel-roll back-chamber 48 inches in diameter by 54 inches long. Interfacing the chamber with the pumping station is a freon-cooled baffle to minimize diffusion pump oil backstreaming. The pumping station provides ~0.5 to 1.0 micron of mercury for 10 mlb thrusters with the baffle in place. With the baffle removed, a factor of 5 lower cell pressure results. Figure 7 shows the vacuum test cell used during the Mark I tests. The cell is rolled back to expose the thrust stand. A test facility schematic diagram is shown in Figure 8. The Mark II thruster tests were conducted in a new high vacuum facility having improved cell performance. Figure 9 is a photograph of the improved thrust stand with the Mark II resistojet in place.

Thrusting performance is measured on this Marquardt-developed thrust stand sized for the 1 to 250 mlb thrust range. The thrust beam is flexured about each orthogonal axis. Flexures in the horizontal plane of the beam permit precise balancing of the beam by the addition of dead weight on the right hand end. The balanced beam is then operated as a single-vertical axis beam with the horizontal plane flexures locked. The vertical axis flexures can be changed for maximum resolution in the thrust range being measured.

Electrical power cables to the thruster are brought onto the beam through water cooled mercury-copper electrode pots. This prevents torquing of the stand as well as thermal expansion effects. Instrumentation are taken off the beam by the bundle of super-flexible wire seen hanging between the two terminal strip panels. Not visible in Figure 9 is a tubing array mounted below the vertical axis. This array permits bringing propellant flows onto the beam and pressure signals off of the beam while minimizing propellant flow momentum forces and Bourdan tube effects. The tubing array and instrumentation wire bundle represent small spring forces which are repeatable and become part of the overall thrust beam calibration.

The thrust beam is calibrated at no flow-cell vacuum conditions by a remotely operated-precision weight calibrator seen as the black box on the left in Figure 9. The calibrator contains a flexured pulley over which a mono-filament nylon line passes. This line attaches to the thruster and has a tare weight pulling down over the pulley. The tare weight and pulley flexure spring forces become part of the beam calibration. Under actual environmental conditions, the beam is then calibrated by adding additional precision weights through a servomotor drive. The calibrator pulls on the beam at the same moment-arm distance that the thruster pushes.

Beam deflection is measured by a position transducer of the linear variable differential transformer type seen in Figure 9 directly below the thruster. At the opposite end of the same beam member to which the transducer is attached is a viscous paddle arm. The paddle is contained in a rectangular can seen covered which contains oil for damping the beam. A second paddle, not visible, is located below the thruster. In this case, the can is also off the beam and, in addition is water cooled. The paddle attaches to an intermediate bracket insulated from the thruster and the thrust beam. This provides a reference temperature heat sink for the thruster mounting bracket and prevents heat from flowing onto the beam. Temperature monitoring of the beam at the thruster end has shown that temperature remains constant within one degree F. Contributing to this good thermal control is aluminum foil laid over the left hand end of the beam. This prevents net thermal radiation from the thruster being captured by the beam structure.

The Marquardt-balanced beam-vertical axis thrust dynamometer is a precision steady-state device. Thrust resolution is 0.01 grams or 0.2 percent at 10 mlb. With the Mark II thruster setup, the perturbed beam oscillates at one cycle per three seconds and is fully damped within 30 seconds following a full scale perturbation.

Steady-state mass flow rate measurements for gaseous propellants are obtained from Brooks Rotameters. These are calibrated at operating pressure and temperature. Optimized scales are used and flow metering errors are kept to within ± 1.0 percent. Liquid water is supplied to the thruster by a precision-positive displacement Milroyal pump. The pump flow rate is calibrated at each data point by observing consumption from a graduated cylinder over 1/2 hour intervals. In this way the error in water mass flow rate is kept within ± 1.0% also. For 10 mlb thrusters, measured specific impulse errors are not more than ± 1.0% for a single propellant and less than ± 1.5% for mixtures of two propellants. Flow metering repeatability is better than 0.2%. This permits observing thrust changes of less than 0.3%, as for instance, when carbon deposition is occurring or cell pressure is being changed.

ENGINE DEVELOPMENT

Mark I Resistojet

Thruster description.- Two Mark I biowaste thrusters were fabricated using platinum-rhodium alloy heater parts and were tested with CO_2 and H_2O prior to the start of the biowaste resistojet program. A third Mark I thruster, also using platinum-rhodium alloy, was assembled during the program to be used in continued tests with other propellants and mixtures. These thrusters were modeled after the life test thrusters described in Reference 4 with minor structural modifications.

Nozzle gometry of the Mark I thruster is identical to the life test thruster. The life test nozzle was optimized for hydrogen propellant with an area ratio of about 30 and a total divergence angle of 44 degrees. With biowaste propellants, nozzle throat Reynolds numbers are higher (about 1200 to 1500 as compared to 450 with hydrogen). Thrusting performance of the Mark I thruster would therefore be nonoptimum (lower) with biowaste propellants. Subsequent biowaste thrusters have nozzles more optimized (larger area ratios and smaller divergence angles) for the biowaste propellant flow conditions.

A bellows was incorporated in the resistojet to provide for relative movement of the heater elements during thermal expansion (see Figure 1). The bellows spring rate was sized to balance the bellows spring force against the hydrostatic pressure loading in the longitudinal direction and to thus unload the innermost heating element. This was essential since the inner element was a slender column of 0.137 cm (0.054 inch) mean O.D. with a length to diameter ratio of about 30. The Mark I thrusters had bellows which were sized for balanced loading with a supply pressure of about 3 atmospheres.

Thruster performance.- Mark I thrusters were tested with CO_2, H_2O, CH_4, and air as propellant. The purpose of the tests was to obtain preliminary data on the biowaste propellants in the concentric tube resistojet design. Measured specific impulses were conservative (low) since the Mark I thruster nozzle geometry was nonoptimum as discussed above and because hard vacuum cell conditions were not achieved. As was

dicovered later, the relatively high back pressure, 50 to 70 microns caused a marked reduction in measured specific impulse. Because of the bellows sizing used in the Mark I thruster, biowaste propellants were supplied at the nominal rated 3 atmospheres pressure to prevent unnecessary loading on the innermost heating element. The Mark I thruster throat diameter was 0.046 cm (0.018 inch) and results in thrusts greater than 10 mlb with CO_2 and H_2O and a 3 atmosphere supply pressure.

Figures 10 and 11 present the data obtained on Mark I thrusters No. 7 and 8 using CO_2 and H_2O, respectively. Table II summarizes the results of these tests. The Table II data correspond to the maximum observed specific impulse. These specific impulses were expected to increase with subsequent biowaste thrusters having optimum nozzle geometries.

The No. 8 thruster test included a water evaporator to provide the thruster with steam. For the Table II data, thruster steam supply temperature was 430°K (774°R). Earlier attempts to operate the resistojet with a liquid water supply resulted in unstable operation generally tending towards water flow without any internal evaporation and with consequent icing in the nozzle. The water resistojet must have a pre-evaporator section whenever the propellant is to be supplied as a liquid. The pre-evaporator can be a separate device close-coupled to the thruster in which feed water is evaporated using either electrical energy or spacecraft waste heat. It is also possible to incorporate the pre-evaporator into the thruster. If electrical energy is to be used in the pre-evaporator this approach would be desirable in order to achieve the highest thermal efficiency.

Methane runs were made with Mark I thruster No. 8. Each time an attempt was made to operate at maximum temperature, thermal decomposition occurred followed by carbon deposition on thruster heater and nozzle parts resulting in loss of mass flow and thrust. During these runs, thrust was allowed to drop to about one-half of design value before the test run was terminated. Between methane runs, the thruster was cleaned of carbon deposits by operating the thruster hot while flowing air through to burn out the carbon.

Figure 12 presents the data for the first methane run. Following the data point corresponding to an electric power to mass flow ratio of 2620 joules/gram, power was increased for the next data point. A significant change occurred in the thruster over a period of from 10 to 20 minutes. This transient was not documented. Thrust and mass flow rate dropped to about 70% of their previous values. Over the next 20 minutes, thrust and mass flow decreased slowly to about 60% of design thrust and then remained at this level for 30 minutes (data point at 6,280 joules/gram) after which the thruster was shut down.

A post test examination revealed a uniform deposit of carbon in the thruster nozzle throat and extending out the divergent section to an area ratio station of from 5 to 10. The thruster nozzle throat design diameter was 0.018 inch (0.046 cm). Drill blanks were inserted through the nozzle throat and indicated that the throat had closed down to about 0.015 inch diameter.

The nozzle throat was reopened to 0.018 inch. A cold mass flow check revealed that a substantial flow restriction had occurred within the thruster. No apparent change in thruster heater resistance was observed, however. An airflow run was then made which cleaned the carbon out of the thruster.

Figure 13 presents data for the second methane run in which the transient was documented. Pretest cold flow data agreed with the Figure 12 cold flow data, indicating that the thruster performance had not changed significantly. Data for the transient occurring between data point 8026 and 8027 are plotted as a function of time in Figure 14. The test operation plan for this run called for obtaining steady state data power settings below the setting at which no apparent carbon deposition occurred in the first test. Once carbon deposition started, the test plan called for going to high power and temperature to observe the effect corresponding to suddenly applying power.

During this testing an anomaly occurred and is indicated in Figure 14. At about 20 minutes after data point 8026, thrust appeared to be dropping and the carbon deposition beginning. Power was then set and maintained between 65 and 68.5 watts for the remainder of the transient. The thrust is seen in Figure 14 to decrease rapidly to 3.5 grams at 37 minutes and then increase suddenly to 4.06 grams at 38 minutes. The rear end of the heater was being monitored by a pyrometer. No visible glow occurred up until time 32 minutes. A slight glow was visible at 36 and 37 minutes. At 38 minutes, the heater no longer glowed.

Thrust then continued to fall off smoothly to 3.2 grams at data point 8027. The exact point at which the heater began to glow visibly again was not noted. At 73 minutes, the heater rear end was glowing at 1070°K. During the entire transient, propellant supply pressure remained constant at 3 atmospheres. The reason for the sudden dip and subsequent recovery at 37 minutes is not understood. It is almost certainly a thruster phenomenon and not the result of instrumentation irregularities.

Referring back to Figure 13, thrust continued to decrease from data point 8027 to 8032 after which the run was terminated. The times at which each of these data points were taken are as follows:

Data Point	Time
8027	1224
8029	1250
8030	1315
8031	1338
8032	1347

The run was then terminated to avoid damaging the thruster. It appears that the thrust would have continued to drop until a point of failure was reached. The final observed heater temperature was 1515°K. Specific impulse (uncorrected for space vacuum) was 220 seconds at the final 5.7 mlb level. Post run cold flow specific impulse was the same as the prerun value (98 seconds) even though thrust had dropped substantially. This indicates considerable carbon blockage in the thruster.

The No. 8 thruster was again cleaned with air and operated a third time with methane. In this run, the last data point showed:

Data Point	8043
Thrust, grams	3.16
Specific Impulse, sec	225
Electric Power, watts	88.6
Pyrometer temperature, ^{o}K	1497

The airflow data obtained were as follows:

Test Date	11/17/69	11/19/69	11/20/69
Cold Flow Thrust, grams	4.40	3.89	4.75
Cold Flow Specific Impulse, sec	75	71	75
Hot Flow Thrust, grams	4.39	3.53	4.18
Hot Flow Specific Impulse, sec	158	153	156
Electric Power, watts	53	47	52
Pyrometer Temperature, ^{o}K	1452	1458	1475

Supply pressures varied slightly between these data, therefore the thrust and power should not be cross compared.

Towards the end of each methane run, carbon deposition rates appeared to become very slow. Power and mass flow data indicate that the methane was essentially undissociated. Therefore, the end of run conditions, and cold flow conditions reflect performance for unreacted methane.

The following data lists the ratio of thrust to supply pressure for cold flow methane with the thruster in the clean condition:

Test Date	Thrust to Supply Pressure Ratio, gram/atm
10/21/69	1.446
11/18/69	1.590
11/19/69	1.651
11/20/69	1.848

Thrust to supply pressure ratio is an indication of the thruster nozzle throat area ratio. These data indicate that the thruster nozzle throat area increased about 28%.

The Serial Number 8 Mark I biowaste thruster was operated with various mixtures of carbon dioxide and methane. Mixture ratios (weight of CO_2 to CH_4) of 3.0, 2.75, 2.5, and 2.0 were used. The mixture ratio of 2.75 corresponds to an equimolar mixture. This represents the theoretical limit for which no solid carbon is formed. For lower mixture ratios (richer in methane) solid carbon theoretically would form.

During this test, no attempt was made to operate at reduced temperatures to establish a carbon deposition threshold. Rather, the thruster was operated at near maximum temperature to establish the effect of carbon deposition on thruster performance.

Thruster supply pressure and heater temperature, measured by a pyrometer sighting on the upstream end of the inner element was held constant. The effect of any carbon deposition in this case is to reduce mass flow and consequently thrust. Except for thrust and mass flow changes associated with the change in the mixture ratios, no change was observed at mixture ratios of 3.0, 2.75 and 2.5. The mixture ratio of 2.5 was maintained for 2 hours. Subsequently, the mixture ratio was reduced to 2.0. Immediately a very slow decreasing thrust and mass flow transient began. This was documented for 3-1/3 hours during which time thrust decreased 3.7 percent or about 1.1 percent per hour. For comparison, the thrust decrease rate observed between data points 8026 and 8027 of Figure 14 for pure methane was 18.5 percent per hour.

At the end of 3-1/3 hours at the 2.0 mixture ratio with thrust still decreasing at the above given rate, the mixture ratio was increased to 2.6. The thrust transient stopped immediately. Thrust was observed to remain constant for 45 minutes after which the thruster was shut down.

Suspecting that carbon deposition might occur at the 2.5 mixture ratio over long periods of time, the thruster was cleaned out (carbon removed) and was operated again at the 2.5 mixture ratio for 6 hours. A very light deposition of carbon was detected amounting to about 1/4 percent per hour decrease in thrust. The effect of carbon deposition on thrust observed for the MarkI platinum alloy thruster tests is summarized as follows:

Mixture Weight Ratio, CO_2 to CH_4	Rate of Thrust Decrease, Percent Per Hour
3.00	0
2.75	0
2.50	1/4
2.0	1.1
0 (pure methane)	18.5

The mixture ratio of 2.75 is the equimolar case which theoretically corresponds to no solid carbon production in the decomposition of CH_4. Statistically, carbon could form at this ratio also. A run duration of the order of 100 hours would be required to properly evaluate this case.

As was discussed in the section on theoretical performance, specific impulse (I_{sp}) can be correlated against propellant molecular weight and a theoretical curve was presented as Figure 6. Figure 15 presents experimental Mark I biowaste thruster

performance. An arbitrary theoretical specific impulse curve through a specific impulse of 155 seconds and a molecular weight of 29 is indicated by the dashed line. The water, air and carbon dioxide data are seen to follow the trend implied by the Figure 6 correlation. Note that in Figure 15 specific impulses are the actual measured values and include nozzle losses as well as frozen flow losses. An unreacted methane data point is shown, and as predicted, falls high in the Figure 15 correlation. The unreacted point was taken from a run after extensive carbon deposition had occurred and the Mark I thruster was changing thrust very slowly. While a slight reaction was still in progress, effectively, the bulk of the propellant passing through the thruster could be considered unreacted. This is verified by power versus mass flow data corresponding to unreacted CH_4. For the data of Figure 15 thrust levels were as follows:

Propellant	Thrust	
	Grams	Millipounds
CH_4	2.7	6
CO_2	6.5	14.3
H_2O	5.75	12.7
Air	4.0	8.8

Had the methane thrust been in the 9 to 14 millipound range, nozzle losses would have been less and specific impulse would have been higher and even more in keeping with the Figure 6 correlation.

Figure 15 indicates that consistent data have been obtained with the biowaste thrusters. These data correspond to visible heating element temperatures of from 1390 to 1500°K. The corresponding actual gas chamber temperature was not measured directly. From energy balance calculations, gas temperature is estimated to be about 100°K higher than the observed heating element temperature. Experimental values in Figure 15, cannot, therefore, be related rigorously to theoretical values in Figure 6 to obtain nozzle efficiencies. In addition, the Mark I nozzle is not of optimum geometry for the biowaste propellants and results in lower specific impulse than an optimum thruster would. In addition, and perhaps more significant, the engine was tested with a high cell back pressure, 50 to 70 microns, which resulted in significantly reducing (10% or more) the measured thrust and resulting specific impulse.

Following these tests, no further work was done on the Mark I thruster because of the severe carbonyl reactions between platinum-rhodium and CO_2 identified by the materials tests.

Concurrently with the Mark I development, a water evaporator unit was being developed. This component is discussed in the following section.

Water Evaporator Development

The electrically heated water evaporator that was designed and fabricated is shown in Figure 16. Figure 17 shows a cross section of the evapoartor. An off-the-shelf 125 watt heater was used for a heat source. This was surrounded by 1/16 inch diameter copper balls to provide the heat transfer surface required for water evaporation and super heating. Thermocouples T_1, T_2, and T_3 are located in the bed of copper balls to monitor the wet to superheated steam interface.

Figure 18 presents preliminary data for the evaporator in which various transient conditions were examined. T_{out} is the temperature measured 1.0 inches downstream in the steam outlet line. Water inlet temperature remained constant at 76°F. The evaporator was insulated with a 1.0 inch thick blanket of Johns-Manville Microlite Type B insulation. The electrical power input to the evaporator was held constant at 60 watts for the Figure 18 data.

The first portion of the Figure 18 test explored the effect of various input water flow rates. Flow rate was increased in steps to essentially flood the evaporator at about the time of 50 minutes in Figure 18. All temperatures are seen to then correspond to a saturation temperature condition indicating two-phase (wet steam) conditions throughout the evaporator. By time 70 minutes, and at a reduced input flow rate of 1.17 grams per minute, the evaporator is seen to recover and again generate superheated steam. Throughout most of the test, conditions at Station T_1 remained saturated at about 260°F. At time 10 minutes and again at time 160 minutes T_1 is seen to be going superheated indicating that the saturated-superheated interface was moving upstream of Station T_1.

At time 100 to 117 minutes, the evapoartor was approaching a steady state condition with a saturation condition at T_1. At time 117 minutes, flow rate was reduced from 1.17 to 1.07 grams per minute and small oscillations begin to appear at T_1. This indicates that the saturated to superheated interface was essentially at T_1. Upstream of T_1, the evaporator would, therefore, contain a two-phase mixture of steam and liquid water. Downstream of T_1, conditions corresponded to superheated steam. Up to time 142 minutes, the evaporator had been operated with the steam outlet at the top and water inlet at the bottom. In this orientation, a one 'g' force was aiding to keep any water toward the inlet end.

At time 142 minutes, the evaporator was inverted by rotating 180° to put the steam outlet end down. Very little effect was noted on the outlet steam temperature for the remainder of the run. Perturbations from time 160 minutes on are primarily due to T_1 going superheated. Fluctuations in T_2 immediately after the inversion (time 142 minutes) indicate that some two-phase water was moving toward station T_2. This test indicates that even in an adverse "one-g" gradient, the evaporator appears to function normally and delivers superheated steam.

Subsequent testing in the inverted position with flow rate increased to 1.17 grams per minute revealed occasional transients where the two-phase region did effectively fall toward the steam outlet end. At all times, the output steam was superheated however. These tests indicate that with proper flow rates, the evaporator can function in an adverse "one-g" environment. The evaporator should, therefore, function normally in a "zero-g" enviornment.

A steady state run was conducted to determine the efficiency of the evaporator. The following parameters were measured at the steady state condition:

Electric power input	58 watts
Pressure	36 psia
Water inlet temperature	76°F
T_1	260°F
T_2	465°F
T_3	530°F
Steam outlet temperature	407°F
Water flow rate	1.125 grams/min.
Thermal efficiency	90 percent

Power losses for these data correspond to 6 watts. Insulation used was nonoptimum and tests on the evaporator are in a room environment. In a vacuum, the insulation effectiveness would greatly increase.

The evaporator insulation was changed to improve thermal efficiency before attempting higher power runs. The evaporator was insulated with a Johns-Manville Min K cylinder 2 1/4 inches in diameter which in turn was covered with Johns-Manville Microlite Type B insulation to an overall diameter of 3 1/2 inches. This reduced the thermal loss to 3 watts corresponding to an efficiency of 95 percent for the above operating conditions.

Efficiency of the evaporator was found to be sensitive to the ratio of flow rate to input electric power. As the evaporator was pushed to make more steam, the efficiency increased. This would be expected as temperatures decrease with increased steaming rate resulting in lower thermal losses. The absolute value of the thermal loss was found to be insensitive to the steaming rate, however.

Typical data for a constant power loss condition are as follows:

Performance for 3 Watt Thermal Loss

Input electric power, watts	40	60	75	100	120
Output steam power, watts	37	57	72	97	117
Thermal efficiency	0.925	0.95	0.96	0.97	0.975
Steam mass flow rate, g/min.	0.80	1.25	1.54	2.15	2.62

Steam output temperatures for these conditions range from 360 to 410°F. Data for the 100 and 120 watt runs indicated that thermal losses increase about 1/2 watt when output steam temperature increases from 370 to 430°F.

The prototype water evaporator was integrated with the thruster and the assembly was mounted on the thrust stand with an axial solenoid valve for propellant control. Delays were caused by a leak which developed in the prototype evaporator. A thin walled (order of 10 mils) electrical heater element was used in the initial configuration. This heater had a seam which required brazing to effect a positive seal. Subsequent operation in the tightly packed bed of copper balls caused a thermal expansion crushing load which in turn opened the brazed seam.

The thin walled heater was replaced by a thicker walled seamless heater having the same outside dimensions. Thus the water evaporation is essentially unchanged from the initial configuration. The new heater had different electrical characteristics, however. The original heater was rated at about 125, whereas the new heater is rated at 175 watts. The new heater proved satisfactory for the thruster tests. While the evaporator was installed on a Mark II thruster, a thermal startup transient run was made with no propellant flow. Figure 19 presents data tracking of the 3 thermocouple temperatures. Power was manually controlled simulating a crude 4 step control from 80 down to 4 watts.

The Figure 19 data show that steaming temperatures (about 300°F is required) are available in about 3 minutes using a maximum power input of 80 watts. Four watts of power were sufficient to hold the evaporator at 500°F. A ready to steam condition of about 300°F could be maintained for about 2 watts of power.

During all of the S/N 002 Mark II thruster testing involving water and water-gas mixtures, temperature T_1 closest to the inlet end of the evaporator remained at a saturated condition. Temperature T_2, about 2/3 of the way from the inlet to the exit end, generally drifted between 350 and 450°F indicating superheated conditions in this region. The T_1 region was apparently in a liquid-steam boiling condition. It is estimated that the inventory of liquid water in the evaporator would be about 1/3 to no more than 1/2 of the available volume in the evaporator. Thus the prototype evaporator is adequately sized for the 12.5 millipound test conditions.

Mark II Resistojet

Design.- Following discovery of the severe carbonyl problem with platinum-rhodium, design of the Mark II thruster was initiated. Since only traces of oxygen were projected to be in the biowaste gases at the time this unit was being designed, platinum-iridium alloys were selected for the critical inner heating elements. Relative to the Mark I thruster, the following changes were made to optimize thruster performance and develop suitable mechanical strength to withstand dynamic stressing in a launch vibration-shock environment.

Heater Assembly

1. Lap joints have been substituted for butt welds in the critical inner heater element.

2. A high thermal resistance support has been provided to constrain the strut end of the heater assembly against radial motion.

3. Annular gas passage supports have been relocated for optimum dynamic strength.

Nozzle Assembly

1. A trumpet shaped nozzle having effectively an area ratio of about 100 and a total divergence angle of 40 degrees has been substituted for the area ratio 32 - divergence angle 44 degree Mark I conical nozzle.

2. Throat entrance radius has been reduced from 0.025 to 0.010 inch to reduce viscous effects at the nozzle throat. Throat diameter remains unchanged at 0.018 inch.

Expansion Bellows and Positive Electrical Connector Assembly

1. A longer-lower spring rate bellows has been incorporated to match thruster material expansion and biowaste propellant pressures.

2. The assembly has been shortened by projecting the bellows into the regeneratively cooled portion of the thruster.

3. A high conduction electrical connector is incorporated.

4. A thermal resistance is introduced between the heater assembly and electrical connector.

5. Insulation has been eliminated from the electrical connector. The connector is a composite structure with improved mechanical strength.

Main Housing and Negative Electrical Connector

1. Thruster mount points have been moved outward to a larger circle radius for improved thrust vector alignment and improved thermal isolation.

2. A high conduction, regeneratively cooled negative terminal attach point is provided.

Insulation and Cover

1. Insulation geometry has been improved for optimum resistance to radial heat transfer and for better mechanical strength.

2. A lightweight aluminum cover with a low emissivity coating is used to reduce inertia loads and improve thermal performance.

Instrumentation

1. The inner element pyrometer viewport is retained.

2. Resistance thermometer instrumentation has been added to measure inner element temperature.

Figure 20 shows the new thruster size and arrangement of the propellant inlet tube and electrical connectors.

Fabrication.- Three Mark II thrusters were successfully assembled using heater elements fabricated from platinum-20% iridium alloy. The parts were fabricated by Engelhard Industries and considerable difficulty was experienced during fabrication because of the properties of iridium. Platinum-iridium is a tough, high mechanical strength material with an ultimate tensile strength in the annealed condition of about 100,000 psi for the 20% iridium alloy. Pt-Ir is similar in some respect to the tougher superalloys and tantalum relative to its machining and forming characteristics. Its difficulty in working is in proportion to the iridium content. The material can be turned on a lathe and milled, but is very abrasive causing rapid tool wear. When reaming, there is a tendency for the material to gall and tear. The alloy can be readily ground and eloxed, however. These are the preferred machining methods. In trying to form the alloy by expanding or stretching, it breaks or cracks, but it can be compressed or swaged effectively.

Figure 21 shows the inner heater element and nozzle parts. Opposite the nozzle end is a short cylinder which is welded to the inner element and machined to form struts. Figure 22 shows the next or outer heater element which is welded internally on the small diameter end to the struts. The cap in Figure 22 closes the strut end of the final inner-outer heater assembly. The outer heater element presented the most manufacturing difficulty, followed second by the inner element. For some perspective on the heater size, the inner element is a 0.040 inch inside diameter tube with a wall thickness tapering from 0.005 to 0.008 inch over a length of about 1.5 inches.

Figure 23 shows the bellows assembly and the insulated heater assembly for the Mark II thruster. An instrumentation wire which will be used to measure the inner element resistance is shown. These parts are joined to form the heater-bellows assembly. This assembly is the working part of the biowaste thruster.

The complete S/N 003 Mark II thruster is shown in Figure 24. Shown alongside is the S/N 001 thruster with its insulation and cover removed. The instrumentation wire is seen projecting through the positive electrical connector. The negative or ground electrical connector can be seen at the propellant inlet port. The Mark II thruster incorporates a trumpet shaped nozzle which offers a compromise between better thrusting performance and increased structural strength.

Performance tests, - Two of the Mark II thrusters, S/N's 001 and 002, underwent extensive performance testing with typical biowaste propellants that do not contain significant amounts of oxygen. The third unit, S/N 003, underwent a simulated acceptance test with hydrogen and then was subjected to a vibration test which simulated launch vehicle environmental conditions. The unit then was subjected to a post-performance test to demonstrate thruster integrity. The thrusters were tested in the improved high vacuum facility capable of achieving cell pressures of 1.0 micron or less for the 10 mlb thrusters.

Performance tests were conducted with a variety of typical biowaste propellants. The following table summarizes these propellants.

Propellant	Weight Mixture Ratio	Thruster Serial Number
H_2	-	001, 003
CO_2	-	001
CH_4	-	001
H_2	-	002
CO_2/H_2O	1.4	002
H_2O/CH_4	1.0	002
CO_2/CH_4	0.5	002
CO_2/CH_4	1.0	002
CO_2/CH_4	2.0	002

Although all Mark II performance tests were conducted in the high vacuum facility, windage and cell pressure corrections must be made to the measured thrusts to obtain actual thrust. Reference 5 presents a detailed discussion on cell pressure and windage effects. Figures 25 and 26 present windage correction factors for hydrogen and carbon dioxide applicable to the Mark II thrusters. For a given mass flow rate, windage effects are more severe for hydrogen than for carbon dioxde. This is expected since spouting

velocity and molecular mean speed of hydrogen is better than 4 times that for carbon dioxide at the same temperature. For given simulator mass flow rates, maximums in the windage correction factor occur at about 4 microns of mercury for H_2 versus from 1 to 2 microns for CO_2. Cell pressure instrumentation included an ion gauge, thermocouple gauge, Magnevac gauge, Alphatron, and a McLeod gauge.

Although hydrogen is not generally considered to be a probable biowaste resistojet propellant, it is used as a convenient test gas because thrusting performance is most sensitive to this propellant. This is especially true if the thrusters are heat transfer surface limited on other propellants. Figures 27 and 28 present performance of the S/N 001 thruster with hydrogen. Propellant supply pressure was held constant at 37 psia for all propellants except methane. The Mark II thrusters deliver from 11 to 14 mlb thrust when hot, depending on the propellant. Because the supply pressure was held constant, engine thrust is higher at the lower power levels (lower gas temperature) because of an increase in mass flow. With hydrogen, it is evident that a specific impulse of about 575 seconds can be achieved at 180 watts of electric power.

A comparison of the pre- and post-vibration test calibrations of S/N 003 on hydrogen propellant are presented in Figures 29 and 30. Flagged symbols are post-vibration test data. These data show that no change occurred in thruster performance as a result of the vibration tests. Figures 29 and 30 can be compared with Figures 27 and 28 for the S/N 001 thruster on hydrogen. Prior to testing the S/N 003 thruster, the high vacuum facility pumps were serviced. A heater in one of the diffusion pumps had been inoperative. Pumping speed has been improved which is reflected by the humping of the thrust curve at lower power-higher mass flow rate for the S/N 003 thruster as compared to the S/N 001 thruster. Cold specific impulse is seen to have been improved by lower cell pressure from 244 seconds for S/N 001 to 260 seconds for S/N 003. During the post-vibration calibration test, the S/N 003 thruster was operated to a specific impulse of 580 seconds on hydrogen propellant. While differences exist at cold flow and partial power between the S/N 001 and S/N 003 data, the hot flow data are essentially identical. This indicates that the nozzle throat sizes were identical in the two thrusters.

Figures 31 through 34 present performance obtained with the S/N 001 biowaste-resistojet with CO_2 and CH_4 propellants. A 30 psia supply pressure was purposely used with methane to drop thrust closer to the 10 millipound design thrust level and to increase propellant stay time in the thruster. In this way, a more realistic condition was achieved relative to the formation of carbon.

For the Figures 27 through 32 data, cold flow cell pressures were 20 and 180 microns, respectively, for carbon dioxide and hydrogen. Corresponding measured cold flow specific impulses were 61 and 244 seconds, respectively. Under hard vacuum conditions, the specific impulses would improve to estimated values of 63 and 260 seconds, respectively, for carbon dioxide and hydrogen. For spacecraft design purposes, a faired curve between these cold flow specific impulses and the maximum power and points of the specific impulse curves in Figures 27 and 31 should be used. It should be noted that the data in Figures 27 through 32 do not necessarily reflect the full capability of the thruster. The thruster was operated to a condition where the inner element temperature, as viewed by an optical pyrometer, was between 1450 and 1500°K (2610 and 2700°R). This was an arbitrary red line criteria for these first tests.

Noting the flatness of the specific impulse curve for carbon dioxide in Figure 31, it would appear that the specific impulse would not exceed 150 seconds with increased power. Flattening of the specific impulse curve indicates that the thruster may be heat transfer surface limited. The Mark II thrusters were assembled with expansion bellows sized for propellant supply pressure of from 37 to 38 psia. This has resulted in a thrust output of 6.1 grams (13.4 millipounds) for hot carbon dioxide. In effect, the thruster is being operated with 34 percent more mass flow than for a 10 millipound design thrust level. If the thruster were resized for 10 millipounds of thrust (smaller nozzle throat or different expansion bellow spring rate) the heat transfer characteristics should improve and a 160-second specific impulse should be possible with carbon dioxide. Hydrogen gas is a better heat transfer fluid than carbon dioxide. With hot hydrogen, the Mark II thruster delivers about 5.2 grams (11.5 millipounds) of thrust. The demonstrated specific impulse of 576 seconds indicates that predicted performance is being achieved with the Mark II thruster on hydrogen.

At the highest power points for both CO_2 and H_2 reported in Figures 27 through 32, inner element temperature per the optical pyrometer were about the same. However, it was noted that the nozzle of the thruster glowed considerably hotter when operating with CO_2 than with H_2. A thermocouple on the outer case at the nozzle end indicated 1020 and 865°K (1830 and 1560°F), respectively, for CO_2 and H_2 operation. Also inner element and overall resistance measured higher corresponding to higher mean heater temperature with CO_2 propellant than with H_2. These facts confirm that the CO_2 gas was not being heated as close to maximum structure temperature as the H_2 gas was. Measured specific impulses related to the predicted performance curves suggest that effective gas temperatures were 1140 and 1410°K (2050 and 2540°R), respectively, for CO_2 and H_2 at the highest power conditions. Resizing to the 10 mlb level should increase the gas temperature for CO_2 operation, resulting in close to predicted performance.

Figure 35 presents data for a typical high power condition (not maximum power) using carbon dioxide propellant to show the effect of cell pressure on thrusting performance. Mass flow rate is constant for these data, thus the change in specific impulse corresponds to the changing thrust with cell pressure. The Figure 35 data have been corrected for windage per the correction curves given in Figure 26.

The Mark II thruster can be compared to the Mark I thruster to indicate changes in thruster performance which have occurred. The Mark I data for CO_2 summarized in Table II corresponds to the same specific impulse demonstrated with the Mark II thruster (Figure 31). Cell pressure for the Mark I test was 52 microns corresponding to a thrust and specific impulse correction factor of 1.06 (ratio of thrust at 0.7 microns to 52 microns per Figure 35). This scaling of the Mark I data should be valid, since the same thrust stand was used for that test. Table III compares pertinent parameters for the Mark I and II thrusters.

These two data points correspond to identical specific impulses and identical electric power per unit of mass flow rate. A slightly improved (by one percent) overall total power efficiency is indicated for the Mark II thruster. This is encouraging, since many structural changes were made to make the thruster suitable for typical launch vibration and acceleration loads.

Inclusion of a thermal dam in the inner case between the bellow assembly and heater assembly has resulted in a significantly lower housing temperature. For the Table III operating conditions, housing temperatures were 465 and 414°K (836 and 745°R), respectively, for the Mark I and Mark II thrusters. Outer case temperatures were found to be higher for the Mark II thruster. Insulation cover temperatures were only a few degrees higher (8°K) for the Mark II. This fact, along with the significantly lower emissivity of the Mark II gold plated cover versus the stainless steel Mark I cover, indicates that the insulation effectiveness has been significantly improved. The Mark II thruster utilizes special cylindrically formed Min K insulation, whereas the Mark I insulation was made from flat slabs of Min K insulation.

The Mark II S/N 002 thruster was tested with water and water-gas mixtures. Figure 36 shows this thruster on the thrust dynamometer stand with a close-coupled water evaporator (also see Figure 37) and with a solenoid valve. A visual flow tube is included in the setup to evaluate the kind of flow being supplied when liquid water-gas mixtures are used. In the Figures 36 and 37 setup, a gas supply line and pressure gauge line were connected between the solenoid valve and the water evaporator, upstream of the visual flow tube.

During runs when carbon dioxide gas and liquid water were supplied to the thruster via the evaporator, indications were noted of instabilities due to the gas-liquid supply system and instrumentation lines going to the evaporator. Small pressure changes would tend, during increasing pressure, to drive some liquid water into the pressure gauge line and into the gas supply line. Subsequently, during decreasing pressure, this stored liquid would pass on to the thruster. For example, with a CO_2 to H_2O weight mixture ratio of 0.2, a ± 2 percent oscillation in thrust magnitude due to thruster chamber pressure oscillation was observed. By eliminating one of the gas lines and making the gas supply and pressure gauge line common, the mixture ratio could be increased to 0.3 for a ± 2 percent thrust variation. A check valve in the supply in an actual thruster spacecraft system would reduce or eliminate this problem.

A piston effect instability is also suspected relative to operation of the water evaporator. The evaporator is seen to be in a horizontal orientation in Figure 37. Liquid water and gas enter from the right hand side and leave as a steam-gas mixture on the left. Insulation used with the evaporator is left off in the Figures 36 and 37 photos for clarity. During operation of the evaporator-thruster system, a 2-inch diameter cylinder of Min K type insulation is placed over the evaporator.

As mentioned earlier, the prototype water evaporator appeared to be suitable for operation in a zero-g environment. This was indicated by successfully operating the evaporator in a vertical position with liquid water entering the bottom end and then inverting the evaporator end for end. The horizontal orientation of Figure 37 is a compromise between the two vertical orientation extremes. For stable operation in the horizontal orientation, liquid water must remain at the right hand or inlet end in Figure 37. Toward the center of the evaporator, a two-phase interface exists and the leaving

end of the evaporator is filled with steam being superheated to the exit condition. The slug of water at the inlet end can be likened to a piston and tends to be pushed toward the exit end when gas enters the inlet end. This phenomenon can cause momentary surging in pressure and, hence, pressure instability.

For typical propellant inlet conditions of 37 psia pressure and 294°K (530°R) temperature, the specific volume ratio of carbon dioxide gas to liquid water is 223. For the mixture ratio of 0.3 condition in which a ± 2 percent thrust variation occurred, the ratio of the actual volume of gas to liquid entering the evaporator is about 70. This would suggest the possibility of a piston effect phenomenon. The 2 percent thrust variation is not appreciable; however, it would be desirable to minimize the variation as it would result in an effective inefficiency in a propulsion system. During operation with water alone, a ± 0.2 percent variation was noted. Experience with gaseous propellant has indicated essentially zero variation in thrust with time for constant power and supply pressure conditions. During runs with water alone, a small carbon dioxide gas bleed was introduced into the gauge line to insure water would not accumulate in that line. This may have contributed to the observed ± 0.2 percent variation. The thruster could be operated to a carbon dioxide to water mixture ratio of 0.1 with no additional increase (from ± 0.2 percent) in the thrust variation.

Various techniques could be used to reduce the effects of gas-liquid instability in the propellant feed system and water evaporator. These were not explored. In order to facilitate the documentation of thruster performance on water and gas-water mixtures, the test setup was changed to input gaseous propellant between the evaporator and the thruster. With this arrangement, only liquid water was supplied to the water evaporator.

Figures 38 through 43 present thruster performance for water and for mixtures of carbon dioxide and water and of methane and water. Arbitrary, but typical, mixture ratios were used. Tolerances in the mixture ratios and thruster supply pressure held during the runs are noted on the performance curves. These do not mean that mixture ratio and thruster pressure are difficult to control. For the tests, a constant displacement-precision pumping system was used for accurate flow metering. In a spacecraft application, some type of pressure regulated propellant feed system would be used. During the thruster tests, successive data point conditions involved changing the water pumping speed, gas flow feed rate, thruster power and water evaporator power. Rather than juggle these variables for precise mixture ratio-supply pressure control, this time was used advantageously to allow the thruster to achieve steady-state thermal conditions. Water flow rates were accurately determined by switching the water pump inlet feed to a 50 ml graduated cylinder and by observing water consumption over a period of time of 20 to 30 minutes.

Figures 38 and 39 present performance for water only performance. A zero thruster power specific impulse of 123.5 seconds with water was obtained. Electrical power (124 watts) was supplied to the water evaporator to make steam for the thruster

while no power was applied to the thruster. The highest specific impulse observed with power to the thruster was 235 seconds. Measured thrust for this condition is 5.59 grams (12.3 millipounds). Calculated overall efficiency for the thruster at the 235 second condition is 70 percent.

Evaporator efficiency calculated to be 94.2 percent for an overall thruster-evaporator efficiency of 65.8 percent. A total electrical power input of 142.1 watts was distributed 48-52% for the thruster (68.1 watts) and evaporator (74.0 watts). These data indicate that the Mark II thruster achieved predicted performance with water propellant.

Cold flow resistance of the S/N 002 thruster is lower (0.028 ohms versus 0.034 ohms) than for the S/N 001 and 003 thrusters. This is the result of having substituted platinum-rhodium alloy tubes for both the outer and inner cases in thruster S/N 002. The cases in 001 and 003 thrusters are of platinum-iridium alloy. All three thrusters have inner and outer heater elements and nozzles made from platinum-iridium alloy. This explains the lower cold flow resistance points shown in Figures 39, 41, and 43. Discontinuities in the resistance data curve fits with the cold resistances, for example see Figure 39, are due to the effect of water evaporator steam heating on the thruster. That is, even at zero thruster power the thruster would be warmed by the steam inlet and have a higher resistance. Cold flow values shown in the figure are for ambient temperature, nonheated conditions.

The thruster plus water evaporator power curve in Figure 38 has the expected characteristic shape. With increasing thruster power, total power decreases slightly. This is the result of having to provide a large power increment for the vaporization of the liquid water supplied to the evaporator and of an increasing specific impulse-decreasing thrust characteristic. Mass flow rate is rapidly decreased with increased thruster power. The combined effect is the relatively flat total power curve shown in Figure 38.

Figures 40 through 43 present the results for the water-gas mixture runs. A maximum specific impulse of 184.5 seconds was measured at a CO_2 to H_2O mixture weight ratio of 1.44. The S/N 002 thruster was also operated on pure CO_2 and found to deliver the same specific impulse for a given electric power per unit mass flow rate as the S/N 001 thruster. Proportioning specific impulses for pure H_2O and for pure CO_2, the mixture specific impulse of 184.5 seconds is found to include 234 seconds on the water portion and 151 seconds on the carbon dioxide portion of the mixture.

The performance of thruster S/N 001 with CO_2 indicated heat transfer limited conditions were occurring with a maximum measured specific impulse of 142 seconds. The above calculation showing an effective specific impulse of 151 seconds on the CO_2 portion of the mixture substantiates the heat transfer limited conclusion. The thruster is not as heat transfer limited on water propellant or with the mixture of H_2O and CO_2.

The water evaporator which supplies heated propellant to the thruster effectively increases the heat transfer surface of the thruster. Thus it does appear that with proper resizing of the thruster to achieve 10 millipounds in the Mark II size, that predicted performance on CO_2 could be realized. The thruster already has demonstrated predicted performance with H_2 and H_2O propellants.

Figures 42 and 43 present performance for a nominal CH_4 to H_2O mixture weight ratio of 1.01. At the highest specific impulse of 226 seconds, the visible inner element temperature was 1245°K (2240°R). Heater element temperature for this condition is estimated to have reached about 1335°K (2400°R). This is well above the carbon deposition threshold temperature being predicted from the bell jar tests on sample heater tubes. This high temperature condition was maintained for 3 hours to observe any effect of carbon deposition on performance. No discontinuities in performance were noted as had occurred with the Mark I thruster. Thrust did decrease slowly, however, at 0.3 percent per hour indicating a slow carbon deposition rate. Relating the thrust change to nozzle throat size reduction from carbon deposition, the deposition rate can be calculated to be about 13 micro-inches per hour. Approximately 8 micro-inches per hour were calculated for the S/N 001 thruster operated on pure methane at a lower heater element temperature of about 1270°K (2290°R).

During operation of the S/N 002 thruster with water, several start-up transients were documented. In all cases, the water evaporator was heated to about 535°K (960°R) before admitting propellant. The following start-up runs were made:

1. Thruster power was left off while water was supplied at a fixed feed rate of 0.04 grams per second. The evaporator exit temperature was maintained by controlling evaporator power.

2. Thruster power was left off while water was supplied from a constant pressure source. The evaporator exit temperature was maintained by controlling evaporator power.

3. Evaporator power was left at a no-flow holding power level of 4 watts. Water was supplied from a constant pressure source. Upon initiation of water flow, thruster power was turned on to 30 watts.

4. Run 3 was repeated except this time the evaporator exit temperature was maintained by controlling evaporator power.

In all cases, a solenoid valve upstream of the evaporator was used to initiate water flow. Therefore, before the start-up both the evaporator and thruster were empty with internal pressures corresponding to cell pressure (about 0.002 microns of mercury). The fixed water feed rate in Run 1 resulted in a very gradual buildup

of pressure as the evaporator was being filled to its normal inventory of water. During the first 10 minutes in Run 1, five thrust disturbances occurred in which thrust was noticed to increase momentarily at the same time a faint-steam-like cloud of vapor and/or water mist left the thruster nozzle. The cloud was barely visible in a strong light beam and dissipated rapidly in the downstream direction. The pulse-like thrust disturbances were sufficient to carry the thrust beam to full travel for a fraction of a second. The momentary thrust increase was undoubtedly due to a large increase in momentary mass flow rate which suggests the clouds contained liquid water or perhaps ice.

The Run 2 start-up also resulted in momentary thrust disturbances, again always increasing thrust. This time 3 disturbances were noted occurring at about 1/2, 1-1/2 and 5 minutes after flow initiation and the wispy clouds could again be barely seen spouting from the nozzle.

The start-up in Run 3 was excellent with no disturbances for the first 2-1/2 minutes. After 2-1/2 minutes, the evaporator cooled off and passed liquid water into the thruster causing thrust to increase. Thrust level became erratic and ice was seen to form around the outer edges of the divergent nozzle section. Icicles formed, some of which were about 2 inches long, and extended from the exit edge parallel to the nozzle axis. It appeared that no ice was forming along the upper portion of the nozzle edge indicating that liquid water was running along the divergent nozzle wall and was being influenced strongly by gravity. The shut-down for this run involved a series of large thrust disturbances due to icing.

Run 4 corresponds to a preferred operation mode where thruster power would be initiated with propellant flow initiation. In this run, a relatively small thruster power was applied (30 watts as compared to about 60 watts at full power). No thrust disturbances were observed.

While thrust disturbances were noted during Runs 1 and 2 when no thruster power was applied, these were not detrimental to the thruster. These disturbances were always towards higher thrust and at no time was there any indication of momentary blockage of the nozzle from ice. Attempts to operate a Mark I thruster without a water evaporator showed severe flow instabilities to occur from a liquid propellant supply. Therefore, the biowaste thruster operating with liquid propellant must have an evaporator. The evaporator must be maintained at steaming temperature or pre-heated prior to initiating propellant flow. The thruster can be operated safely without thruster power provided it is supplied by steam from an evaporator. A water resistojet thruster control should include evaporator temperature as well as propellant pressure override signals on thruster power. In addition, the evaporator temperature signal should override the propellant solenoid command. In this way propellant flow will not be initiated with a cold evaporator and thruster power will not be applied with either a cold evaporator or inadequate supply pressure. This in effect provides a double safety on the thruster.

Figures 44 and 45 present detailed performance curves for the CO_2-CH_4 mixture ratio of 1.0 condition. While documenting performance of the Mark II, S/N 002 thruster on CO_2-CH_4 mixtures, additional carbon deposition data were obtained. The thruster was operated for extended periods of time at tempeature conditions for which thrust decreased slowly. This thrust change was related to carbon deposition in the nozzle throat. The following table indicates the results of these tests:

MARK II S/N 002 THRUSTER CARBON DEPOSITION DATA

Weight Mixture Ratio, CO_2/CH_4	Run Time, Hours	Measured Specific Impulse, Seconds	Estimated Max. Structural Temperature, ^oK (^oR)	Carbon Deposition Rate, Micro-inches/hour
1.0	6.0	178.5	1220 (2200)	18
1.0	42.5	168.5	1110 (2000)	0.5
2.0	39.2	157	1165 (2100)	0.25
0.5	17.9	180	1165 (2100)	0.5

These data compare favorably with the sample heater tube (bell jar experiments) data presented in Figure 40 of Reference 1. The three points of deposition rate less than unity indicate a higher threshold temperature than suggested by Figure 40 of Reference 1. The correlation is, of course, indirect relating maximum heater temperature to the deposition rate in the colder nozzle throat. The data above should best serve to suggest the specific impulses which may be possible with CO_2-CH_4 mixtures.

Again, projecting performance of the biowaste resistojet with the optimization suggested above, higher specific impulses should be possible. The optimization will not only improve nozzle performance but reduce the temperature difference between the chamber gas temperature and heater wall threshold temperature. This in effect maximizes the specific impulse for a given threshold temperature. Estimating that chamber gas temperature will be about 55^oK (100^oR) lower than the effective heater wall threshold temperature, performance on methane/methane mixtures was predicted and is presented as Table IV. The case of a H_2-CH_4 mixture is included to indicate the improvement in performance which should be possible with a small hydrogen addition to methane. It was pointed out in Reference 1 that hydrogen is known to be a good carbon deposition retarder. A factor of five reduction in deposition rate is possible with a 12 percent addition of hydrogen to methane, for example. Hydrogen would also result in substantially higher specific impulses because of the higher threshold temperature and lighter molecular weight propellant mixture.

In the course of obtaining the carbon deposition data, a total reduction in throat diameter of 360 micro-inches (180 micro-inches deposition thickness) occurred. The thruster was then operated to near full power on CO_2 (chamber gas temperature about 1450^oK or 2600^oR) to evaluate the effectiveness of CO_2 as a carbon remover. The possibility of CO_2 serving as a carbon gasifier was discussed in Reference 1. No

doubt the thruster had a buildup of carbon in the heater section corresponding to more than 180 micro-inches. This assumption is based on sample heater tube tests reported in Reference 1 and the fact that heater wall temperatures are significantly higher than the nozzle throat wall temperature.

The carbon stripping test (full power on CO_2) was comprised of a one hour run followed by a 23 hour run. The 24 hours of hot time was interrupted to obtain a cold flow calibration after the first hour to determine how effectively carbon was being removed. Unexpected results occurred, however. It is believed that carbon in the heater section proper was being removed by the carbon dioxide. However, the nozzle throat continued to close with an additional deposit of carbon 240 micro-inches thick. It appears that during the carbon gasification process in the heater section, unreacted carbon particles were being freed by erosion and subsequently deposited on the colder nozzle throat surface. Most likely gasification was occurring at the throat but at a much slower rate than for the deposition process.

An anomaly was observed approximately 20 minutes after power-up for the one hour hot run. The dynamometer thrust recorder was turned on 20 minutes into the run just in time to document a 1.7 percent step-up in thrust level. Power and thruster pressure were constant. The anomaly was due to a sudden increase in throat size. Pre-post cold flow calibrations verified that the thrust had decreased during the start-up (prior to the observed thrust step-up) indicating that a small particle of macroscopic order of size had blocked the nozzle throat. The thermal expansion during start-up may have caused a flake of carbon to pass from the heater to the nozzle throat. In view of the 180 micro-inches deposited in the throat with methane mixtures, deposition in the much hotter heater section would probably be measured in mils (several thousand micro-inches). Thinner deposits would occur at threshold conditions and present a lesser carbon problem.

Had the thruster been operated longer on CO_2, the gasification of heater carbon deposits should have gone to completion. Probably the deposition noted in the nozzle throat would be reversed and lead to eventual removal of all of the carbon. For the Mark II thruster, gasification of carbon does not occur quickly. This situation could be improved by incorporating a thermal dam in the nozzle diverging section or in the outer pressure case near the junction of the nozzle to the case. Nozzle throat temperatures would be increased and affect a reduction in condensation of carbon and an increase in local gasification. On the other hand, deposition rates with biopropellants containing methane might be increased relative to chamber gas temperature and effective specific impulse.

Figures 46, 47, and 48 compare performance data from all of the various propellants tested. The points of highest specific impulse for any given propellant do not represent maximum capability of the thruster. Rather, the data reflect heater temperatures for propellants and mixtures not containing methane which approach from 1600 to 1670°K (2900 to 3000°R). Whereas, the melting point of the heater

material is 2080°K (3750°R). This margin of at least 420°K (750°R) ensures long life. Lower operating temperatures are used when methane is present because of decomposition of the methane and deposition of solid carbon on the heater surfaces and in the nozzle throat.

The performance presented in Figures 46 through 48 are for a thruster design supply pressure of 37 psia except for CH_4 data shown in Figure 47. The performance on CH_4 were obtained with a thruster supply pressure of 30 psia. At design pressure, the thrust and electric power for CH_4 would scale up by the factor 37/30. Overall efficiency would not change significantly as the result of a trade-off effect. That is, at the higher mass flow rate corresponding to design pressure, the heat exchanger would be working harder (lower heater efficiency), however, nozzle Reynolds number would be higher (higher nozzle efficiency).

At design presure, the thrust is nearly the same for all propellants and falls off slightly with increased specific impulse (increasing gas temperature and decreasing Reynolds number. The humping of the thrust curve for H_2 (Figure 46) at the low I_{sp} end is the result of a higher cell pressure which occurs at the higher mass flow associated with cold flow. Mass flow rates can be found from the thrust curves by dividing thrust by I_{sp}. In Figure 48, the thrust levels should not be compared in terms of the different propellants since some carbon-deposition (which lower thrust) was permitted with the mixtures containing CH_4.

The overall total power efficiency η_O is the useful axially directed power leaving the thruster nozzle ratioed to the sum of the electric and propellant power put into the thruster.

$$\eta_O \triangleq \frac{F \times I_{sp}}{20.8\,(P_e + P_i)} \qquad (2)$$

Thrust F is in grams, I_{sp} in seconds, P_e is electric power in watts, and P_i is the propellant power at the thruster inlet in watts. The overall total power efficiency is the product of the thruster heater efficiency and nozzle efficiency.

$$\eta_O = \eta_H \times \eta_N \qquad (3)$$

For cold flow data, (the lowest specific impulse point on the performance curves except for propellant containing H_2O) η_H is 1.0 and η_O equals η_N. The higher Reynolds number CO_2 flow reflects a nozzle efficiency of 0.855 whereas η_N is 0.77 for the H_2 flow having a lower Reynolds number. Actually, the cell pressure effect mentioned has lowered the H_2 cold flow efficiency. In hard vacuum, the cold flow I_{sp} would increase to 270 seconds and η_N would be about 0.80. For powered flow, η_H decreases from 100% and so does η_N decrease further as the result of decreasing Reynolds number and higher viscous losses. For example, at 575 seconds for H_2, η_O is 0.67 which results from η_H of 0.92 and η_N of 0.73.

Hydrogen is an excellent propellant from a heat transfer point of view. While the Mark II thruster operates at a high efficiency (67%) with heated hydrogen, it does not perform as well on CO_2 (47.5%) and CH_4 (52%). The Mark II design was sized for a hot thrust of 11.5 mlb (5.25 grams) and 13.5 mlb (6.15 grams) on H_2 and CO_2, respectively. Nozzle Reynolds number is higher for CO_2 than for H_2 and results in a higher η_N of about 0.80 with CO_2. This means that η_H is about 0.60 on CO_2 at 13.5 mlb and the thruster is exhibiting heat transfer surface limited conditions. A resizing of the nozzle throat for an actual 10 mlb of thrust and a 20% increase in heat transfer surface area should move the CO_2 performance up to an I_{sp} of at least 165 seconds with η_O greater than 60%. Methane performance would be improved also by a proportionate amount. Performance on hydrogen would increase slightly to an overall efficiency of 69% at 580 seconds.

The fact that the Mark II thruster, as sized, is heat transfer surface limited is shown dramatically by the performance on H_2O (Figure 47). The dashed curves of efficiency and power correspond to the thruster alone while the solid curves include the water evaporator discussed previously. Note that the thruster at 235 seconds I_{sp} has an η_O of 0.70. As a heat transfer fluid, H_2O can be compared to CO_2 which is seen in Figure 47 to be showing heat transfer surface limitations also. The water evaporator, in effect, has increased the heat transfer surface of the thruster and resulted in an η_H of 0.91 with an η_N of about 0.77.

The relative effectiveness of the various propellants as heat transfer fluids can be seen by comparing heat transfer surface area requirements. A simple relative comparison follows by recognizing that the local per unit area heat transfer rate is proportional to gas thermal conductivity.

$$\dot{q} \sim k \tag{4}$$

where the Nusselt number is constant for the highly viscous laminar flow and the local wall to gas temperature difference is considered to be the same for all propellants. The overall heat transfer requirement for the same thrust and same gas temperature rise is proportional to the product of the mass flow rate and gas specific heat. Using the definition of specific impulse, again for the same thrust

$$\dot{Q} \sim \dot{m}C_p \sim C_p/I_{sp} \tag{5}$$

The area required is seen to be proportional to these variables as follows:

$$A = \frac{\dot{Q}}{\dot{q}} \sim \frac{C_p}{k\, I_{sp}} \tag{6}$$

At typical conditions compatible with operation with methane and using mean values of the gas properties, the above parameter ratioed to its value for H_2 propellant is about 2.3, 2.1, and 1.7 for H_2O, CO_2, and CH_4, respectively. Therefore,

relative to performance with H_2, these other propellants require about twice the heat transfer surface. The thruster is considered oversized relative to the H_2 requirements. The nozzle resizing and 20% increase in heat transfer surface will, in effect, provide about a factor of 1.4 increase in heat transfer capability which is considered adequate.

The high area ratio nozzle, was chosen for improved structural rigidity to provide desirable design margins for the vibration requirements. It was known that nozzle performance would be compromised. Relative to a conical nozzle of the same area ratio, the trumpet shaping is believed to have minimized the compromise. With a reduced area ratio nozzle optimized for the 10 mlb thrust flow conditions, the following improvements in nozzle efficiency are predicted:

	Nozzle Efficiency, η_N	
Propellant	Mark II	Improved
CO_2	0.80	0.82
H_2O	0.77	0.79
CH_4	0.81	0.83
H_2	0.73	0.76

These values are based on chamber-gas temperatures of about 1555°K (2800°R) for CO_2, H_2O and H_2 and less than 1100°K (2000°R) for CH_4. Overall total power efficiencies would be increased by the ratio of the improved-to-Mark II nozzle efficiencies.

Projecting the experimental performance for the Mark II thrusters with optimizations which include the following:

1. Nozzle throat resizing for a nominal 10 mlb of thrust.
2. Approximately 20% increase in heat transfer surface.
3. Optimized nozzle expansion geometry.

Performance predictions were made for a 10 mlb biowaste resistojet of the Mark II type and the results are presented in Table V.

For convenience in interpreting the overall efficiency definition back to electric power, power in the gas in watts is given by:

$$P_i = k\dot{m} \tag{7}$$

where $\dot{m}$ is in grams per second, and the constants k are as follows for ambient propellant inlet conditions of 25°C (77°F):

Propellant	Constant, k
CO_2	213
CH_4	625
H_2	4200

In the case of H_2O, k is (-1892) for the liquid and 937 for 500°K (900°R) steam. The η_O of 0.72 above for water is for the thruster receiving steam and includes the water evaporator.

The effect of cell pressure on thruster performance is shown to be significant at cell pressures above one micron for 10 mlb size thrusters. Figure 49 presents these data normalized arbitrarily to the measured value at 2μ. Thus, the relative cell pressure effect is seen to be more prominent for the lighter H_2 propellant. Between 1 and 10μ, I_{sp} is seen to change 3.5 and 7 percent, respectively, for CO_2 and H_2. From the curve fits, it appears that hard vacuum performance has not yet been reached at the 1μ level. It would appear that I_{sp} measured in the Marquardt facility for hot flow conditions are conservative being within about 1% of hard vacuum conditions.

A note of caution is in order based on the above. Any attempt to determine nozzle performance as a function of Reynolds number (in seeking the optimum nozzle, for instance) must consider ambient pressure effects. In addition, windage effects on dynamometer calibrations must be considered. Care must be exercised in interpreting experimental nozzle performance for use on thrusters to be used in the hard vacuum of space.

Figure 50 presents the electrical characteristics measured on the S/N 001 thruster during tests with CO_2, H_2, and CH_4. Since the CH_4 data are for a reduced supply prssure, a power comparison with CO_2 and H_2 should be made by scaling CH_4 power up by the factor 37/30 or about 1.23. The end point on the CH_4 curve would move up along a constant resistance line corresponding to constant temperature.

The Figure 50 data indicate that resistance would offer a temperature limiting signal for the control of power regardless of the propellant being used. For operation with methane and methane mixtures, a reset to a lower limiting resistance could be used for control. The data of Figure 50 are for the overall thruster electrical characteristics. Similar data were obtained from the inner element voltage connection with resistance ranging from 0.026 ohms cold to 0.054 ohms hot. The inner element resistance would provide better power control during transients, and for the Mark II design, it is recommended for a control signal rather than the overall terminal resistance.

Vibration tests.- The S/N 003 thruster successfully competed shock (30 g's), acceleration (8g's) and vibration (10 g^2/Hz) tests conducted by an independent testing laboratory. The lower level random vibration test achieved a calibrated overall 'g' value of 17.65 rms. A higher level random vibration test was added to subject the thruster to a more severe vibration environment. In this test an overall 'g' value of 35.7 or twice the contractual requirement was successfully achieved.

A photograph of the vibration test setup is shown in Figure 51. Leak test instrumentation was used between each test to monitor thruster condition. In addition to leakage tests, thruster cold resistance was measured between each test. No change occurred in thruster cold resistance throughout the test program. Thruster leakage rate remained zero throughout the vibration test and the post-vibration test hot firing.

Figure 52 shows the electrical connector end of the S/N 003 thruster in the vibration mounting bracket taken after the high level random vibration test. Dust is seen on the housing which is powdered Min K insulation and which is believed to have been scraped from the Min K cylindrical block by the 1/4 inch diameter instrumentation hole seen in the housing face. Some Min K powder was also seen to dust out around the thruster heater assembly at the nozzle end. No harm occurred to the S/N 003 thruster and the Min K insulation remained tight in the insulation cover. Long duration vibration at the high level may present a problem, however. It is recomended that a thin foil wrapping around the Min K insulation be incorporated in any flight-type thruster to prevent chaffing. The electrical connectors and braided cables used during the test are seen in Figure 52. These presented no problem. As was shown in Figure 29, there was no performance difference of the thruster before and after the vibration and shock tests.

Design verification tests.- Two Design Verification Tests (DVT) were conducted with the Mark II thrusters. The objective of the first DVT test was to determine the maximum performance available with hydrogen propellant. In support of this test, the S/N 001 thruster was installed in the high vacuum facility during June 1971 for operation to destruction (over temperature) on hydrogen propellant. The thruster was initially operated up to the previous maximum performance level which was approximately 180 watts. Power was then increased in about 5 watt increments. The thruster was operated at each power setting for a minimum of 15 minutes to assure temperature stabilization. The last data point taken prior to the burnout power setting was a power setting of 203 watts. At this power setting, the data indicated a specific impulse of 628 seconds. Thruster failure occurred approximately 5 minutes after power was increased to 209 watts.

Thruster failure was evidenced by a sudden "open circuit" in the electrical circuit. Disassembly of the thruster revealed that the inner heater element, which was Pt-20Ir, had parted approximately 7/8 inches upstream of the nozzle throat. The various components are presented in the photographs of Figures 53 through 55. Operation of the thruster was normal up to the time of failure and failure occurred in the anticipated mode. An examination of the center element, shown in Figure 55, indicates

the element failed in tension. This is indicated by a slight necking down and separated grains in the immediate vicinity of the break. The bellows was designed to keep the tube in slight tension. All of the heater parts were clean and in good condition except for the area where the inner element separated.

Following the tests, a metallographic examination of the inner heating elements and nozzle was made. Figure 56 shows two longitudinal cross-sections of the inner heating element. The locations of these sections are identified in the upper photograph. The section at Point D shows considerable grain growth but the tube was still in good condition at that location. The Section at Point E is where the tube failed and the "cast structure" indicates incipient melting.

This incipient melting is further shown in Figure 57 at Section A, which is a transverse cross-section. The large grain growth prior to melting is evident in both the cross-section and in the external view having a magnification of 25. Figure 58 shows sections at Points B and C. Here large grains are again evident. All of the sections show that the inner tube remained clean with no evidence of corrosion or attack. The exit nozzle and outer heating elements also were very clean and showed no abnormal grain growth.

The second DVT test was carried out on the S/N 002 thruster. The objective of this test was to demonstrate 250 hours firing time and 250 pulse cycles using as propellants CO_2 and CO_2-CH_4 mixtures. This test was not completed because of shorting which occurred in the thruster. A total of about 222 hours of hot firing time (I_{sp} above 130 sec) with about 186 on-off cycles was accumulated. The following list shows the significant events which occurred during this test.

Events	Accumulated Time Above 130 Seconds, Specific Impulse, hrs
Performance calibration with $CO_2/CH_4 = 1.0$	1.8
Carbon deposition run, $CO_2/CH_4 = 1.0$ and $I_{sp} = 178$ sec	7.9
Carbon deposition run, $CO_2/CH_4 = 1.0$ and $I_{sp} = 167$ sec	12.8
Carbon deposition run, $CO_2/CH_4 = 1.0$ and $I_{sp} = 169$ sec	57.5
Pre-Pulsing Documentation, $CO_2/CH_4 = 1.0$ and $I_{sp} = 163$ sec	64.2
Pulsing Run - 182 cycles, $CO_2/CH_4 = 1.0$ and $I_{sp} = 163$ sec	95.5

Events	Accumulated Time above 130 Seconds, Specific Impulse, hrs
Post-Pulsing Documentation, $CO_2/CH_4 = 1.0$ and $I_{sp} = 164$ sec	96.6
Performance calibration with $CO_2/CH_4 = 2.0$	97.3
Carbon deposition run, $CO_2/CH_4 = 2.0$ and $I_{sp} = 157$ sec	137.4
Performance calibration with $CO_2/CH_4 = 0.5$	139.8
Carbon deposition run, $CO_2/CH_4 = 0.5$ and $I_{sp} = 180$ sec	181.1
Carbon deposition run, $CO_2/CH_4 = 1.0$ and $I_{sp} = 175$ sec	195.9
Carbon Burnout on CO_2, $I_{sp} = 133$	220.3
Pulsing run, 4 cycles, CO_2 (center tube shorted)	222

Shortly after the last pulsing test began, a voltage fluctuation was noticed and the thruster did not heat up as rapidly as it had on previous startups. At that point, the thruster was shut down to get a resistance check under cold conditions. The resistance check indicated that under cold conditions, no short circuits existed in the engine and the power supply checked out satisfactory under a dummy load. Testing was resumed but again evidence of a short was present under hot conditions. Therefore, testing was terminated as it was suspected that the inner element was shorting out under high power conditions.

At the time of removal from the altitude chamber, the engine was not in a shorted mode and a nitrogen pressure check showed essentially no leakage (about 0.07 psi/hr at 24 psia).

Figure 59 is a plot of the performance history of the thruster showing specific impulse versus accumulated run time for all conditions where the specific impulse was above about 130 seconds. Indicated on the figure are the propellant mixtures used at various time intervals as well as the type of runs being conducted. Operation of the thruster appeared normal until the inner element began to short circuit.

Following removal from the facility, the thruster was disassembled in order to determine the cause of failure and evaluate the condition of each significant component. Figures 60 and 61 are photographs of the disassembled components. The majority of the larger components were in excellent condition following the test.

Some difficulty was experienced in taking the thruster apart. The heater assembly was difficult to remove from the stem shown in the center of Figure 60. Evidently, the tight tolerances in the region of the spacers (used to keep the elements apart) plus the high temperature effects combined to render the bellows nonfunctional because of binding. This binding was probably responsible for the inner element bending and shorting out.

The inner element is shown in Figure 61. When the cut was made to separate the inner element from the heater element (also shown in Figure 61), the inner element sheared off at the nozzle throat section. The heater elements upstream of the nozzle throat were very clean and showed no evidence of carbon deposits. The nozzle was clean at the throat entrance but was coated internally in some of the divergent section. The inner element has a definite bend about 0.4 inches upstream of the throat station. A pock mark at that point indicated that the inner element did touch the upper part shown in Figure 61 and did dap weld itself during high power operation. Evidently it broke away during low power operation or cool down. These heater parts were then sent to the Metallurgical Lab for examination.

The metallographic examination was completed and Figures 62 through 64 are micro-photographs of the various heater components which were fabricated from Pt-20 Ir. Figure 62 shows a cross-section of the exit nozzle. The top left photo shows the overall nozzle. The throat area was relatively clean, but some deposits appear downstream of the throat. A close examination of the parts revealed that this deposit was braze material which apparently originated from the joint where the tube and nozzle were brazed together. There is no evidence that this braze material was detrimental to the thruster operation. When first disassembled, the braze material appeared black which indicates it was probably covered by a very thin layer of carbon. This brazed material was deposited on the expansion surface. A very thin layer (approximately 0.0003 inches thick) also is evident in the throat area by the X500 picture in the lower left. This deposit also seems to be primarily braze material.

An etched cross section is shown to the lower right in Figure 62. The grain size in this photo is very evident and is representative of the "as received" material. This photo also shows the nozzle did not get hot enough to cause significant grain growth. Figure 63 shows a cross section of the inner tube element. As is evident, the material is in good condition although there has been considerable grain growth, as is shown in the etched crossed sections. Some of the wall thickness is composed of single grains. This grain size should be compared with that shown to the lower right in Figure 62. There is no evidence of chemical attack, however, the wall thickness of the inner tube is tapered by design to increase the tube temperature near the throat. This is accomplished by maintaining a constant tube I.D. but varying the O.D. A comparison of the unetched cross sections through sections A and C reveal that the I.D. has not changed. Sections A and C are located 1.4 inches and 0.4 inches upstream of the throat, respectively. The outer heating element cross section is shown in Figure 64. Here again there was no evidence of chemical attack but there was considerable grain growth.

Alternate Engine Designs

One of the basic objectives of this program was to establish a Mark III design, resulting from the Materials Studies and tests on the Mark I and II thrusters. The Mark III design was to be compatible with all of the biowaste resistojet propellants, if possible. Results from the materials tests showed that the Mark I thruster was not compatible with CO_2 because of carbonyl reaction with its Pt-Rh center tube and the Mark II thruster was not compatible with CO_2 containing 0.25 to 1.5% oxygen because of oxidation of its Pt-Ir center tube. Results from the materials tests showed that TD-Pt was the best center tube material with Pt, Pt-Pd and low concentration rhodium alloys also having relatively satisfactory oxidation and carbonyl resistant properties. However, all of these materials have lower strength than does either Pt-Ir or Pt-Rh and could not be directly substituted in the Mark I or Mark II designs. Therefore, alternate thruster designs were examined.

Two approaches to the use of lower strength materials were evaluated, the first considered only minor modifications to reduce stresses while the second concerns alternate methods of supporting the center tube.

Mark II stress reduction.- The previous vibration stress analysis of the Mark II biowaste resistojet was made for a maximum power spectral density of 2 g^2/cps. Analytical predictions of the natural frequency of the heater tubes were combined with assumed amplification factors to predict a maximum load factor of 700 g's for a standard division of 3σ. This load factor would cause a stress on the inner heater of 28,000 psi under transverse acceleration and 73,500 psi under axial acceleration. Neither TD-Pt or Pt-Pd have sufficient strength to withstand such stresses. However, it was thought that the assumed amplification factor, which cannot be predicted theoretically, may be quite conservative. Therefore, to obtain more realistic design information for analsis of this critical area, additional instrumentation and tests were added to the ruggedized resistojets which were undergoing dynamic environment tests on NASA Contract NAS 1-9601. The additional tests included sinusoidal sweeps at the beginning and end of the dynamic environment test program to define the natural frequencies and amplification factors for the critical components of the thruster. Detailed instrumentation which was recorded during these sinusoidal sweeps included a micro-miniature accelerometer mounted on the heater tube stem to monitor the heater tube dynamic response characteristics in the axial direction. Analysis of these data verified that the actual amplification factors for the heater tube were substantially less than previously used in the structural analysis. The structural analysis model which used a conservative amplification factor of twenty to twenty-five for the critical heater tube was approximately five times greater than the actual dynamic response characteristics exhibited by these ruggedized resistojet assemblies.

This new design information was incorporated into a preliminary update of the structural analysis of the existing Mark II thruster design to determine its maximum vibration capability when fabricated from lower strength materials such as TD-Pt or

Pt-Pd. Figure 65 presents the results of this analysis for the critical heater element at its natural resonance frequency as compared to the work statement requirements and previous off-limit tests conducted by Marquardt on the Pt-Ir Mark II biowaste resistojet.

A number of Mark II design changes also were identified which could further reduce the stresses in the heater tube. The most promising of these appeared to be design modifications which would lower the weight of the innerbody assembly so significantly that lower inertial loads would be imposed on the critical heater tube element. This could be accomplished by using lower weight materials in the low temperature areas and by reducing the size of noncritical parts. The potential capability of this approach is also shown in Figure 65. This capability is based on preliminary analyses and further design and analysis would be required to finalize these design modifications. However, because of the encouraging progress made in the alternate method of supporting the center tube, no further work was done in attempting to reduce the stresses in the basic Mark II design.

RD-1 resistojet.- Previous tests of Mark II biowaste engines have pointed out various aspects of the design which are quite critical and require high strength materials plus careful fabrication to ensure satisfactory operation. Specifically, a high strength material is required for the center tubes because of large vibration and acceleration loads imposed during the boost phase. Also, a precision bellows assembly is required to keep the center tube in tension to prevent shorting out during both steady state and cycling operation. Despite the care and precautions taken, shorting still occurred sometimes. With the fairly recent realization that as much as 1.0% oxygen might be in the biowaste gases, as evidenced by MDAC life support tests, the problem of the Mark II design became even more critical because of the fairly rapid oxidation characteristics of Pt-Ir alloys. To circumvent some of these difficulties, a modified Mark II design was established and evaluated. Results with this design, designated RD-1, were very encouraging.

Figure 66 is a schematic drawing of this concept which may be compared with the Mark II concept shown in Figure 1. Perhaps the most significant difference between these designs is the replacement of the rigid strut connector in the Mark II with a flexible spiral connector in the RD-1 design. This flexible electrical connector takes up the differential expansion of the concentric tubes and thus eliminates the need for the expansion bellows. To prevent shorting of the center tube against the second tube, aluminum oxide microspheres separate the two. These design changes permitted the use of lower strength materials for the center tube.

In support of this concept, several component tests were conducted. Aluminum oxide microspheres were temperature cycled between approximately 500°K and 1500°K with no indication of cracking or spalling as determined from dye penetrant (fluorescent) inspection. A flexible electrical connector (spiral element) also was fabricated and tested.

Spiral element tests: To permit thermal expansion of the center tube heating element, the rigid attach struts at the forward end of the center tube in the Mark II design were replaced by a flexible electrical connection. This connector is in the form of a narrow flat sheet of metal which is attached to the center tube and wrapped around it (forming a spiral) and attached to the second tube. To prove this concept, a spiral element was welded to a tube and cycled on and off in one of the bell jars. The unit was fabricated from platinum and attached to an existing Pt-Ir tube. The unit was cycled 6000 times at temperatures between 650°K and 1500°K and then an additional 8340 times at temperatures between 560°K and 1600°K. This latter temperature variation is believed to be representative of actual engine operation. The tube expanded and contracted approximately 0.010 inches each cycle. The unit was still functioning after the accumulation of 14,340 cycles which demonstrated the feasibility of this concept.

Component engine: A simplified breadboard engine that permitted testing of a center tube and microspheres was fabricated. A photograph of this unit is shown in Figure 67. The cold gas entered the tube shown behind the unit, passed through the annulus containing the microspheres and then passed through the center tube and exited out the tube to the right. Two optical windows were located on the side of the unit. One window permitted a view of the center tube and the other a view of the microspheres. Thus, when operating at high temperature, the temperatures of the center tube and microspheres could be measured with a pyrometer. The unit was designed so that the microspheres and center tube could be readily removed from the unit for examination.

The component engine was tested with methane to evaluate the carbon deposition characteristics of the microspheres. The unit was operated with methane for 113 hours with a center tube temperature of about 1050°K. Under this condition, the microsphere temperature was about 980°K, or just above the carbon deposition threshold temperature. The unit was then taken apart and examined. The center tube had a carbon deposition buildup of about 0.004 inches on its exterior surface and the microspheres had buildups that were less than 0.00025 inches. Photographs of the center tube and a microsphere after exposure to CH_4 are shown in Figure 68. Also included is a clean microsphere for comparison. As is evident from the photo, the carbon on the tube was not too adherent.

The unit was then reassembled and was subjected to 27 hours exposure to CO_2 (with 1.5% oxygen) with a wall temperature of 1367°K. After this cycle, the unit was again taken apart and examined. All traces of carbon were removed from the microspheres and tube, indicating the short exposure with CO_2 was successful in stripping out the carbon. Measurements taken

during this test indicated that the microspheres operated at a temperature that was from 50 to 100°K lower than the center tube temperature. Because the center tube of this component engine was fabricated from Hastelloy X, its operating temperature was limited. An actual engine with a platinum alloy tube would operate at a faster rate. The pressure drop across the component engine was about 2.65 psi, at a CO_2 flow rate of 0.03 gm/sec. while carbon was on the tube and microspheres. After carbon removal, the pressure drop was 0.92 psi at the same flow rate.

R&D biowaste engine: A used Mark II biowaste engine (S/N 002) was modified to incorporate a spiral element and microspheres. A photograph of this unit, designated RD-1, is shown in Figure 69. Externally, the unit differs little in appearance from the Mark II. This engine was first tested with hydrogen and then with CO_2. The objectives of these tests were:

1. To demonstrate that a low strength material, platinum, could be used for the center tube.
2. To demonstrate that expansion of the center tube could be accommodated by a flexible electrical connector, thus eliminating the requirement for a bellows.
3. To demonstrate that aluminum oxide spacers could be used to prevent contact between the first and second heater tubes.
4. To demonstrate that these modifications would not cause a reduction in performance relative to the Mark II thruster.
5. To pinpoint areas needing further evaluation and development.

The first four objectives were fulfilled during the early tests and the last objective was fulfilled by cycling the unit off and on until failure occurred. This failure verified some of the design concepts considered desirable but were not believed to be cost effective for the initial unit.

Operation and performance was in general about as expected. The following table summarizes the performance for the two engines with hydrogen and CO_2.

Engine	Propellant	Power Level (watts)	I_{sp} (sec)
Mark II	H_2	140	505
RD-1	H_2	140	525
Mark II	CO_2	80	142
RD-1	CO_2	80	135

Performance of the RD-1 thruster was better than the Mark II with hydrogen but was not as good with CO_2.

During testing with hydrogen, performance deteriorated with time. At 140 watts power, the initial specific impulse was 545 seconds, but after several days of operation at various power settings, and including 400 cycles of on-off operation, I_{sp} had deteriorated to 525 seconds. This level was still higher than that of the Mark II. However, at about 80 watts power with hydrogen, performance deteriorated from 385 seconds to about 360 seconds which is below that of the Mark II. The unit was then tested on CO_2 and this deterioration accounts for the lower performance level of the RD-1 thruster on CO_2. As discussed below, this performance deterioration was the result of damage to the spiral element.

The engine, as tested, operated with a higher spiral connector temperature than desired. With hydrogen, this limited the maximum power level to about 150 watts. Also, there was some decrease in overall resistance of the unit from its initial value. This probably is the result of movement of the spiral element. It was believed that the element heating problem could be corrected by a slight alteration in the spiral design, but the resistance change may be more difficult to correct.

Prior to testing with CO_2, the engine was cycled off and on 400 times with hydrogen. During these cycles, the "on" power level was between 135 and 140 watts. To conserve time, the "off" cycle did not permit the engine to cool down completely but the spiral element housing, which could be viewed with an optical pyrometer, cycled from about 1350°K (90% of full temperature) to a temperature below the incandescent level, approximately 900°K.

Following the steady state runs, the engine was cycled on CO_2. The unit failed after a total of 2200 cycles, including the 400 cycles on hydrogen, had been accumulated. After disassembly of the unit, it was evident that the center tube, which was platinum, had failed. Examination of the disassembled unit revealed that the microspheres, designed to prevent the center tube from shorting out, had worked their way into the spiral housing and had jammed the spiral, rendering it nonfunctional. The unit continued to cycle with the restrained center tube trying to expand and contract until failure of the center tube occurred. The unit was operating at night, unattended, when failure occurred. The center tube was both broken in two and partially collapsed, nearly sealing the exit, when discovered the next morning. It was obvious that the restricted exit had allowed temperatures in the unit to reach nearly the melting point of platinum before the internal circuit was open enough to prevent flow of current. Essentially all of the microspheres were in excellent condition upon removal. Several in the immediate vicinity of the spiral had become distorted due to the excessively high temperature and loading prior to engine failure. The spiral was in relatively good shape, considering the abuse it took.

This first test of the modified Mark II engine was considered highly successful and very encouraging. The tests identified several areas where improvements could and should be made.

RD-2 resistojet.- The RD-1 thruster was redesigned and designated RD-2. The redesign was intended to: (1) prevent migration of the microspheres into the spiral housing area, (2) reduce the spiral element operating temperature and (3) minimize the thermal expansion requirements of the spiral element. In support of this design, several subelement tests were conducted.

Migration of the microspheres could easily be prevented by a simple ring located at the entrance to the spiral element housing. To reduce the spiral element operating temperature, the spiral element cross-sectional area was increased to 0.004 $in.^2$. A unit was tested in a bell jar, but bending of the center tube occurred after about 1275 cycles. This result indicated that the spiral was too stiff and a second unit was fabricated having a cross section of 0.0028 $in.^2$. This unit also was tested and appeared to operate satisfactorily although there was a 9.6% reduction in resistance during the test. After 12,500 cycles, the test was stopped and the unit was removed from the bell jar. Upon close examination, it was discovered that the inner weld, where the spiral was welded to the inner tube, had failed. It is not known just when failure occurred, but it is believed that failure could be prevented by employing a double weld at that point.

In order to reduce the thermal expansion requirements of the spiral element, it was planned to change the material of the second tube from platinum to Haynes alloy HS 188. This material has a higher coefficient of thermal expansion than the platinum alloys and is advertised as having good oxidation properties in air at temperatures up to 2000°F. To check out the compatibility of this material in the resistojet system, a tube was made and tested in the bell jar facility. As with the other tubes tested in the bell jars, fine Pt wires were spot welded to the tube to serve as sight indicator points for taking optical pyrometer temperature readings. The tube was operated at about 1480°K (2210°F). After 89.8 hours, the tube failed by developing several leaks.

Figures 70 and 71 are photographs of the tube after the test. The results indicate that at least at temperatures around 2200°F there was a reaction between the Pt wires and No. 188 tube material. Platinum appears to be depleted from the wires at the point of contact as is evident from the lower photograph of Figure 71. The major leak is shown in the upper photo of Figure 71. The tube was cross-sectioned and Figure 73 shows two sections of the tube. The top view as at a temperature of about 1400°K (2520°R). There is little evidence of corrosion at the 1400°K temperature, but significant corrosion both inside and outside occurred at 1480°K. The outside of the tube was exposed to vacuum at about 1 micron. The inside was CO_2 plus 1.5% oxygen at 32 psia. These results indicate HS 188 can operate up to about 2000°F, but not above this temperature.

This 2000°F temperature is too marginal for the second tube in the biowaste thruster and since no satisfactory substitute material was found having the desired large coefficient of thermal expansion, the decision was made to redesign the spiral element. The redesign allowed the use of platinum or platinum alloys for the second tube and made the expansion characteristics of the overall system more compatible with platinum alloy expansion characteristics.

RD-3 resistojet - The RD-3 thruster retains the desirable features of the RD-1 engine, but is designed to overcome some of the deficiencies identified during testing of the RD-1 and its components. As with the RD-1, the RD-3 thruster is designed to be compatible with low strength materials such as TD-Pt, uses aluminum oxide to prevent contact between the center tube and second tube, and employs a flexible coil to conduct power from the second tube to the center tube thus eliminating the requirement for an expansion bellows.

Design and fabrication of the RD-3 thruster were completed and limited checkout tests were conducted. However, the data were not obtained in time to be included in this report. It is planned to further test the unit on the follow-on program which will be a DVT (Design Verification Test) type program. This DVT program should result in a demonstration that the RD-3 concept using TD-Pt will meet all of the currently projected requirements for a biowaste resistojet thruster.

CONCLUSIONS AND RECOMMENDATIONS

1. Results from this program have shown that the concentric tube resistojet using noble metals for the center tube heating elements can be an efficient thruster using biowaste propellants from life support systems of manned space station concepts.

2. The currently projected biowaste gases from the expected life support systems for a manned space station/base concept include CO_2, CH_4, H_2O, N_2 and up to 1.0% O_2. To achieve efficient operation and high specific impulse, metal temperature in the thruster must operate for long duration at temperatures approaching 1700°K (3060°R). Noble metals, primarily platinum, are required in order to operate at this temperature with these corrosive propellants. Carbon deposition characteristics, when operating with CH_4, will limit temperatures to about 1700°R.

3. Based upon the high temperature materials tests, thoriated platinum (containing 0.6% ThO_2) appears to offer the best promise of meeting the requirements with all of the biowaste gases. The presence of the finely divided thoria is very effective in improving the high temperature strength properties by inhibiting excessive grain growth at elevated temperature and is effective in suppressing oxidation and evaporation at high temperature. Platinum-rhodium with a rhodium content of 20% suffered from carbonyl attack when CO_2 was tested although a 5% rhodium content appeared satisfactory. Platinum-iridium alloys suffered from excessive oxidation with CO_2 containing 1.0% oxygen. Platinum-palladium operating temperatures were limited by excessive metal evaporation and pure platinum suffered from oxidation attack at the higher temperatures.

4. The Mark I thruster proved the feasibility of and demonstrated high performance of the early biowaste resistojet. However, this thruster was not suited for pure CO_2 propellant because its center tube was fabricated from platinum-rhodium. The Mark II incorporated some improved features. A comparison of thrusting performance of the Mark II thruster against the Mark I thruster indicates that no performance penalty occurred from the redesign features incorporated into the Mark II thruster. Changes were made in the Mark II structure to achieve greater mechanical strength necessary to withstand the shock and vibration loads of handling and launching of a biowaste resistojet into space. Other changes were incorporated to improve thermal performance of the thruster and, as a result, the Mark II thruster was slightly more efficient.

5. A Mark II thruster successfully passed a severe vibration environment test to 1.0 g^2/Hz with a total overall G rms value of 35.7. Pre and post-vibration test calibration served as a simulated acceptance test prior to launch. Hot firing anneals the heater elements making them structurally weaker than the "as received" from fabrication condition. The S/N 003 thruster was operated to a specific impulse of 572 and then 580 seconds on hydrogen, respectively, during the pre- and post-vibration test calibration.

6. Thruster performance tests have been completed with the Mark II thruster on H_2, CH_4, H_2O, CO_2, CO_2/H_2O, H_2O/CH_4 and CO_2/CH_4 representing typical biowaste propellants and mixtures. High efficiency (66%) performance at 575 and 235 seconds specific impulse on H_2 and H_2O, respectively, has been demonstrated. Performance with CO_2 and CH_4 is lower than predicted indicating heat transfer limited conditions. A nozzle throat size reduction for an actual thrust of 10 mlb coupled with a heat transfer surface area increase of 20% is recommended. In addition, nozzle performance can be improved with an optimized nozzle expansion ratio. With these minor changes, the following performance should be possible with the concentric-tubes resistojet concept:

Propellant	Chamber Gas Temperature, ^{o}K (^{o}R)	Specific Impulse, Seconds	Overall Total Power Efficiency
H_2	1555 (2800)	590	0.71
H_2O	1555 (2800)	240	0.72
CO_2	1555 (2800)	170	0.62
CH_4	890 (1600)	205	0.67
$CO_2/CH_4 = 0.5$	970 (1750)	185	0.66
$H_2O/CH_4 = 0.5$	1030 (1850)	225	0.69

7. The water evaporator prototype was tested successfully. "Zero-g" environmental potential was demonstrated as well as high thermal efficiency. The prototype evaporator was found to be conservatively sized by about a factor of two for the 10 mlb biowaste resistojet. For predicted performance calculations, a 3 watt thermal loss is considered realistic for the water evaporator.

8. The Mark II biowaste resistojets can operate for short periods of time to 628 seconds impulse on hydrogen propellant. A further increase in power will result in failure in tension. Improvements in the ceramic spacer design would have to be incorporated to prevent binding between the outer and adjacent concentric tubes during prolonged cycling operation.

9. The RD-1 thruster design demonstrated that the concentric tube resistojet could be redesigned to permit the use of lower strength materials such as platinum or TD-Pt and that an efficient design could result. The RD-1 design also demonstrated that ceramic spacers could be used to effectively prevent contact and resulting shorting between the center and second tubes in the biowaste resistojet.

10. Experience from the RD-1 thruster plus the RD-3 design studies and limited test results indicate that the RD-3 thruster with its TD-Pt heater elements will meet the desired objectives of a biowaste resistojet.

11. It is recommended that the RD-3 thruster be further evaluated and subjected to a DVT (Design Verification Test) type program to demonstrate that the thruster concept is capable of meeting the requirements for a flight type unit operating reliably on all currently projected biowaste propellants.

REFERENCES

1. Phillips, D. G.: Technology Development of a Biowaste Resistojet - Volume I

2. Bliss, J. R., and Greco, R. V.: Design and Operational Characteristics of an Integrated Biowaste Resistojet System. AIAA Paper 71-686, AIAA 7th Propulsion Specialist Conference, Salt Lake City, Utah, June 1971.

3. Piscotta, A: Report of the Development of the Manned Orbital Research Laboratory (MORL) System Utilization Potential; Task Area IV MORL System Improvement Study, Douglas Aircraft Co., (MSSD) Report SM-48819B, January 1966.

4. Page, R. J., and Short, R. A.: Definition of a Resistojet Control System for the Manned Orbital Research Laboratory, Final Report, Volume V, Resistojet Design and Development. NASA CR-66604, May 1968.

5. Yoshida, R. Y, et al: Resistojet Thruster Life Testa and High Vacuum Performance. NASA CR-66970, July 1970.

EVACUATED CONCENTRIC TUBES RESISTOJET CONCEPT

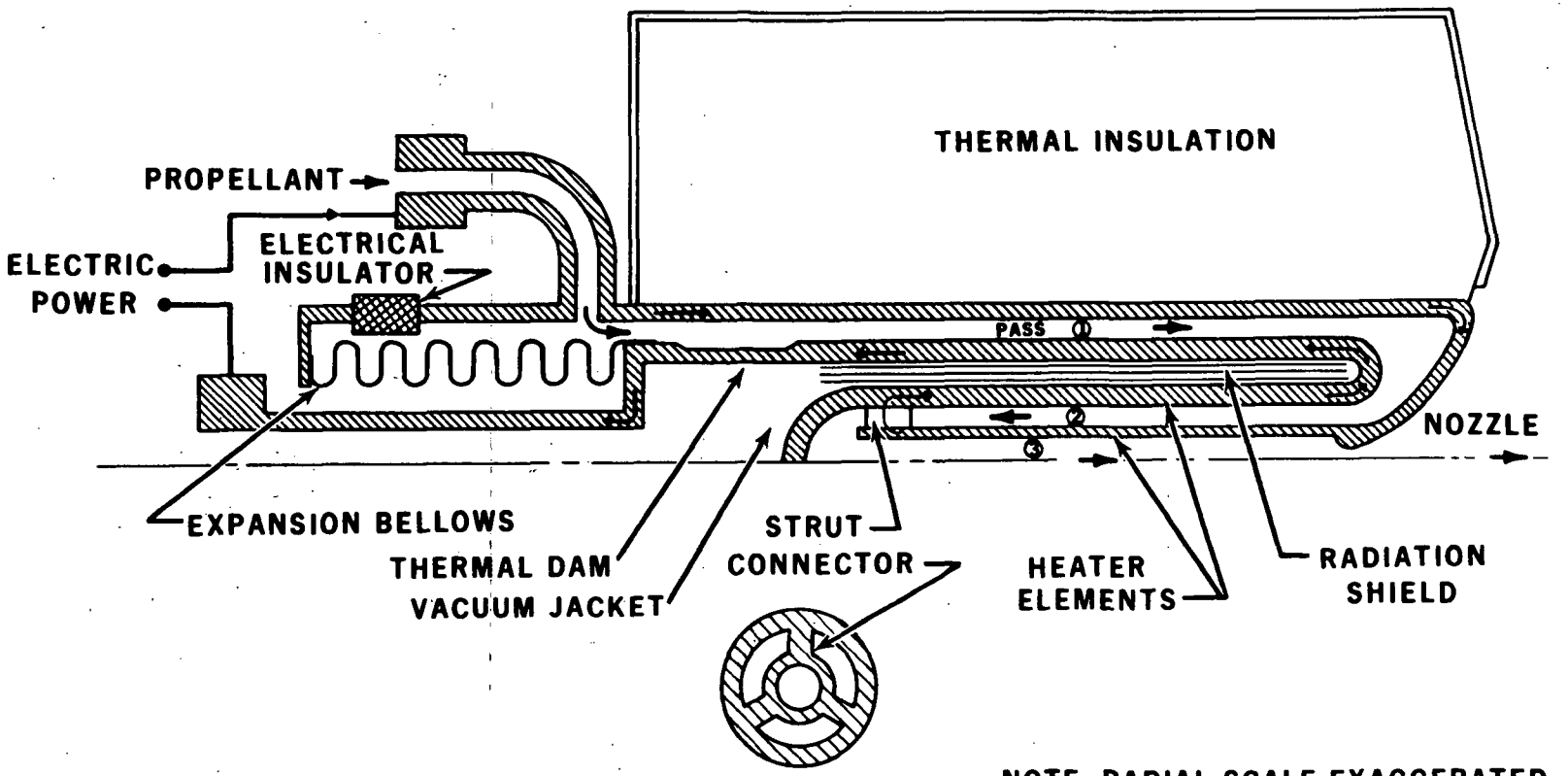

Figure 1

V8294-1

EXPECTED PERFORMANCE OF 10 MLB RESISTOJET

CHAMBER PRESSURE = 2 ATM

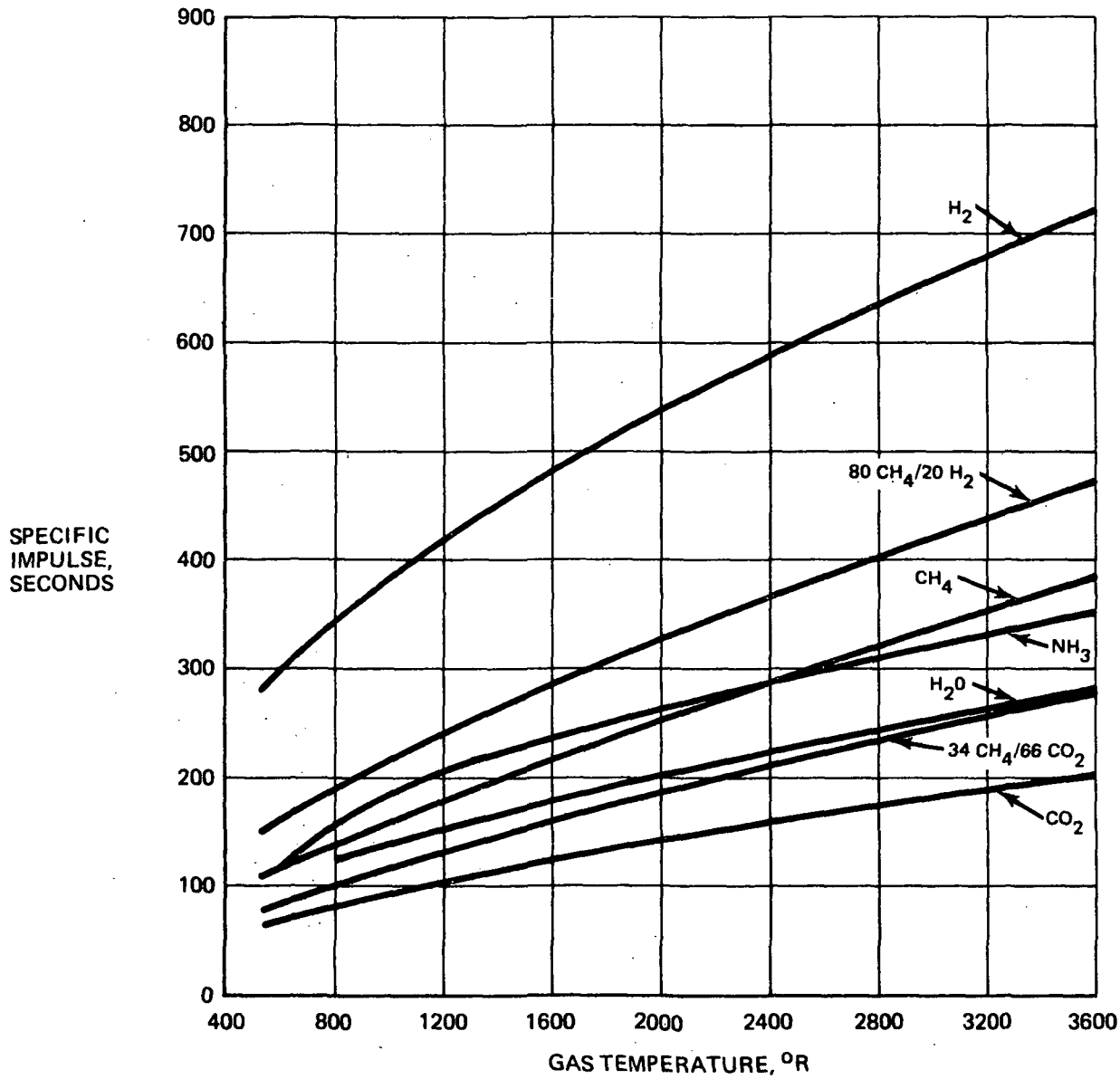

Figure 2

EXPECTED PERFORMANCE OF 100 MLB RESISTOJET

CHAMBER PRESSURE = 2 ATM

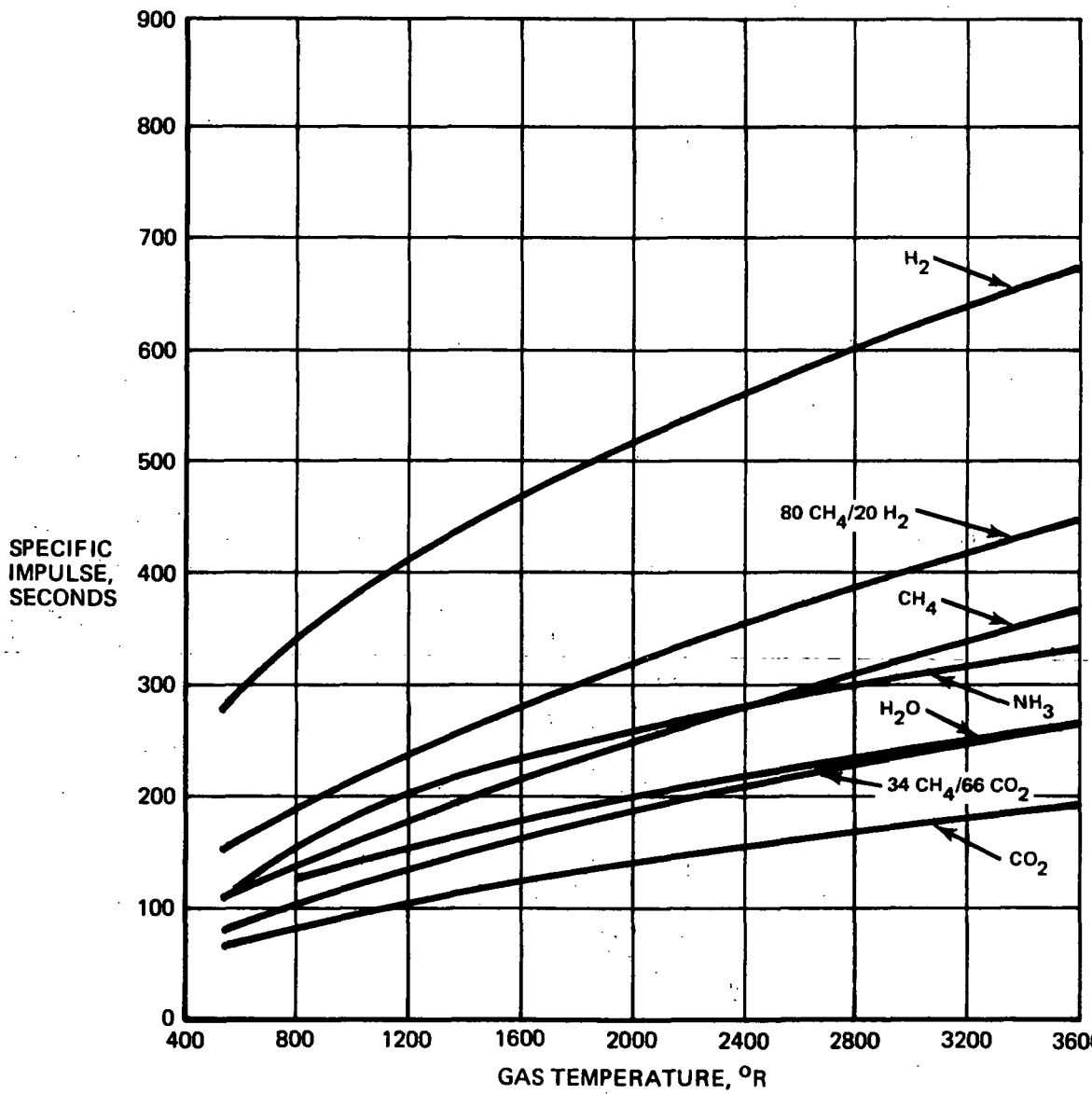

Figure 3

ELECTRIC POWER REQUIREMENTS OF 10 MLB RESISTOJET

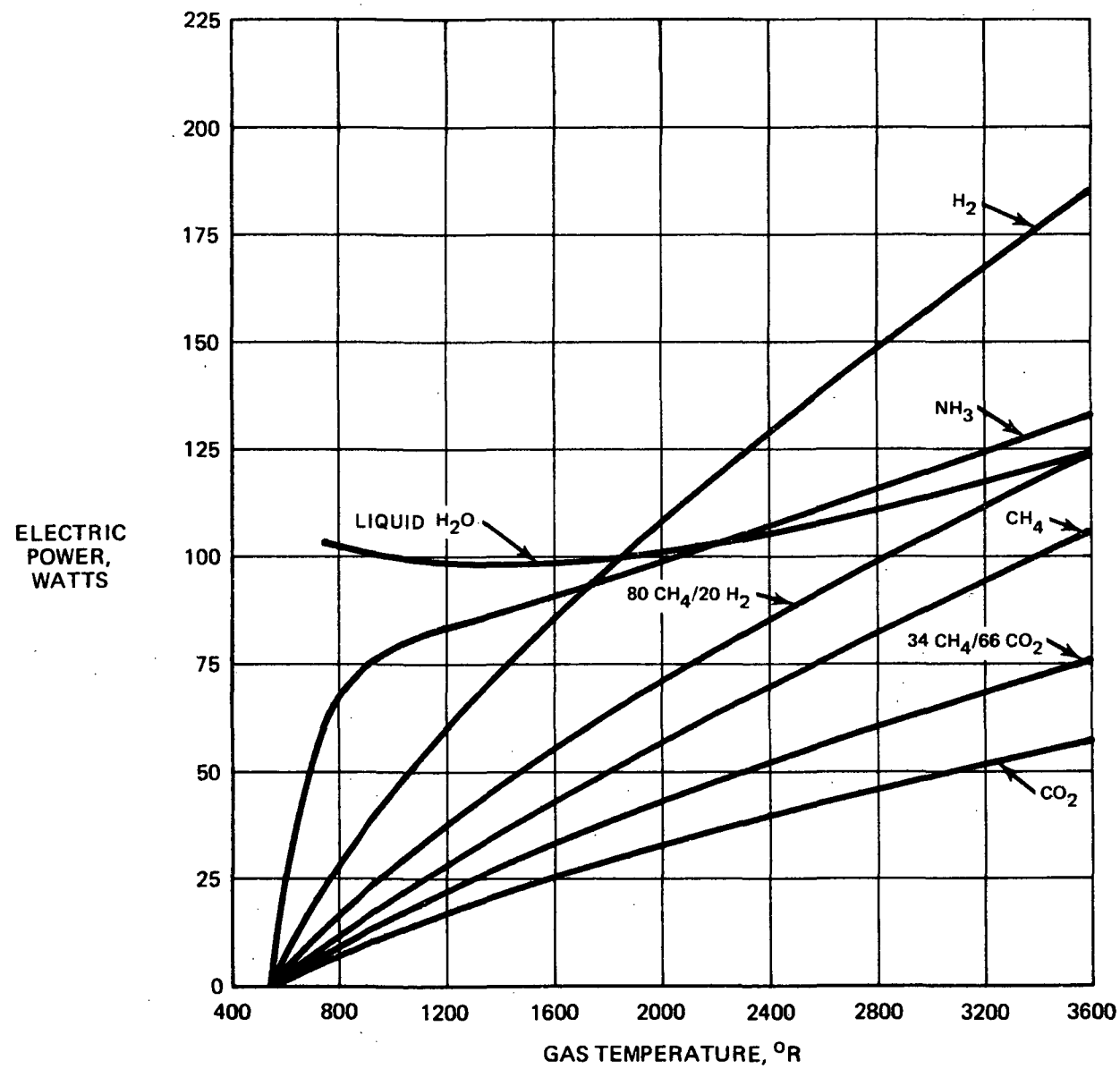

Figure 4

ELECTRIC POWER REQUIREMENTS OF 100 MLB RESISTOJET

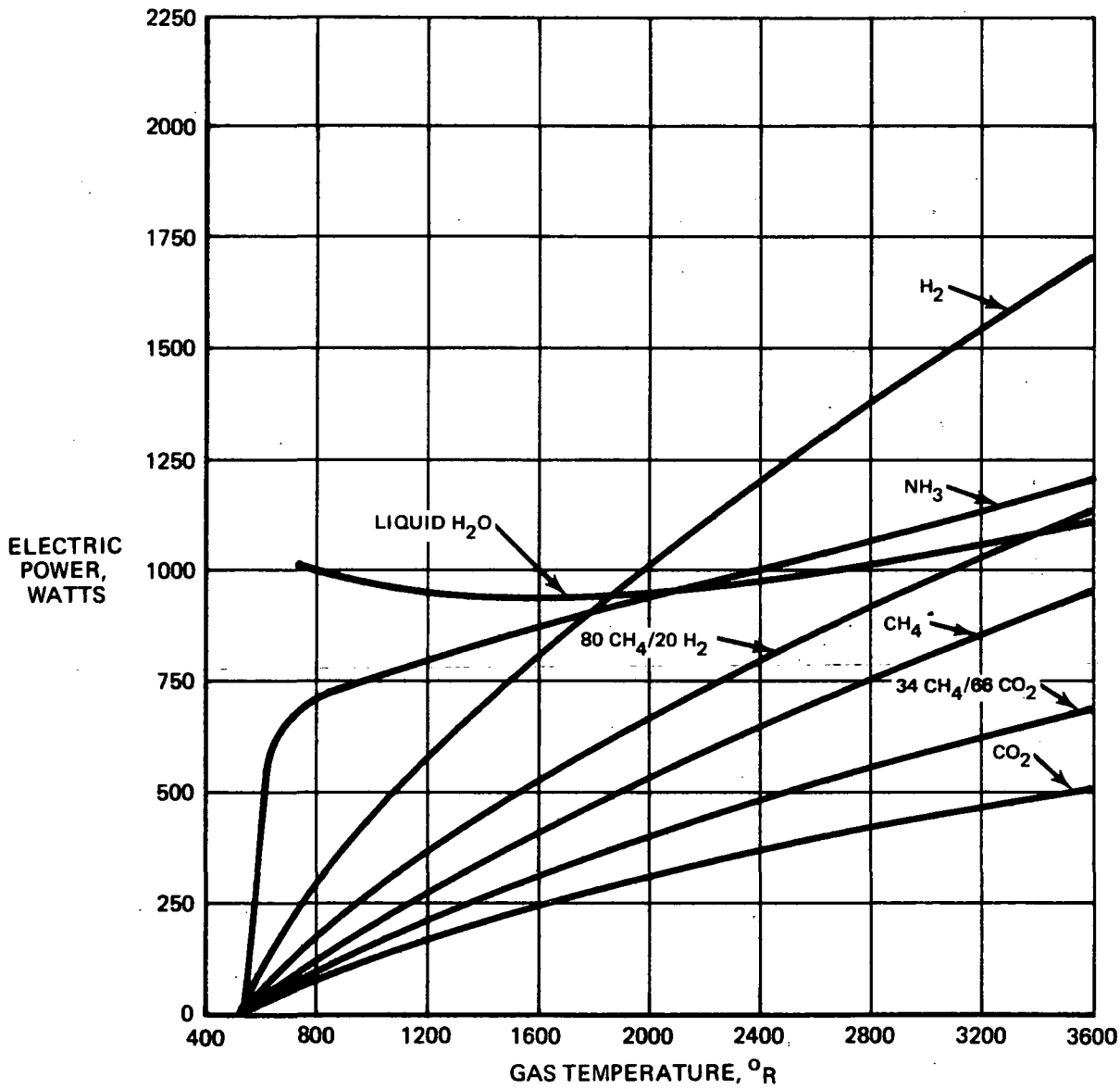

Figure 5

IDEAL FROZEN FLOW SPECIFIC IMPULSE CORRELATION

CHAMBER TEMPERATURE = 3000°R (1667°K)
CHAMBER PRESSURE = 1 TO 2 ATM.

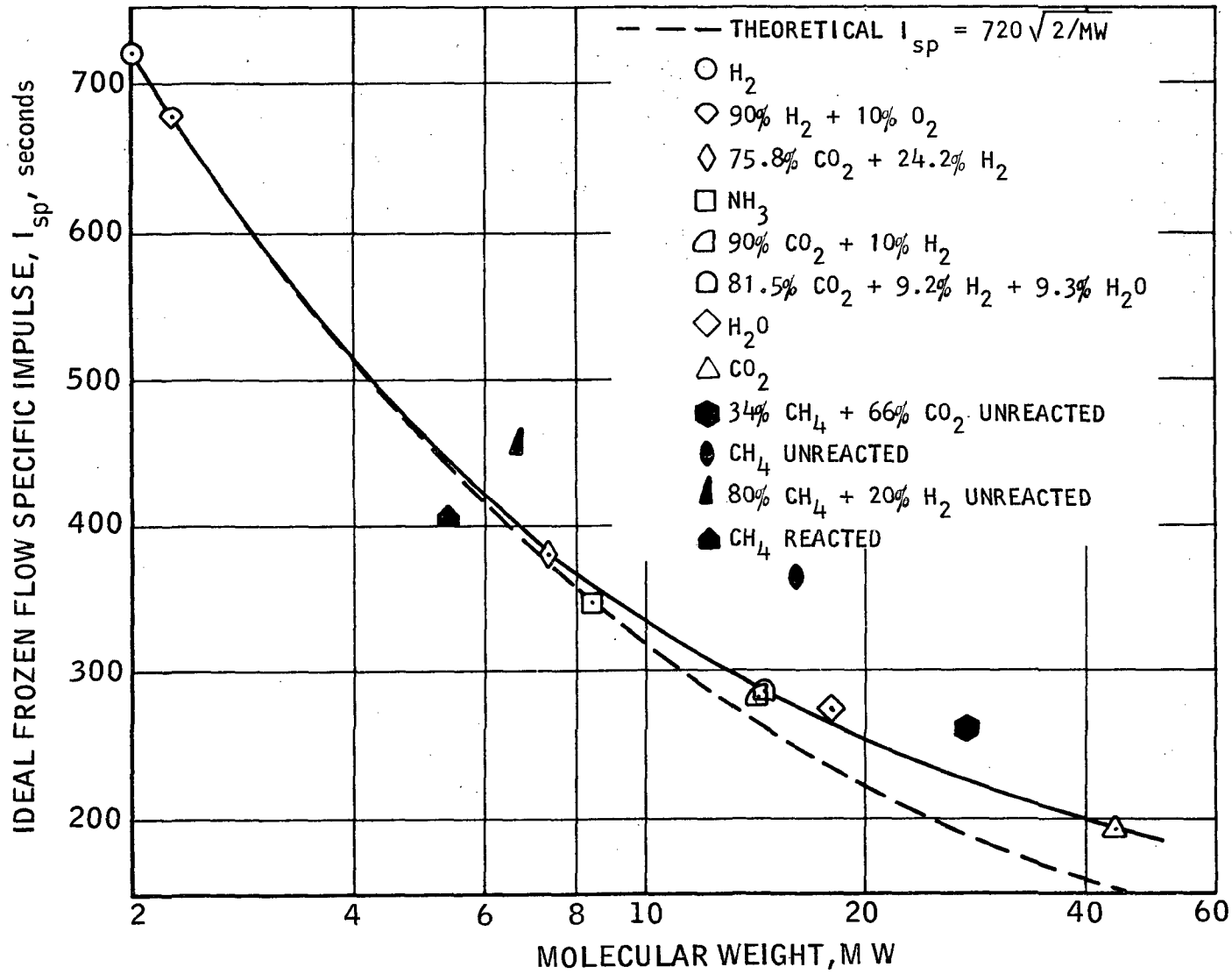

Figure 6

V7902-7

BIOWASTE RESISTOJET TEST EQUIPMENT

NEG. 9482-3

V7416-3

Figure 7

BIOWASTE RESISTOJET TEST SCHEMATIC

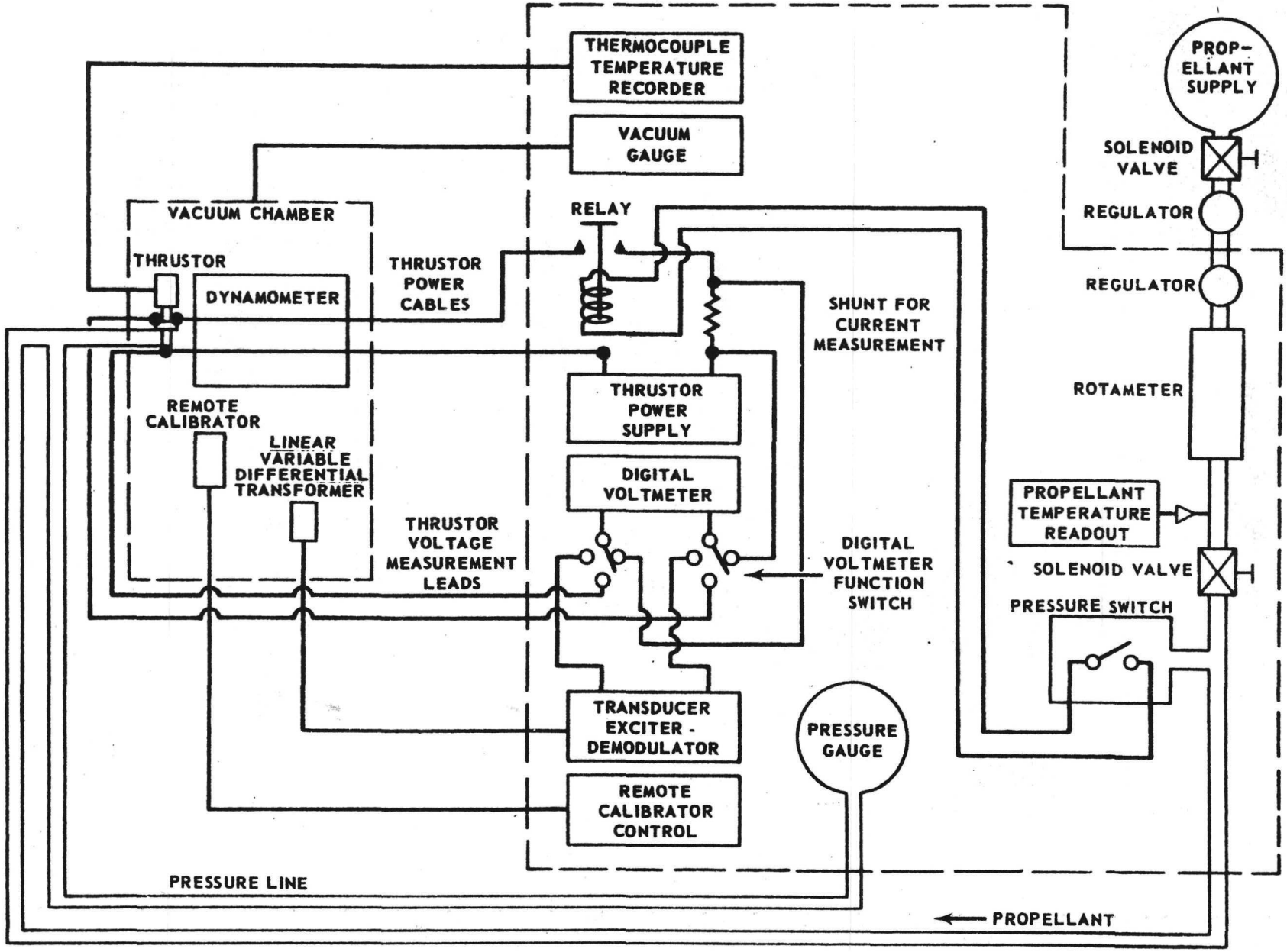

Figure 8

MARK II BIOWASTE RESISTOJET ON THRUST DYNAMOMETER STAND

NEG 9883-17

V8294-5

Figure 9

BIOWASTE RESISTOJET TEST

MARK I ENGINE NO. 7
2-26-69
DATA POINTS

CARBON DIOXIDE
SUPPLY PRESSURE 3 ATM
7020-7027

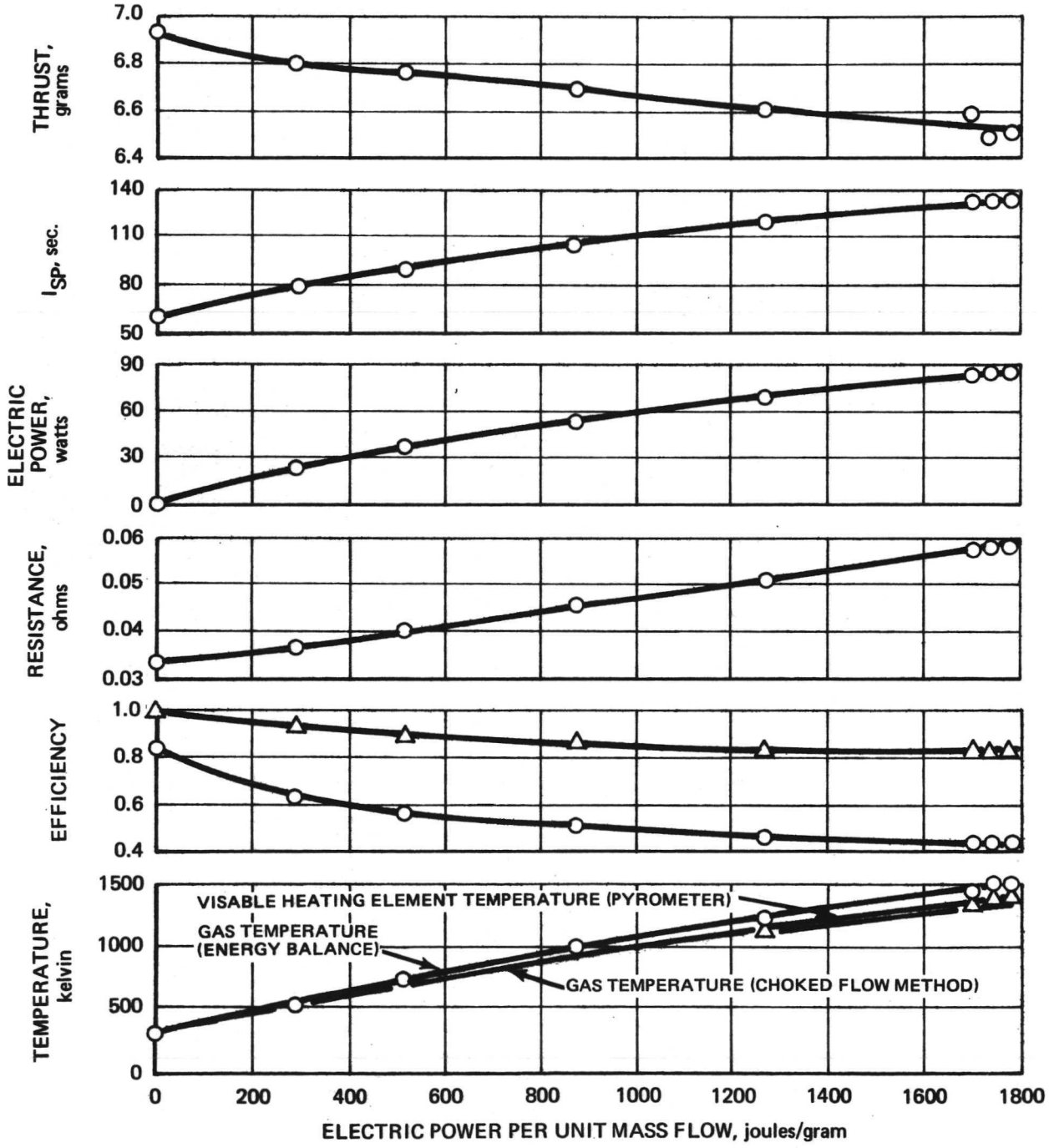

Figure 10

BIOWASTE RESISTOJET TEST

MARK I ENGINE NO. 8 WATER
5-15-69 SUPPLY PRESSURE 3 ATM
DATA POINTS - 8001 - 8005

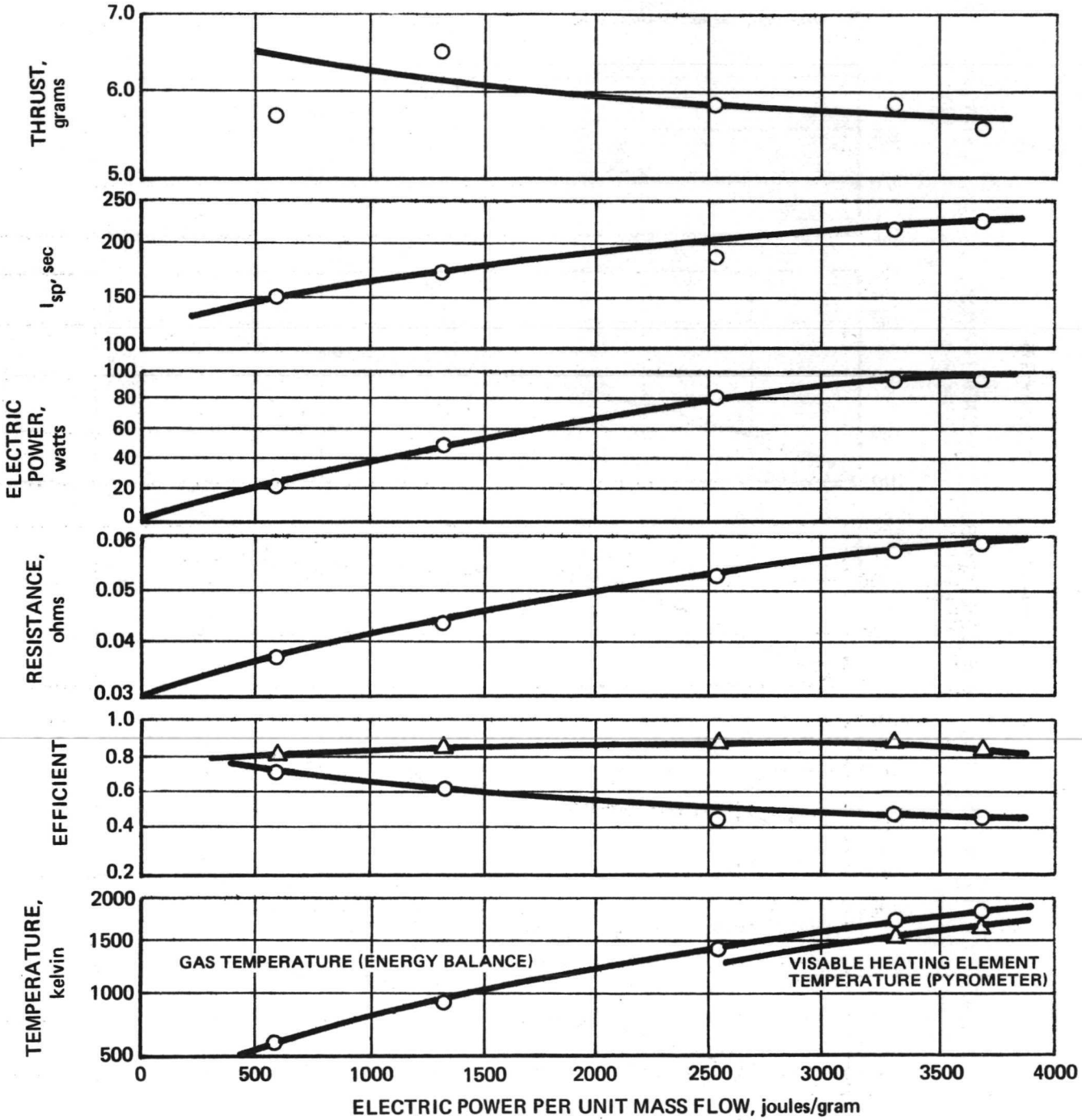

Figure 11

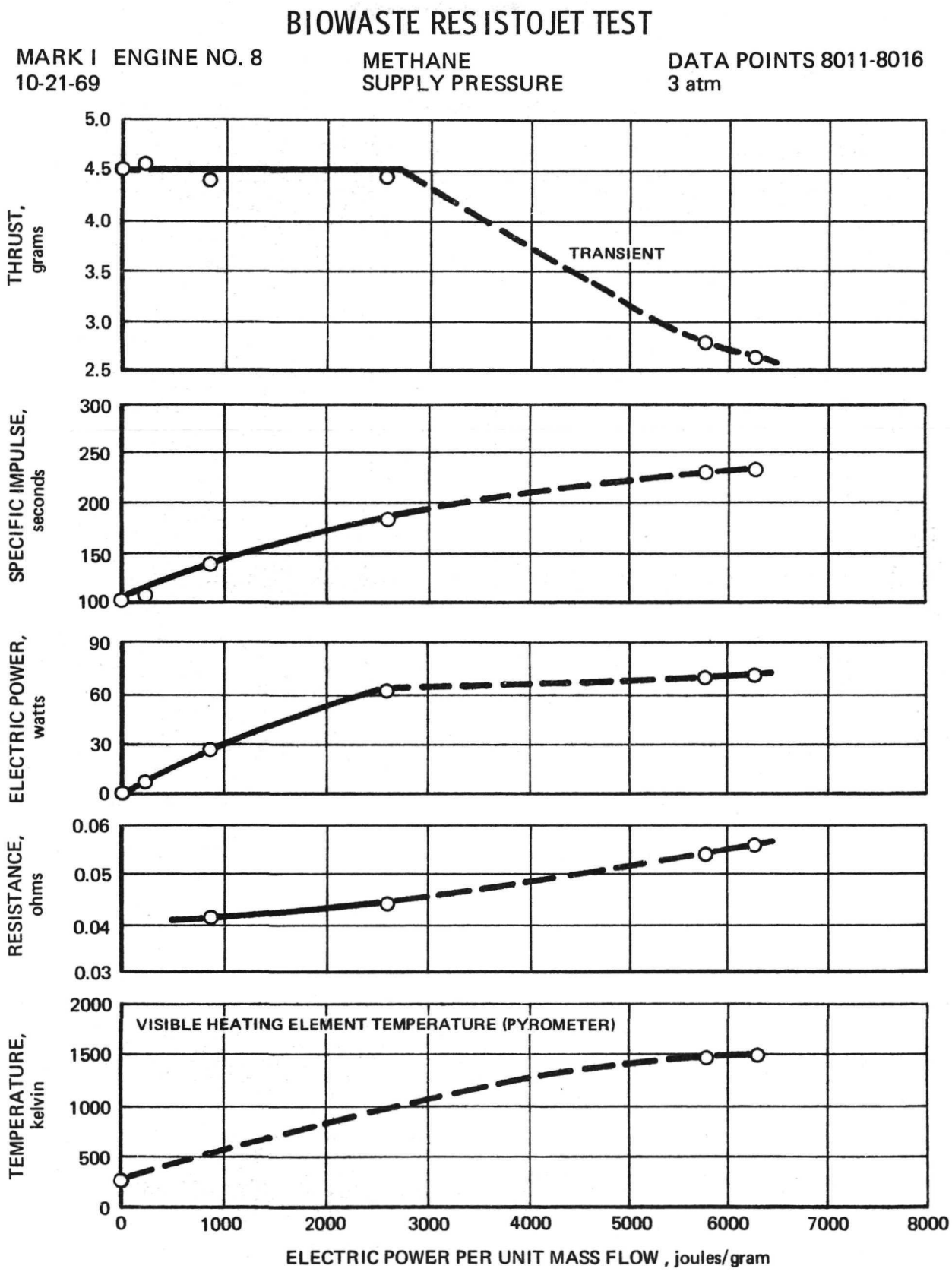
BIOWASTE RESISTOJET TEST
MARK I ENGINE NO. 8
10-21-69
METHANE
SUPPLY PRESSURE
DATA POINTS 8011-8016
3 atm
THRUST, grams
5.0
4.5
4.0
3.5
3.0
2.5
TRANSIENT
SPECIFIC IMPULSE, seconds
300
250
200
150
100
ELECTRIC POWER, watts
90
60
30
0
RESISTANCE, ohms
0.06
0.05
0.04
0.03
TEMPERATURE, kelvin
2000
1500
1000
500
0
VISIBLE HEATING ELEMENT TEMPERATURE (PYROMETER)
0
1000
2000
3000
4000
5000
6000
7000
8000
ELECTRIC POWER PER UNIT MASS FLOW , joules/gram

Figure 12

BIOWASTE RESISTOJET TEST - METHANE PROPELLANT

MARK I ENGINE NO. 8
11/18/69

DATA POINTS 8024 - 8034
SUPPLY PRESSURE = 3 atm.

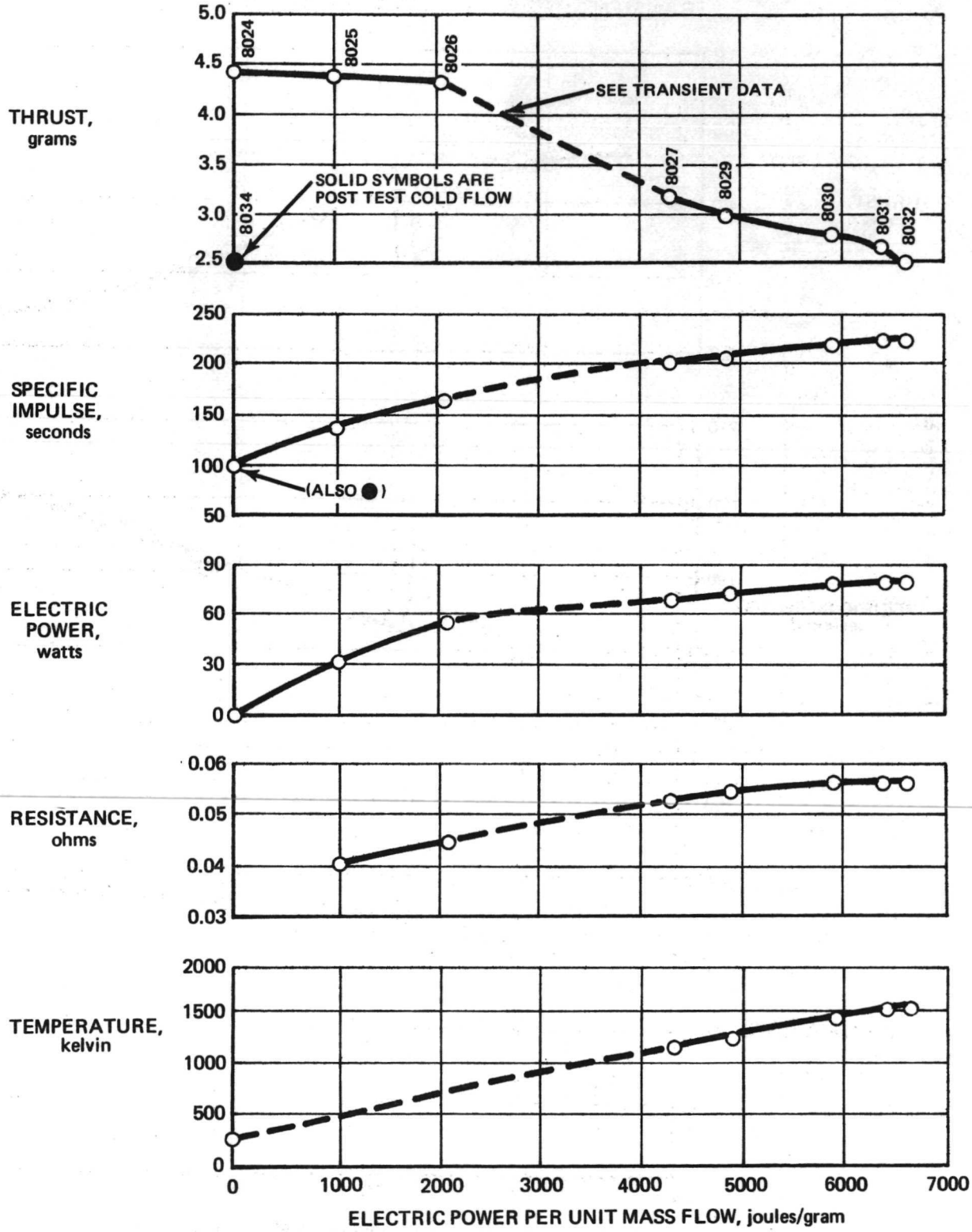

Figure 13

BIOWASTE RESISTOJET TEST - TRANSIENT DATA

MARK I ENGINE NO. 8
METHANE PROPELLANT
TRANSIENT BETWEEN DATA POINTS 8026 AND 8027
11/18/69

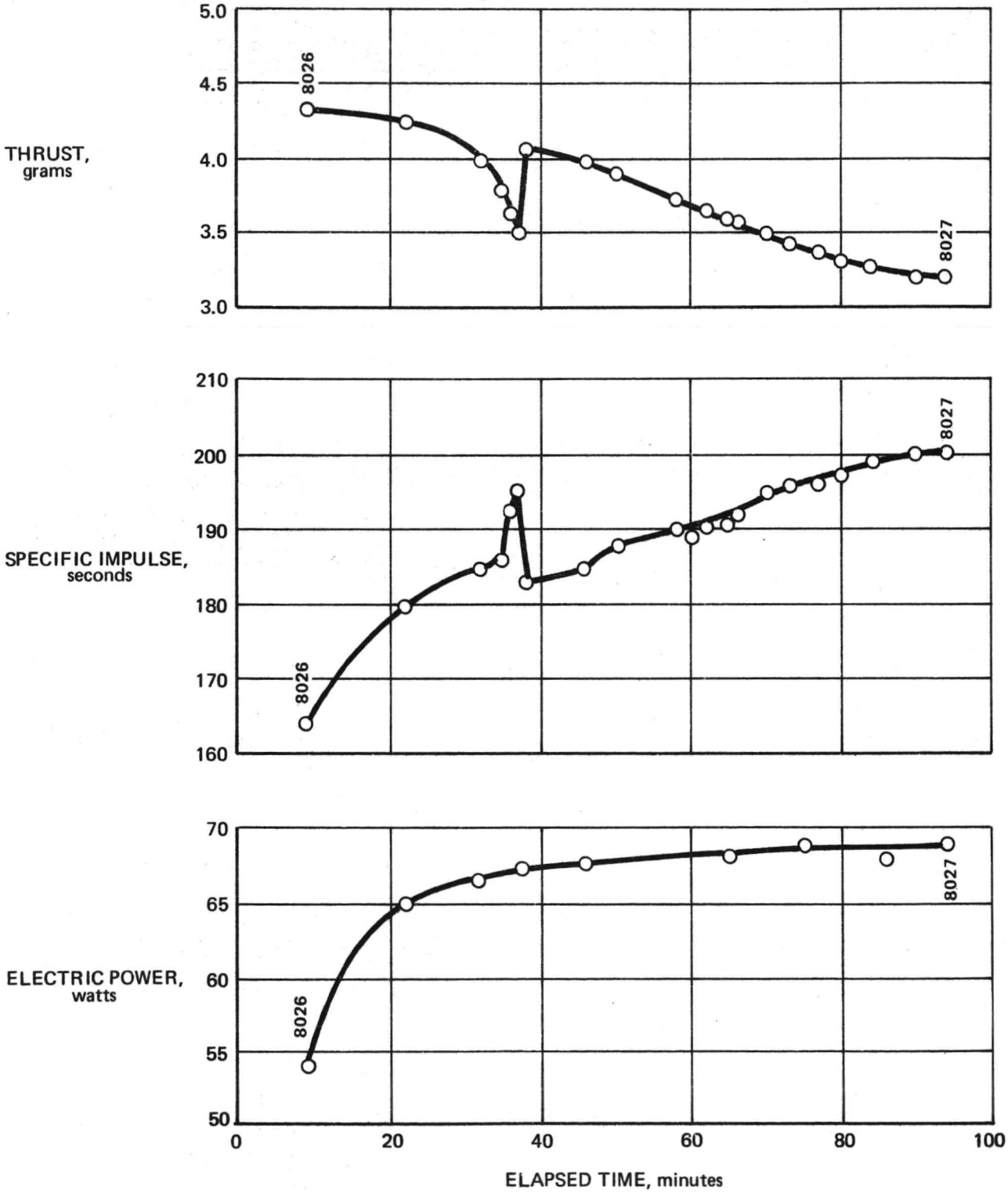

Figure 14

CORRELATION OF EXPERIMENTAL SPECIFIC IMPULSE WITH PROPELLANT MOLECULAR WEIGHT

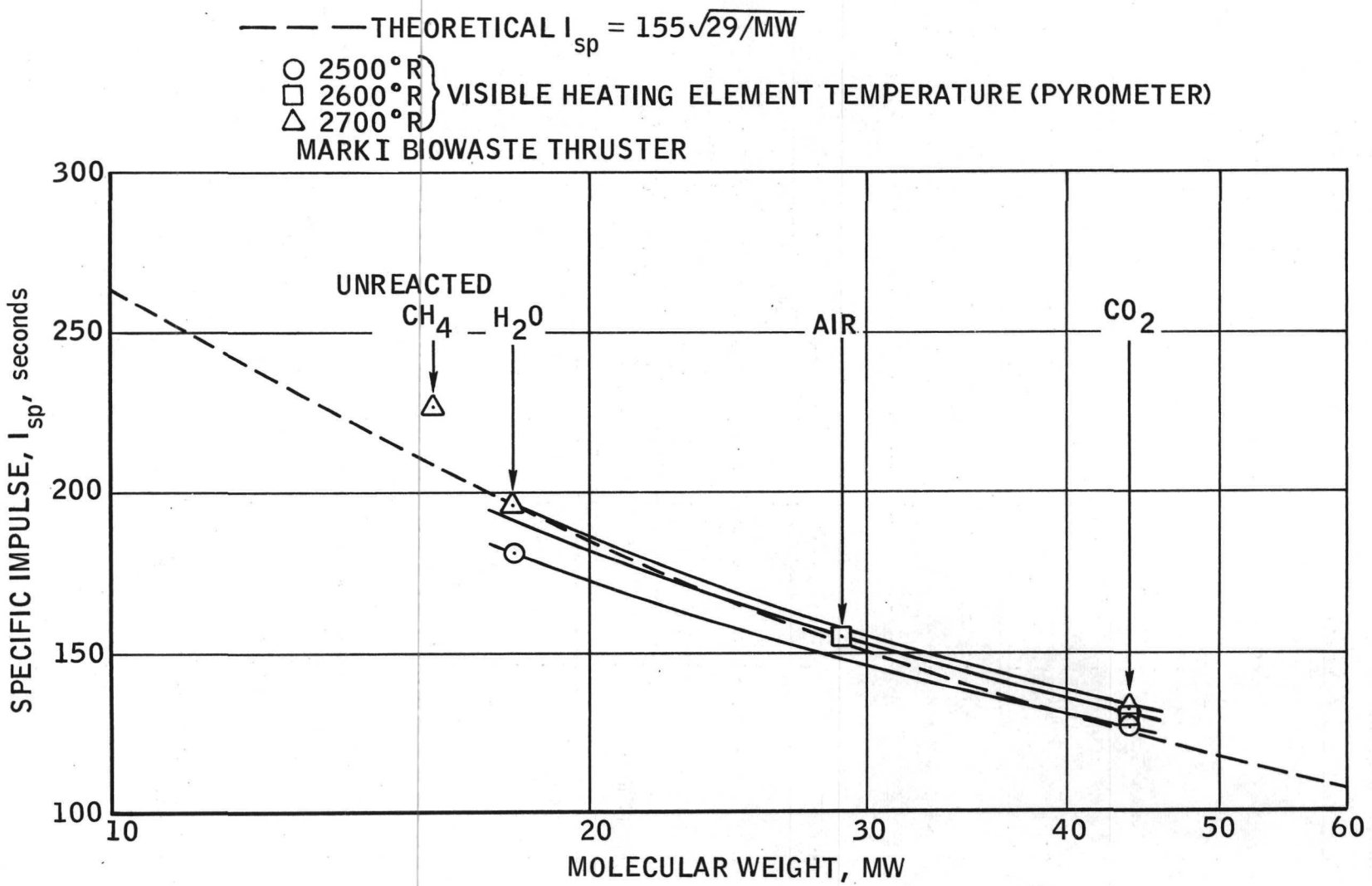

Figure 15

V7902-6

BIOWASTE RESISTOJET WATER EVAPORATOR

Figure 16

NEG. 9805-1

V7984-3

BIOWASTE RESISTOJET WATER EVAPORATOR

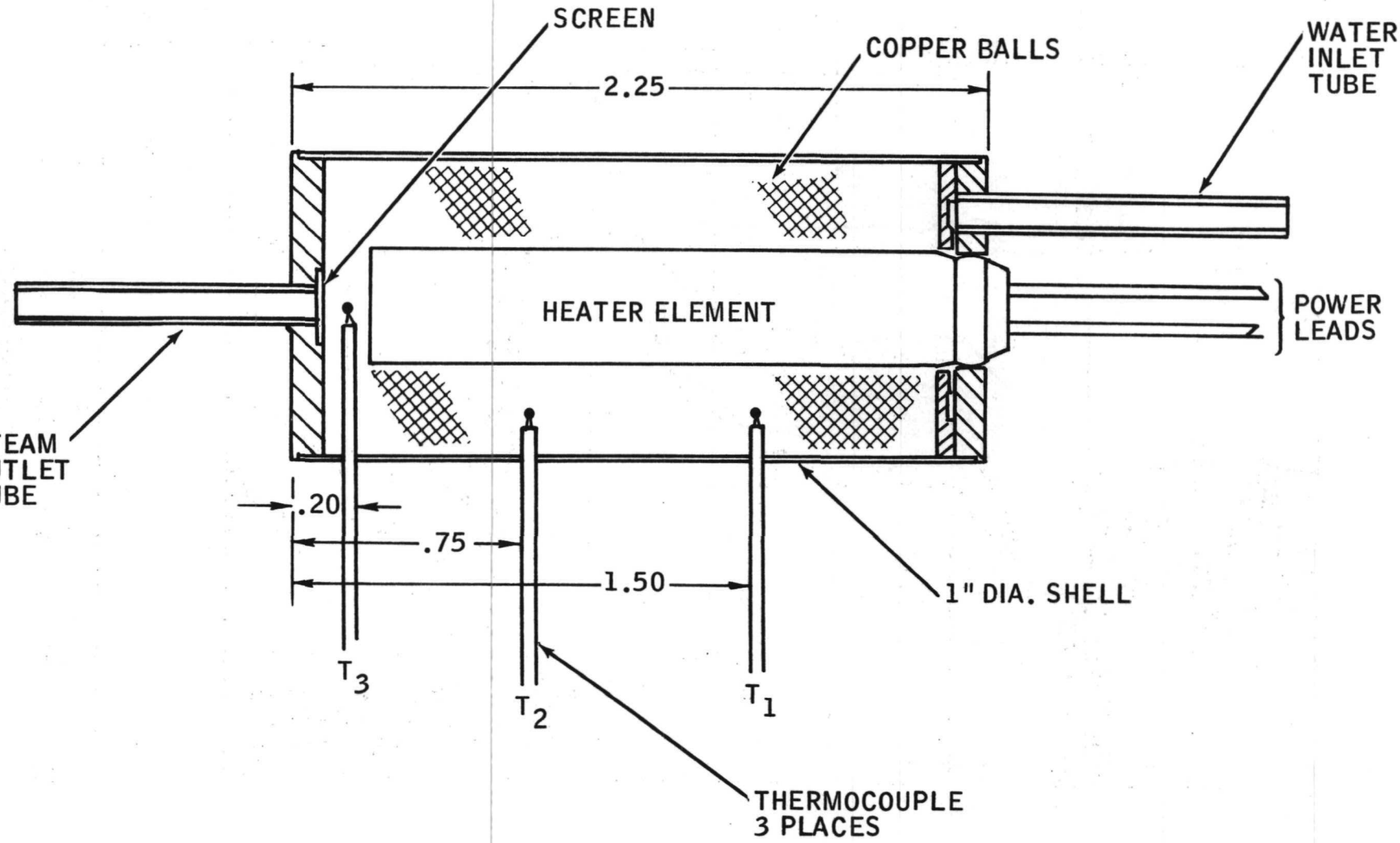

Figure 17

V8035-3

WATER EVAPORATOR TEST TEMPERATURE HISTORY

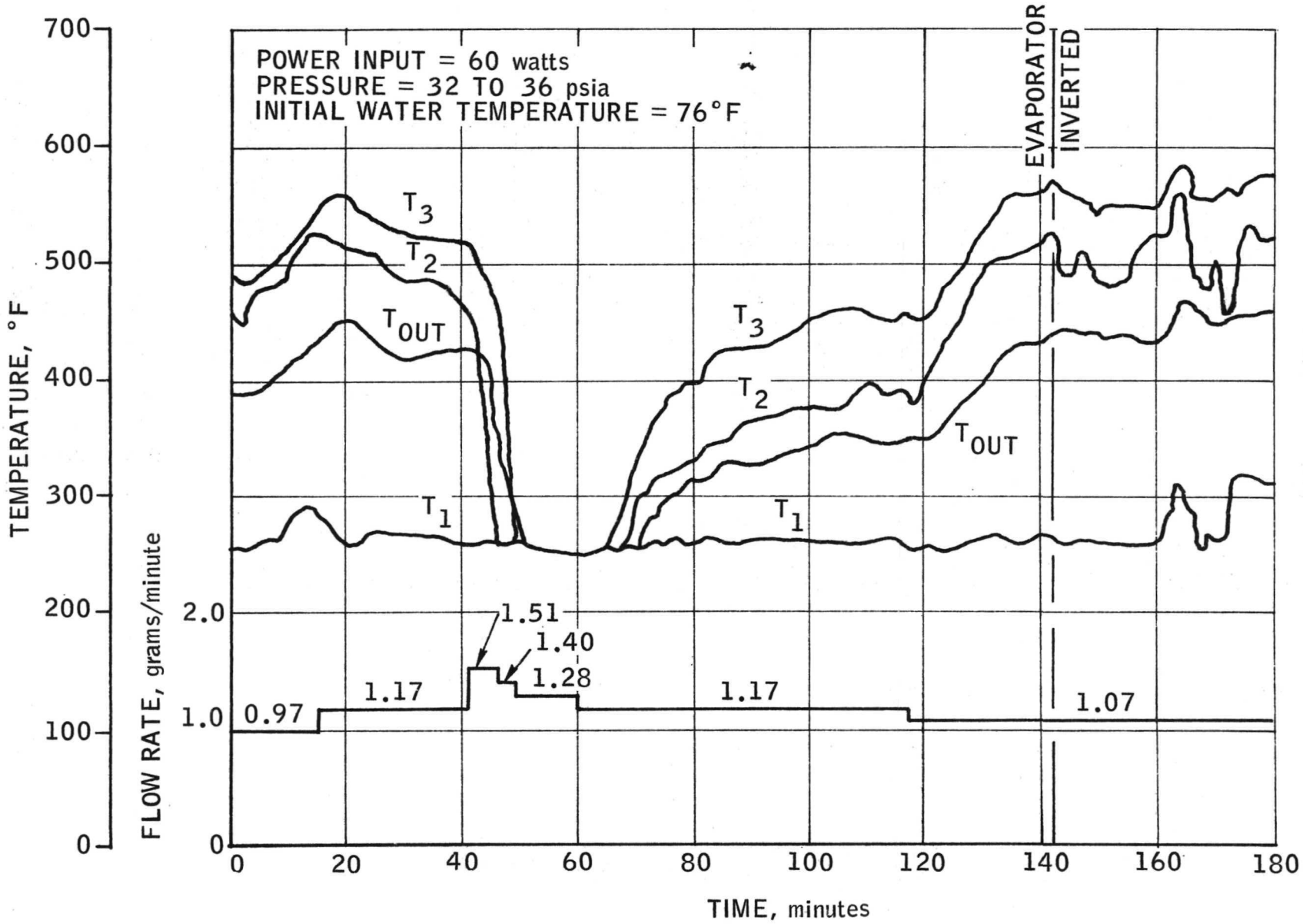

Figure 18

WATER EVAPORATOR THERMAL START-UP TRANSIENT

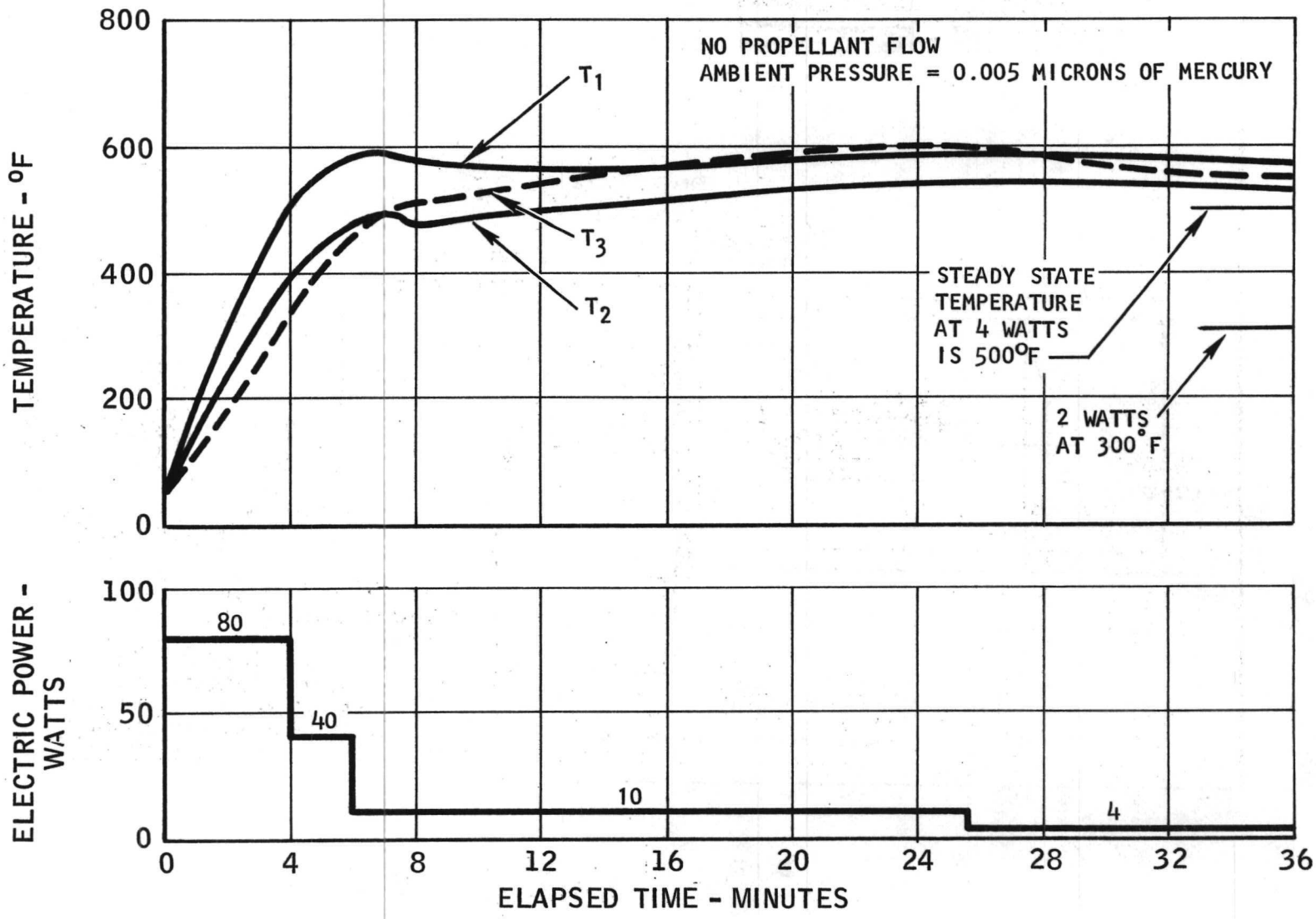

Figure 19

V8418-1

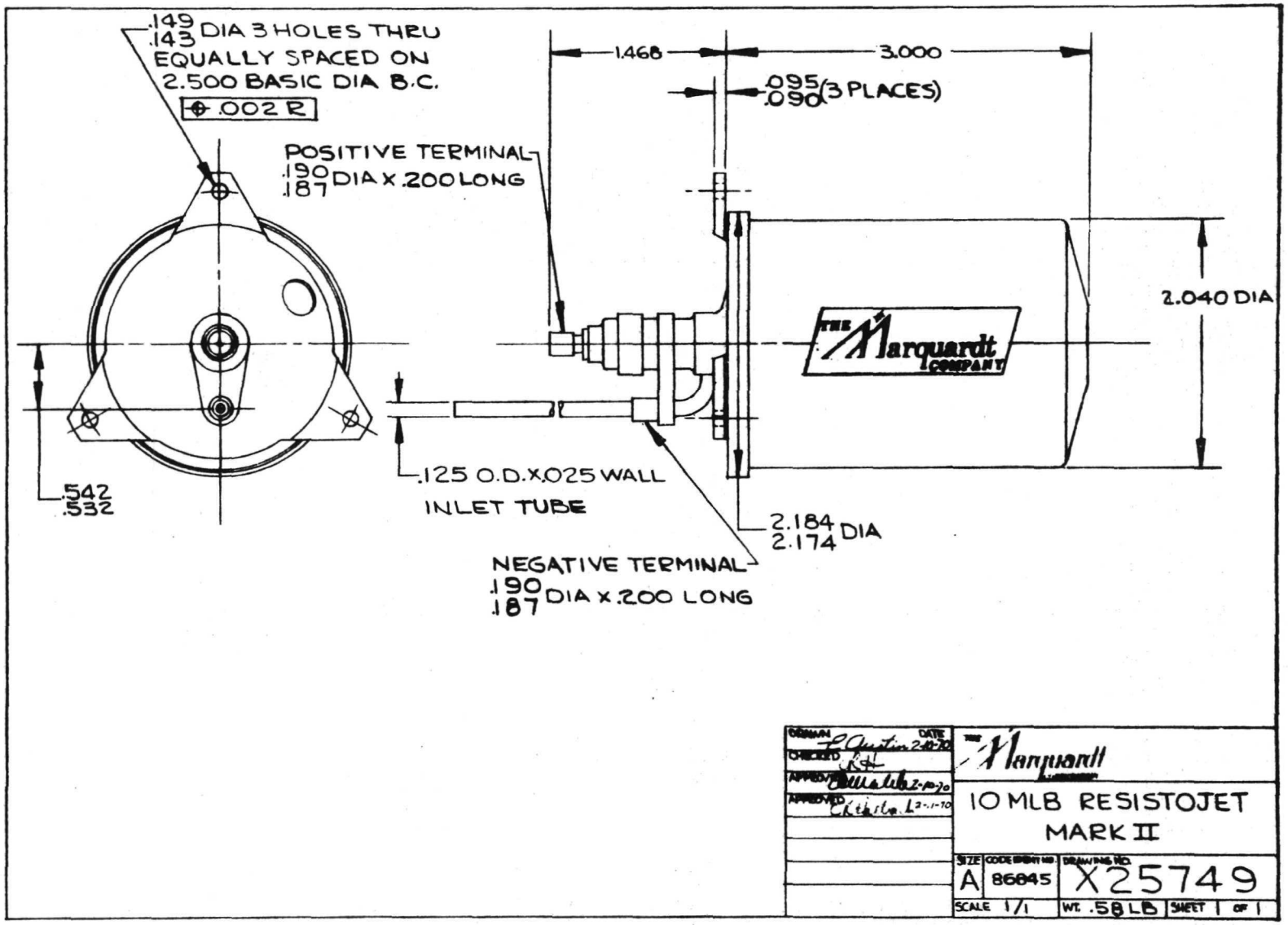
.149
.143 DIA 3 HOLES THRU
EQUALLY SPACED ON
2.500 BASIC DIA B.C.
⌖ .002 R
POSITIVE TERMINAL
.190
.187 DIA x .200 LONG
1.468
3.000
.095
.090 (3 PLACES)
2.040 DIA
THE Marquardt COMPANY
.542
.532
.125 O.D. X .025 WALL
INLET TUBE
2.184
2.174 DIA
NEGATIVE TERMINAL
.190
.187 DIA x .200 LONG
DRAWN L. Austin 2-10-70
CHECKED
APPROVED
APPROVED C. Kibler 2-11-70
THE Marquardt COMPANY
10 MLB RESISTOJET
MARK II
SIZE A
CODE IDENT NO. 86845
DRAWING NO. X25749
SCALE 1/1
WT. .58 LB
SHEET 1 OF 1

Figure 20

MARK II BIOWASTE RESISTOJET – INNER HEATER ELEMENT AND NOZZLE

NEG. 9883-1

V8190-2

Figure 21

MARK II BIOWASTE RESISTOJET OUTER HEATER AND CAP

NEG. 9883-4

V8190-1

Figure 22

MARK II BIOWASTE RESISTOJET
INSULATED HEATER ASSEMBLY AND BELLOWS ASSEMBLY

NEG. 9883-8

Figure 23

V8237-2

MARK II BIOWASTE RESISTOJETS WITH AND WITHOUT INSULATION

NEG. 9883-10

Figure 24

E. P. L. TEST CHAMBER WINDAGE EFFECT

HYDROGEN FLOW THROUGH SIMULATOR
NITROGEN ADDED TO VARY CELL PRESSURE
TEST DATE 9/24, 9/25, 10/3 AND 10/19/70

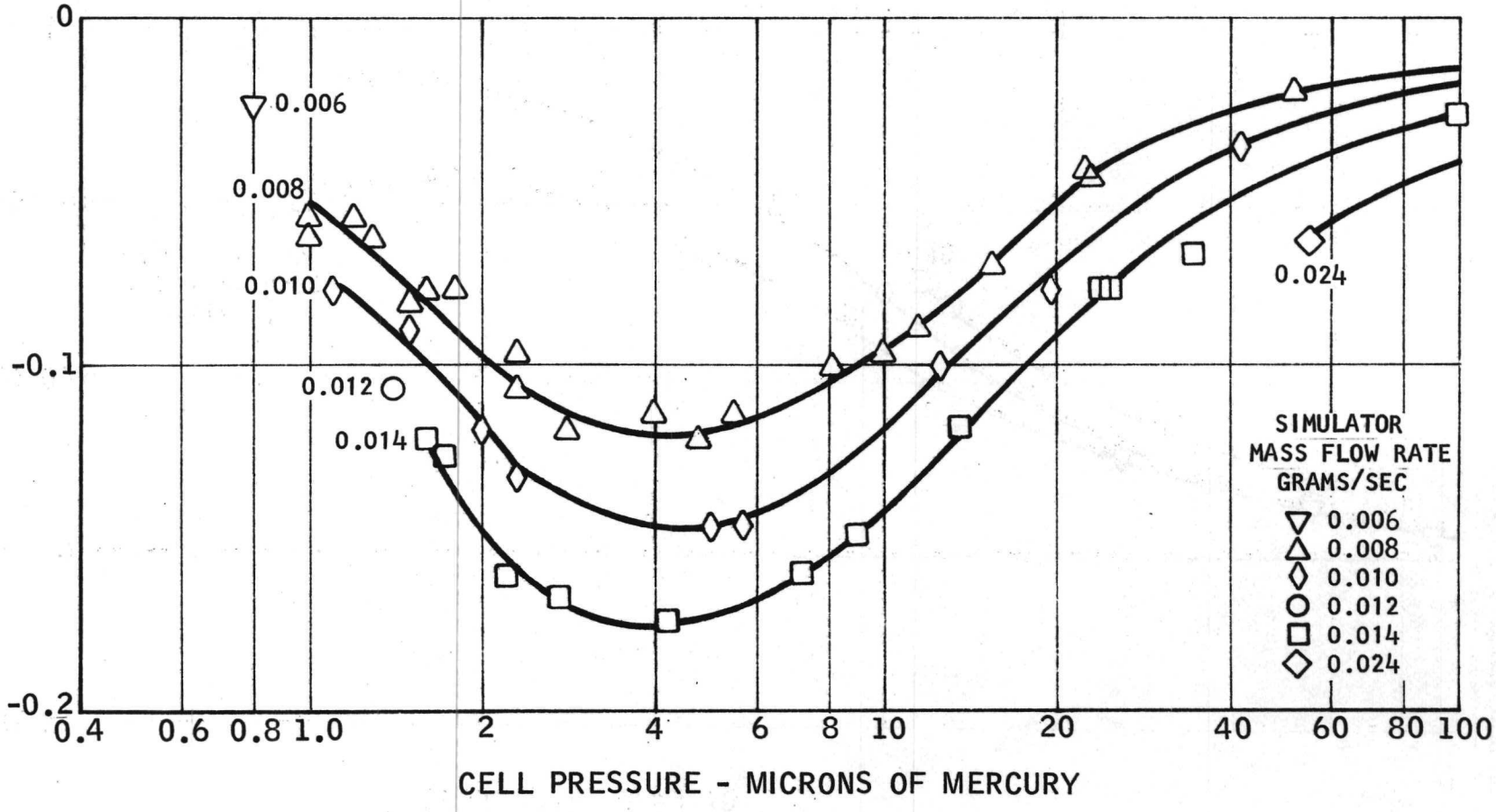

Figure 25

V8349-7

E. P. L. TEST CHAMBER WINDAGE EFFECT

CARBON DIOXIDE FLOW THROUGH SIMULATOR
NITROGEN ADDED TO VARY CELL PRESSURE
TEST DATE 9/23/70

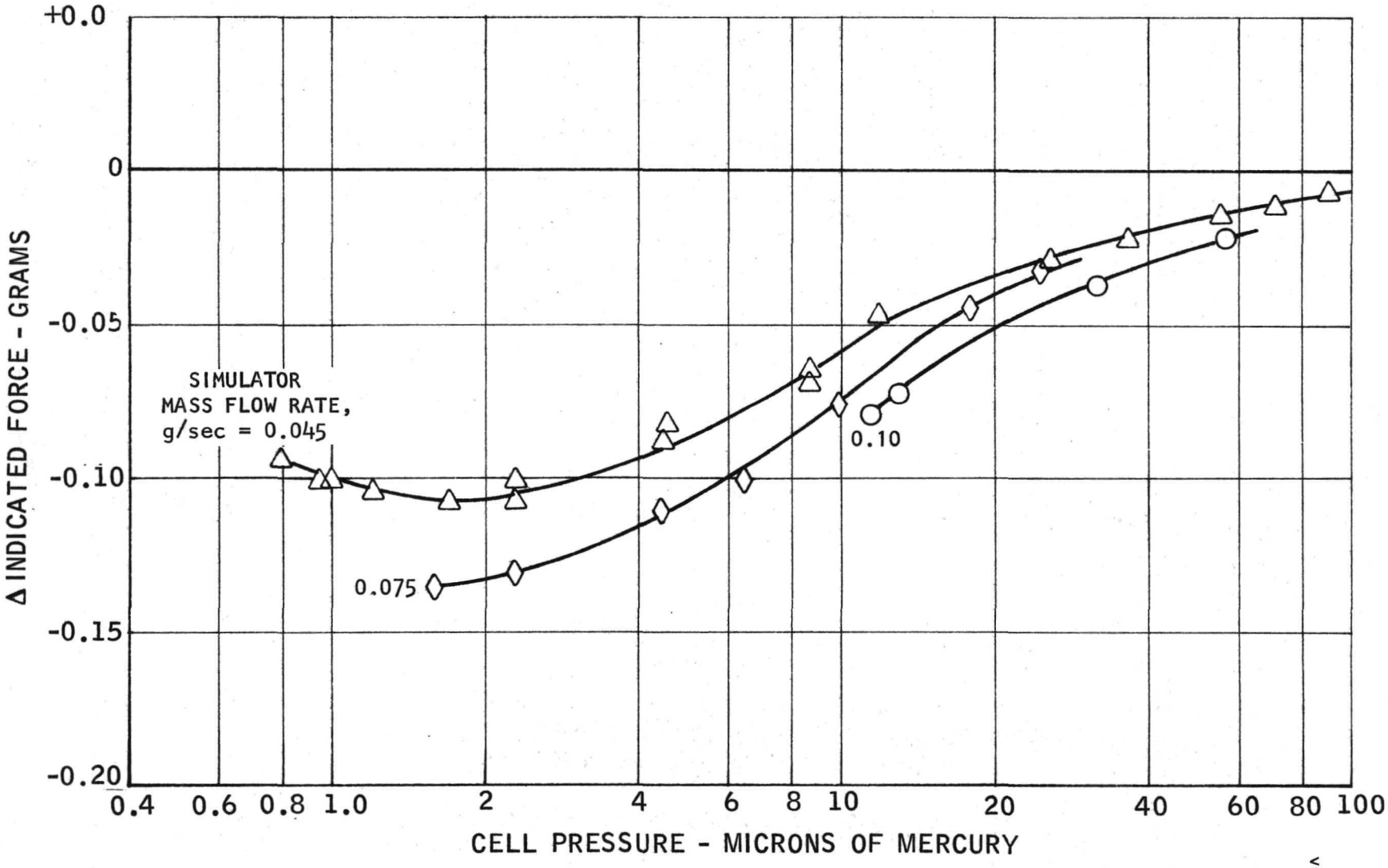

Figure 26

V8322-1

BIOWASTE RESISTOJET TEST

MARK II, S/N 001
9/25 - 9/29/70
DATA POINTS 1025-1038

HYDROGEN
SUPPLY PRESSURE - 37 PSIA

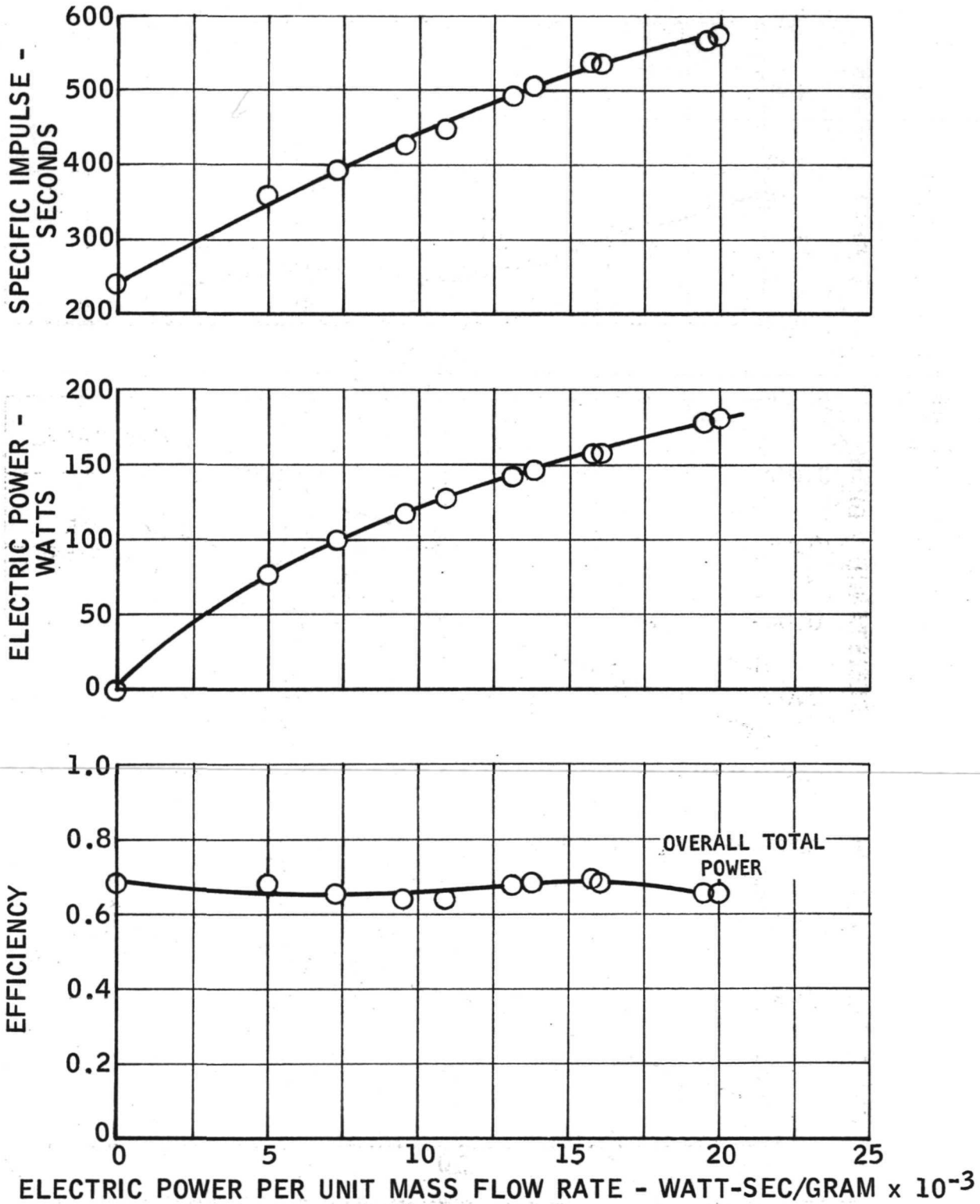

Figure 27

BIOWASTE RESISTOJET TEST

MARK II, S/N 001
9/25 - 9/29/70
DATA POINTS 1025-1038

HYDROGEN
SUPPLY PRESSURE - 37 PSIA

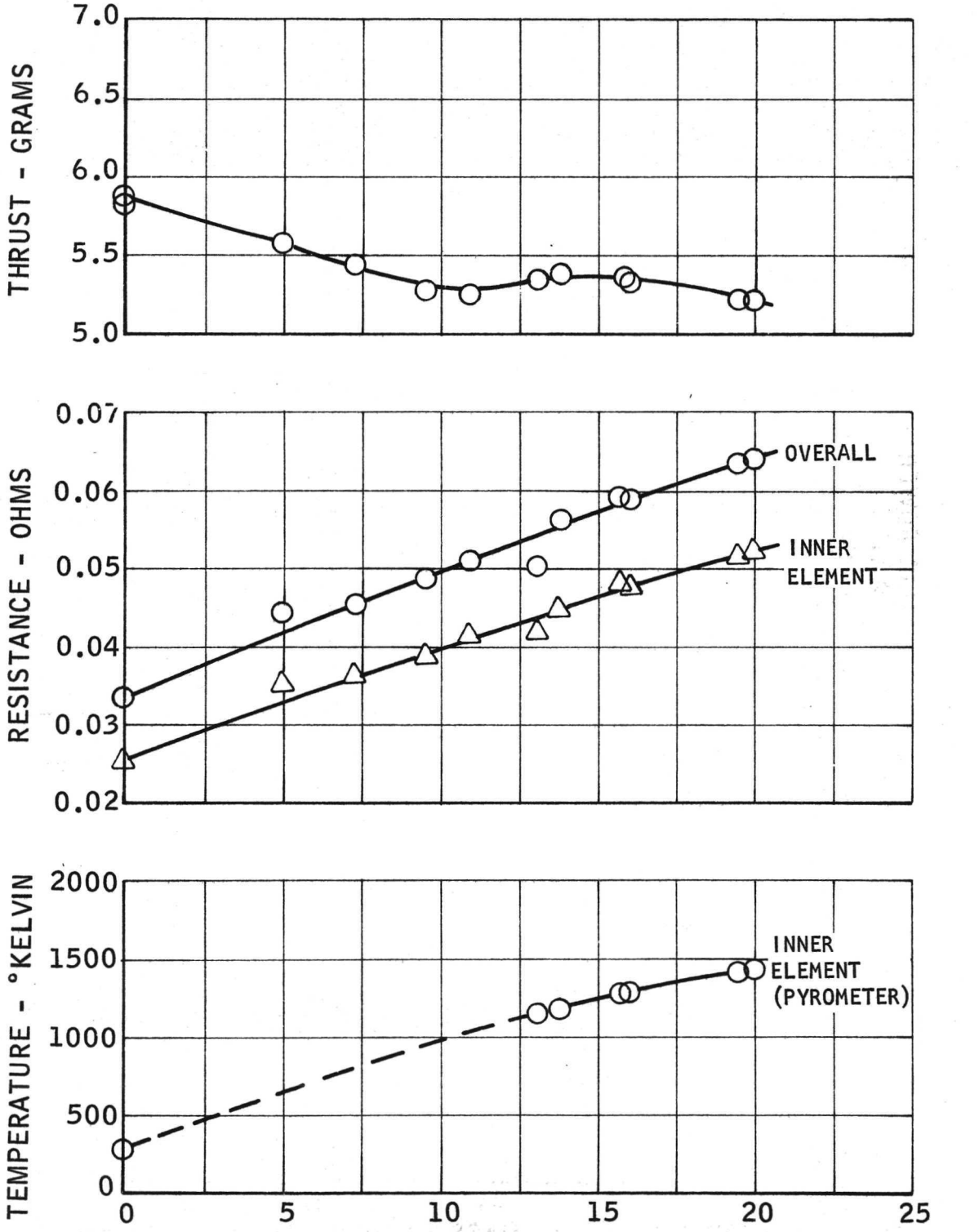

Figure 28

BIOWASTE RESISTOJET TEST

MARK II, S/N 003
10/19/70
DATA POINTS 3001-3010

HYDROGEN
SUPPLY PRESSURE - 37 PSIA

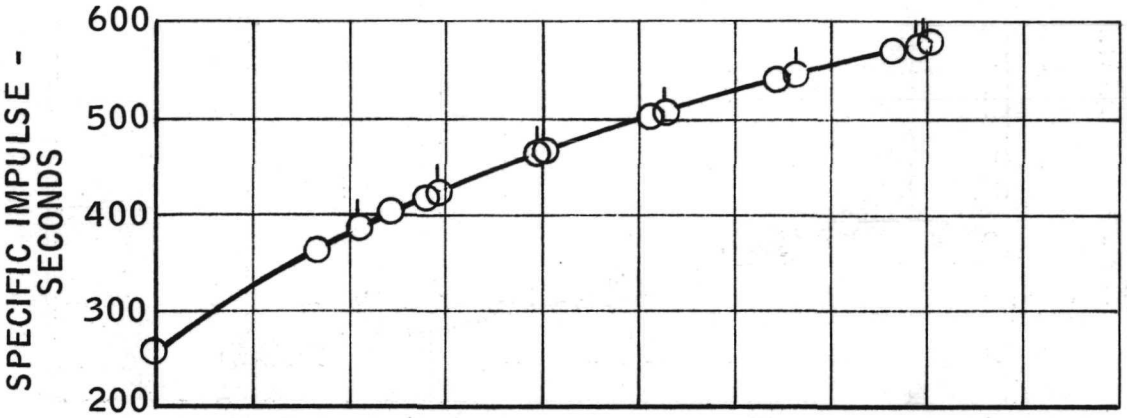

FLAGGED SYMBOLS ARE FROM POST-VIBRATION TEST CALIBRATION
DATA POINTS 3020-3028 ON 11/9/70

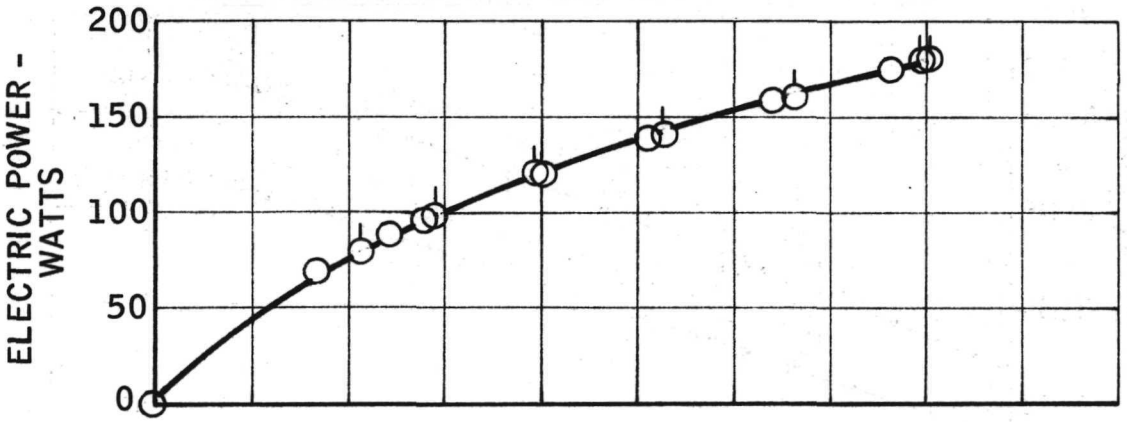

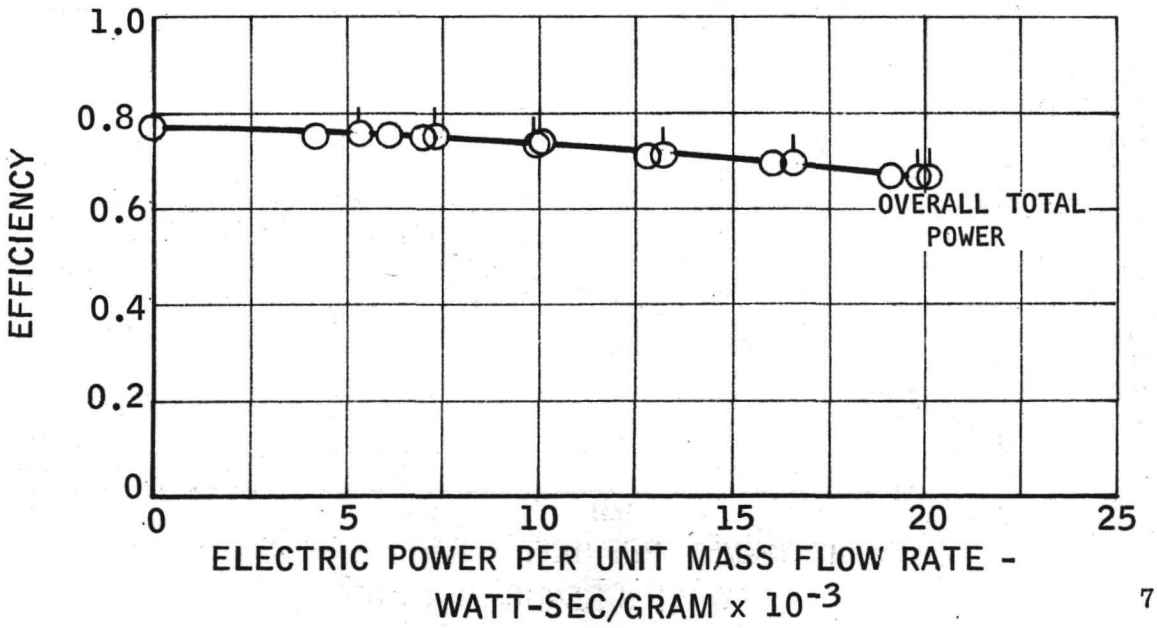

Figure 29

V8349-3

BIOWASTE RESISTOJET TEST

MARK II, S/N 003
10/19/70
DATA POINTS 3001-3010

HYDROGEN
SUPPLY PRESSURE - 37 PSIA

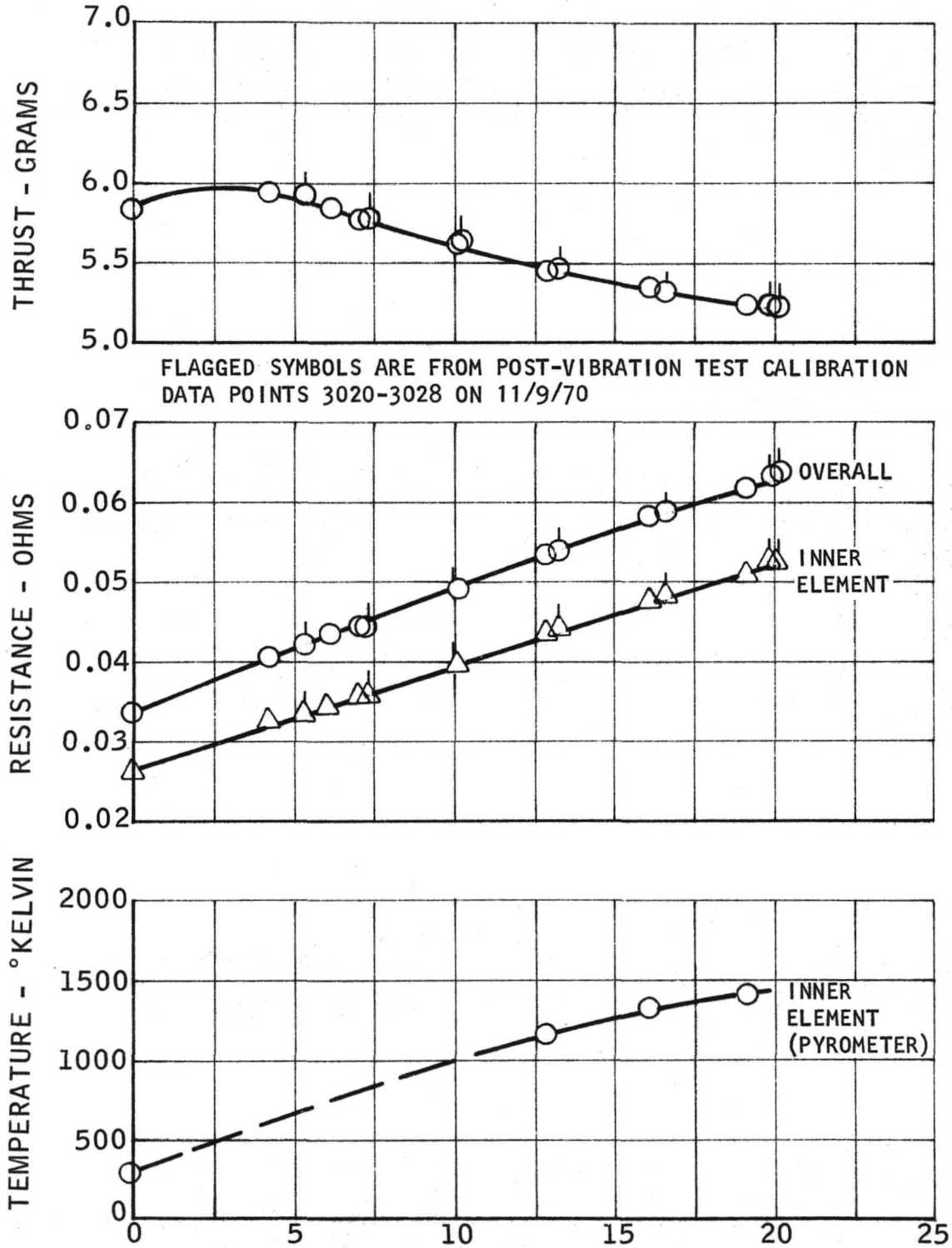

Figure 30

BIOWASTE RESISTOJET TEST

MARK II, S/N 001
9/22 - 9/23/70
DATA POINTS 1005-1024

CARBON DIOXIDE
SUPPLY PRESSURE - 37 PSIA

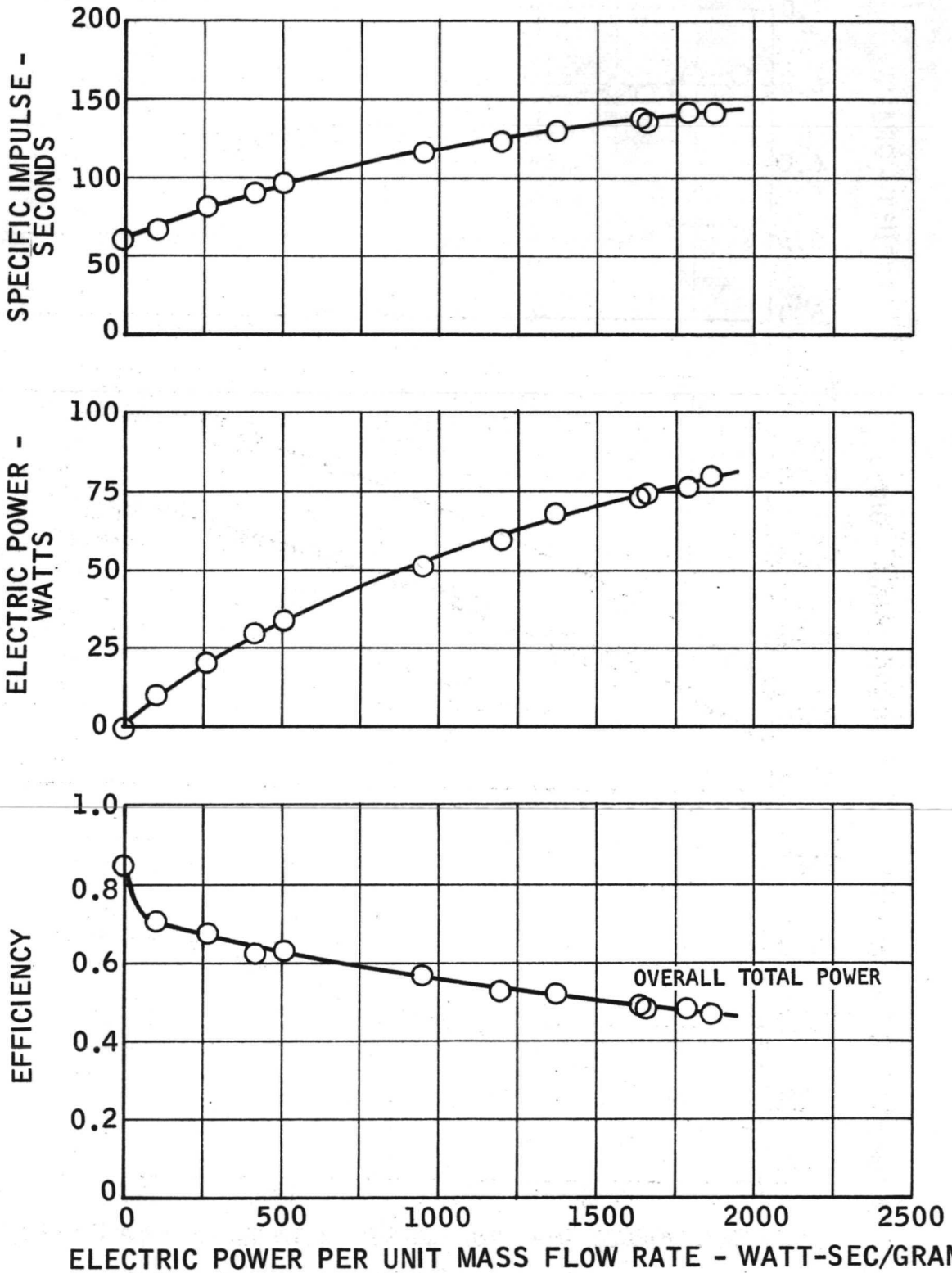

Figure 31

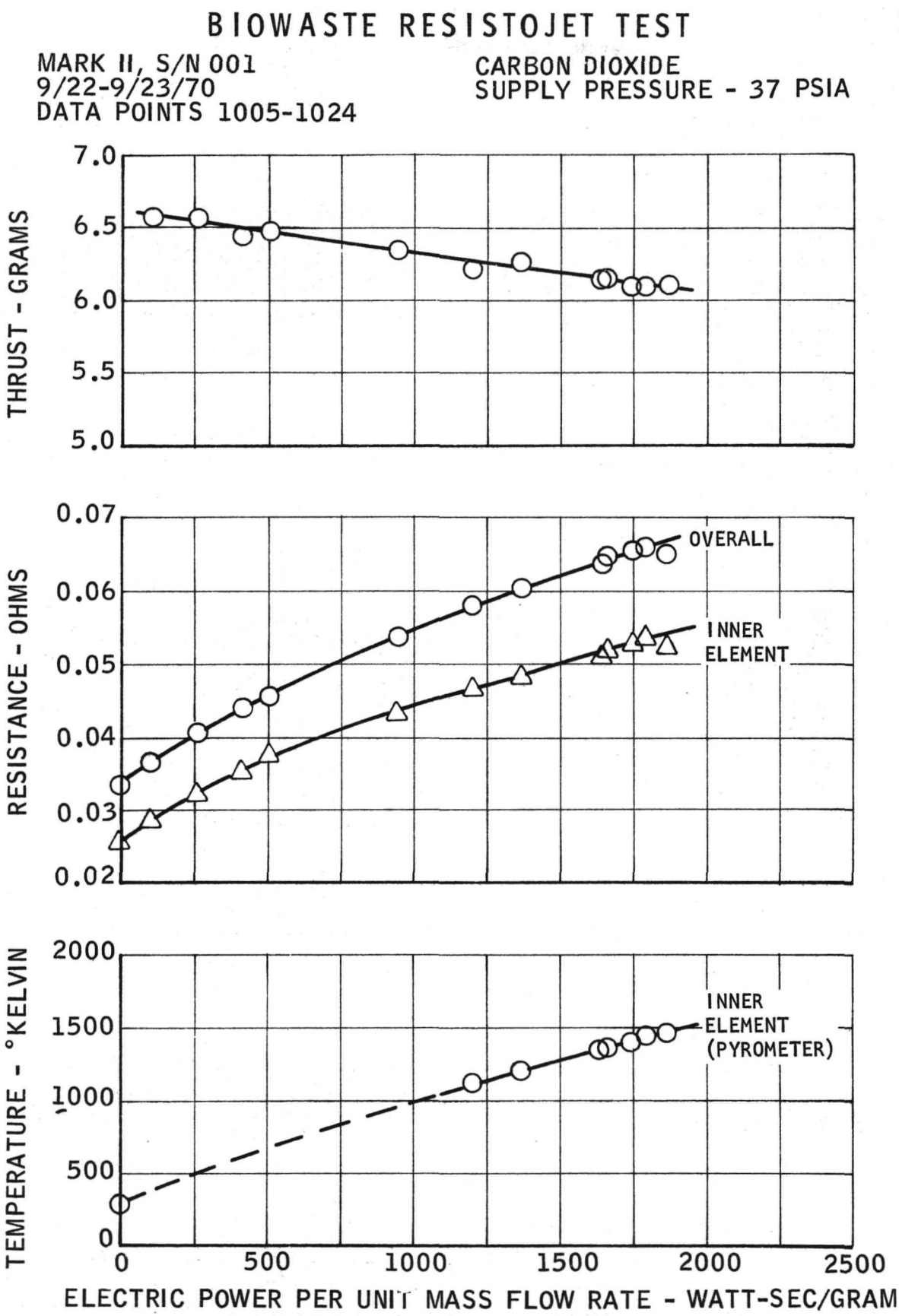
BIOWASTE RESISTOJET TEST
V8322-4
MARK II, S/N 001
9/22-9/23/70
DATA POINTS 1005-1024
CARBON DIOXIDE
SUPPLY PRESSURE - 37 PSIA
THRUST - GRAMS
7.0
6.5
6.0
5.5
5.0
RESISTANCE - OHMS
0.07
0.06
0.05
0.04
0.03
0.02
OVERALL
INNER ELEMENT
TEMPERATURE - °KELVIN
2000
1500
1000
500
0
INNER ELEMENT (PYROMETER)
0
500
1000
1500
2000
2500
ELECTRIC POWER PER UNIT MASS FLOW RATE - WATT-SEC/GRAM

Figure 32

BIOWASTE RESISTOJET TEST

MARK II, S/N 001
10/9 - 10/15/70
DATA POINTS 1039-1079

METHANE
SUPPLY PRESSURE - 30 PSIA

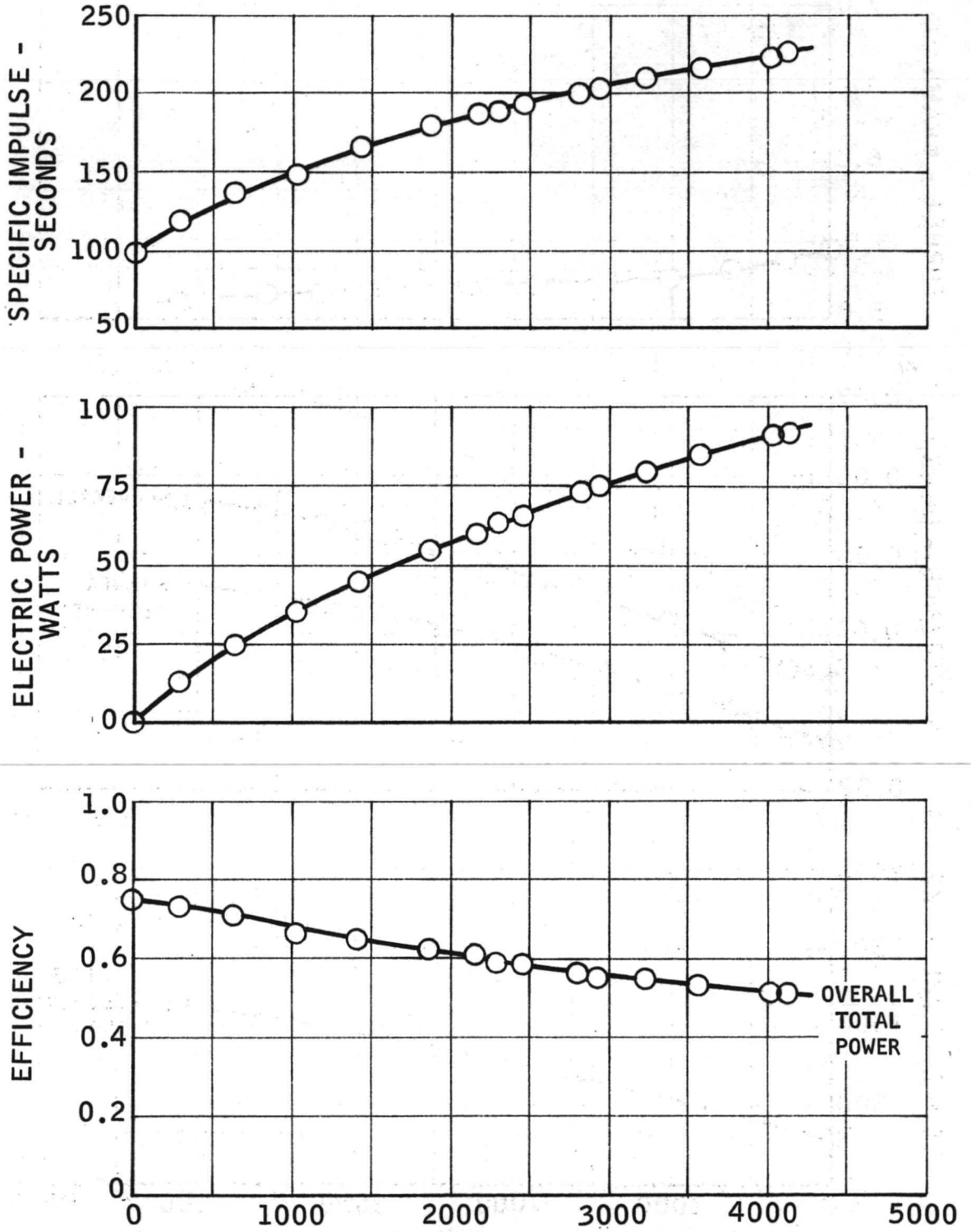

Figure 33

V8349-4

BIOWASTE RESISTOJET TEST

MARK II, S/N 001
10/9-10/15/70
DATA POINTS 1039-1079

METHANE
SUPPLY PRESSURE - 30 PSIA

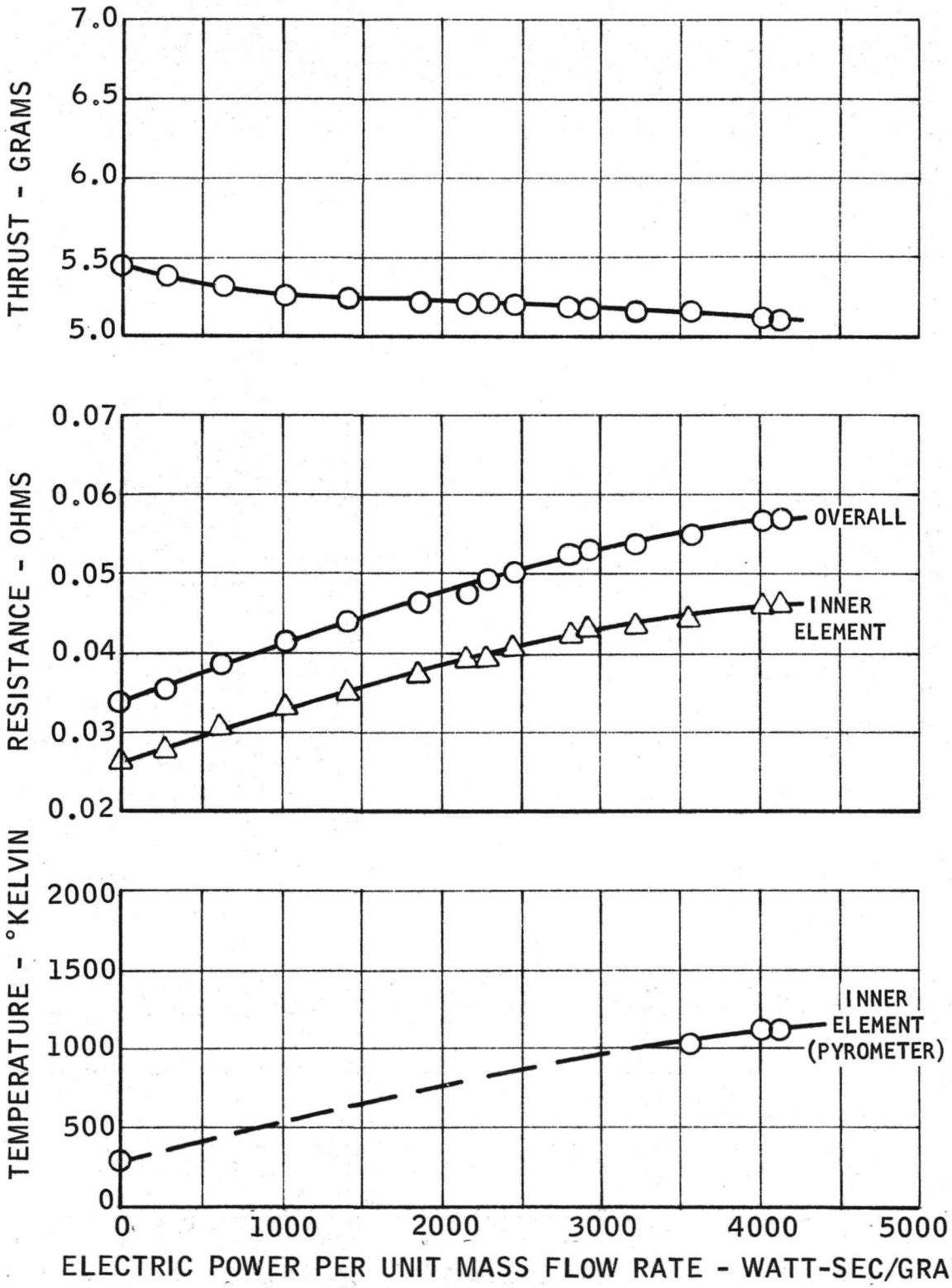

Figure 34

CELL PRESSURE EFFECT ON MARK II BIOWASTE RESISTOJET PERFORMANCE

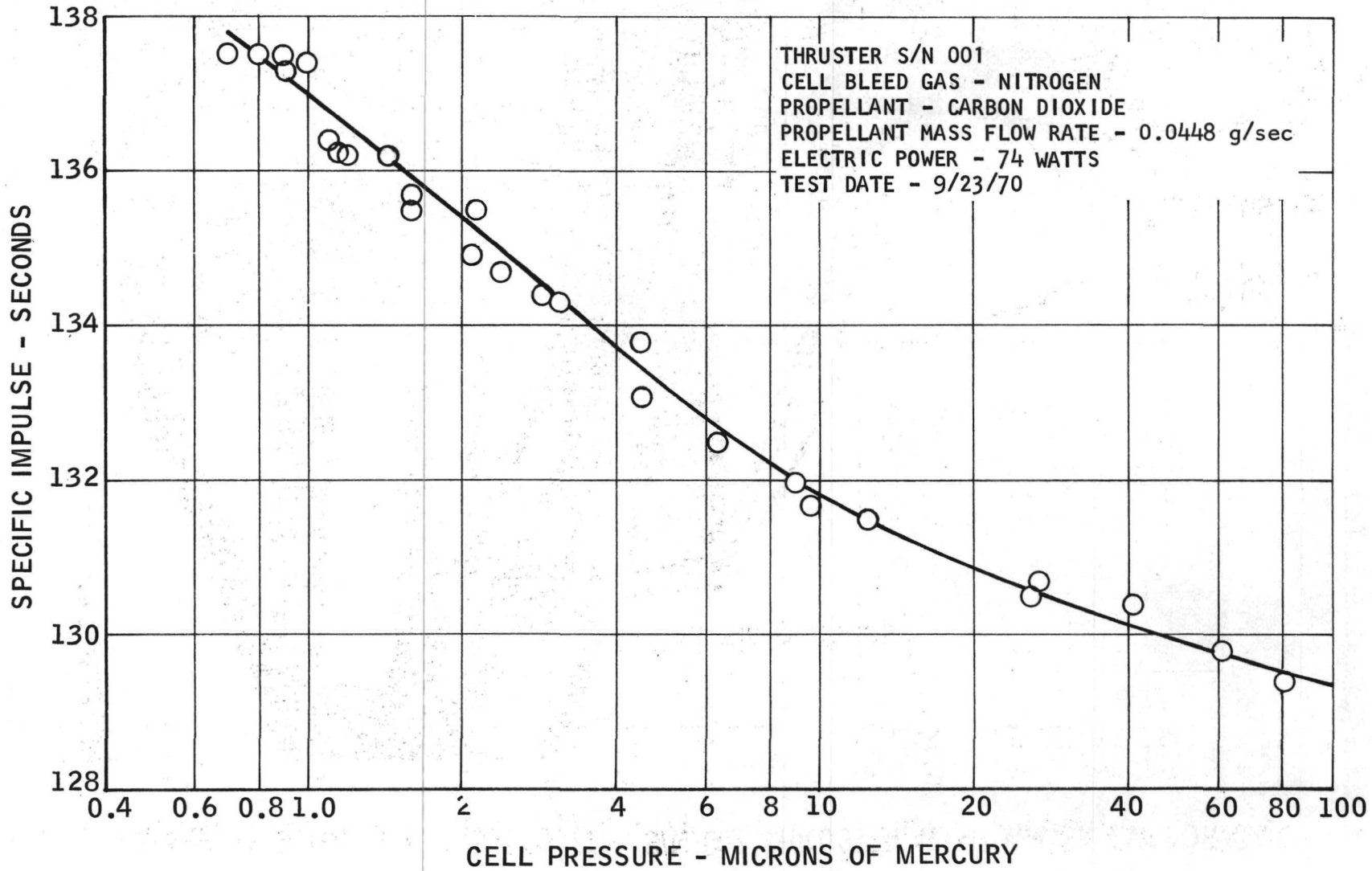

Figure 35

V8322-5

MARK II BIOWASTE RESISTOJET - S/N 002 THRUSTER WITH WATER EVAPORATOR

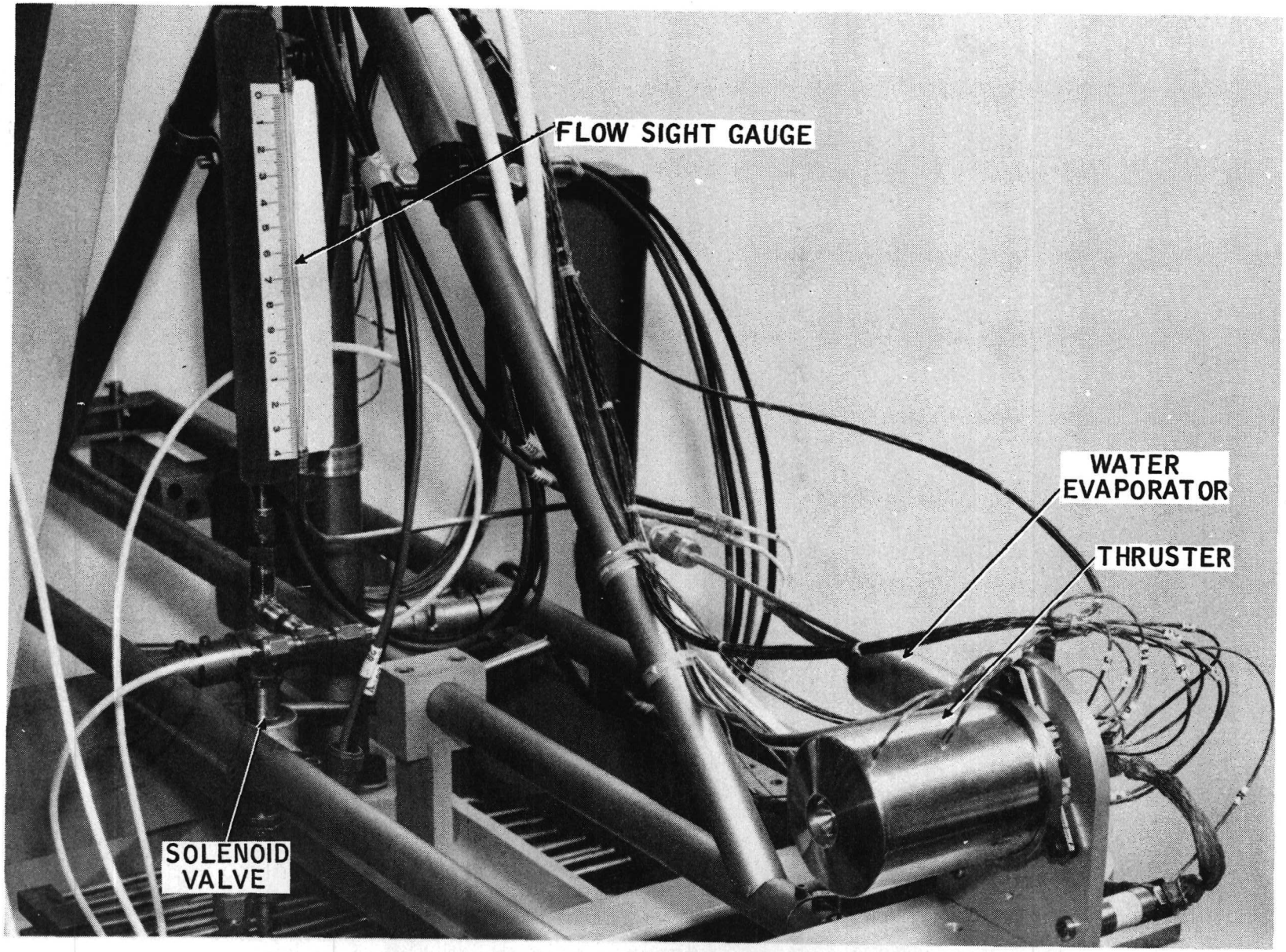

Figure 36

MARK II BIOWASTE RESISTOJET - S/N 002 THRUSTER WITH WATER EVAPORATOR

NEG. 9961-1

V8390-1

Figure 37

V8418-3

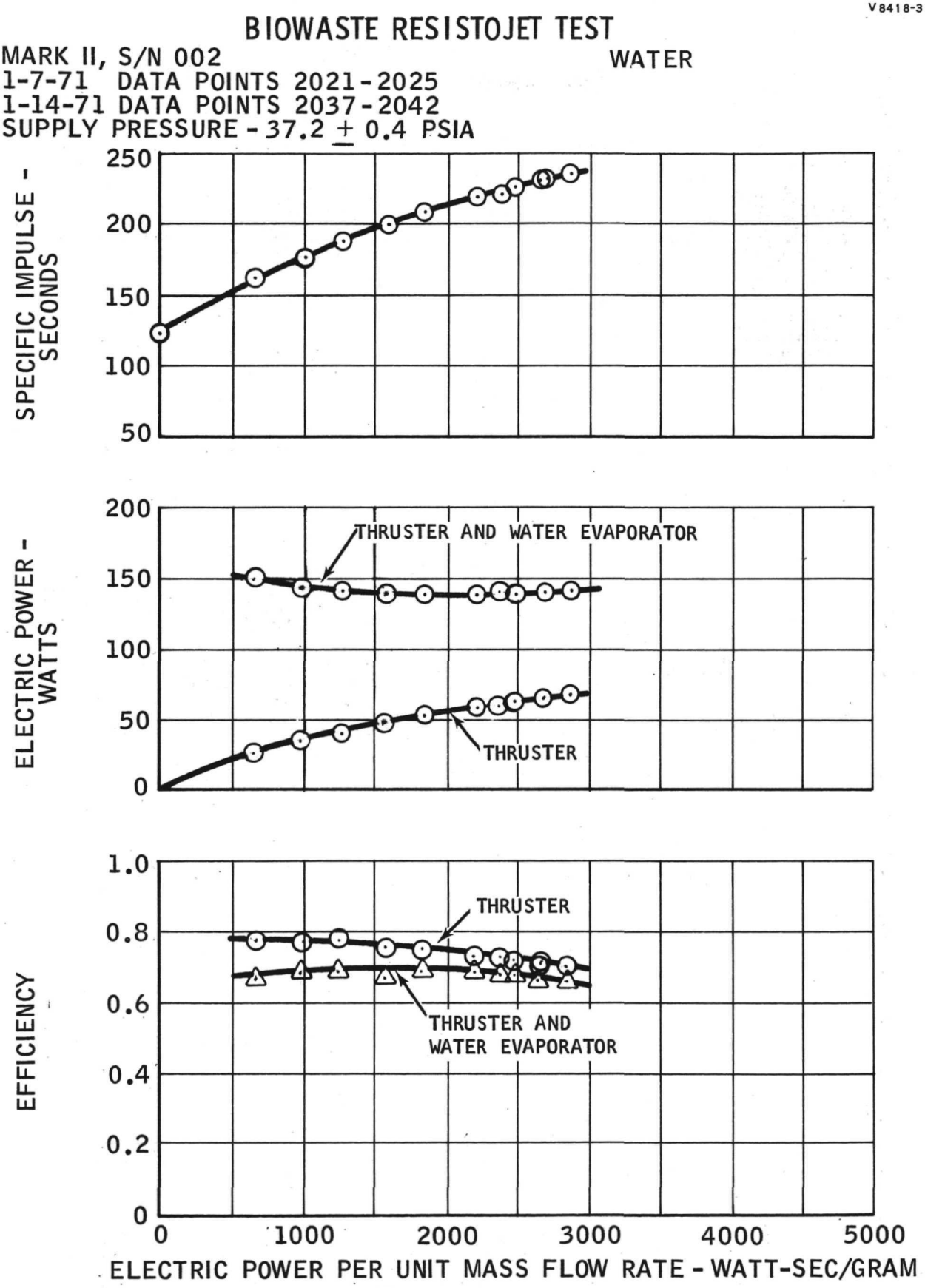

Figure 38

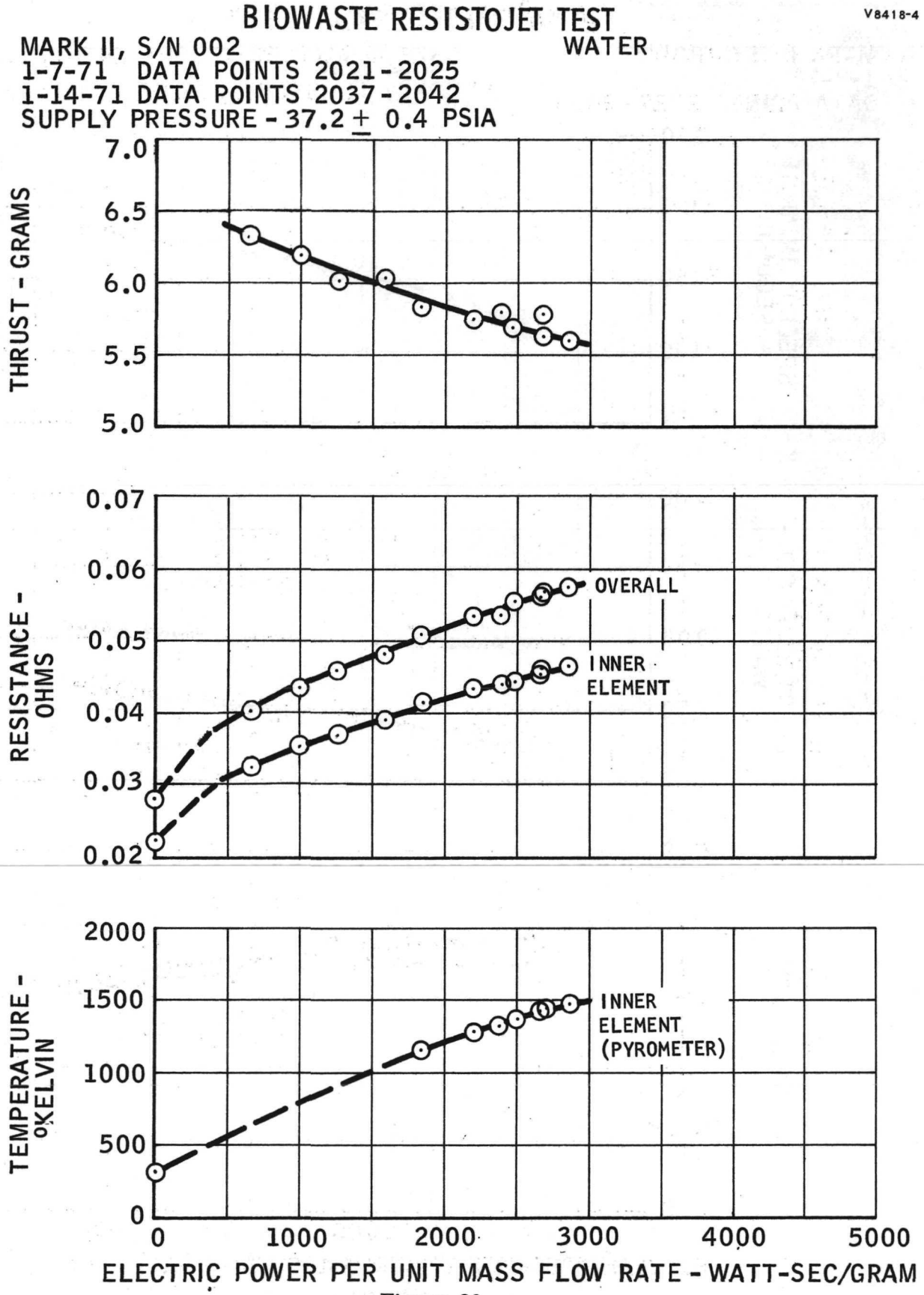
BIOWASTE RESISTOJET TEST
V8418-4
MARK II, S/N 002
WATER
1-7-71 DATA POINTS 2021-2025
1-14-71 DATA POINTS 2037-2042
SUPPLY PRESSURE - 37.2 ± 0.4 PSIA
THRUST - GRAMS
7.0
6.5
6.0
5.5
5.0
RESISTANCE - OHMS
0.07
0.06
0.05
0.04
0.03
0.02
OVERALL
INNER ELEMENT
TEMPERATURE - °KELVIN
2000
1500
1000
500
0
INNER ELEMENT (PYROMETER)
0
1000
2000
3000
4000
5000
ELECTRIC POWER PER UNIT MASS FLOW RATE - WATT-SEC/GRAM

Figure 39

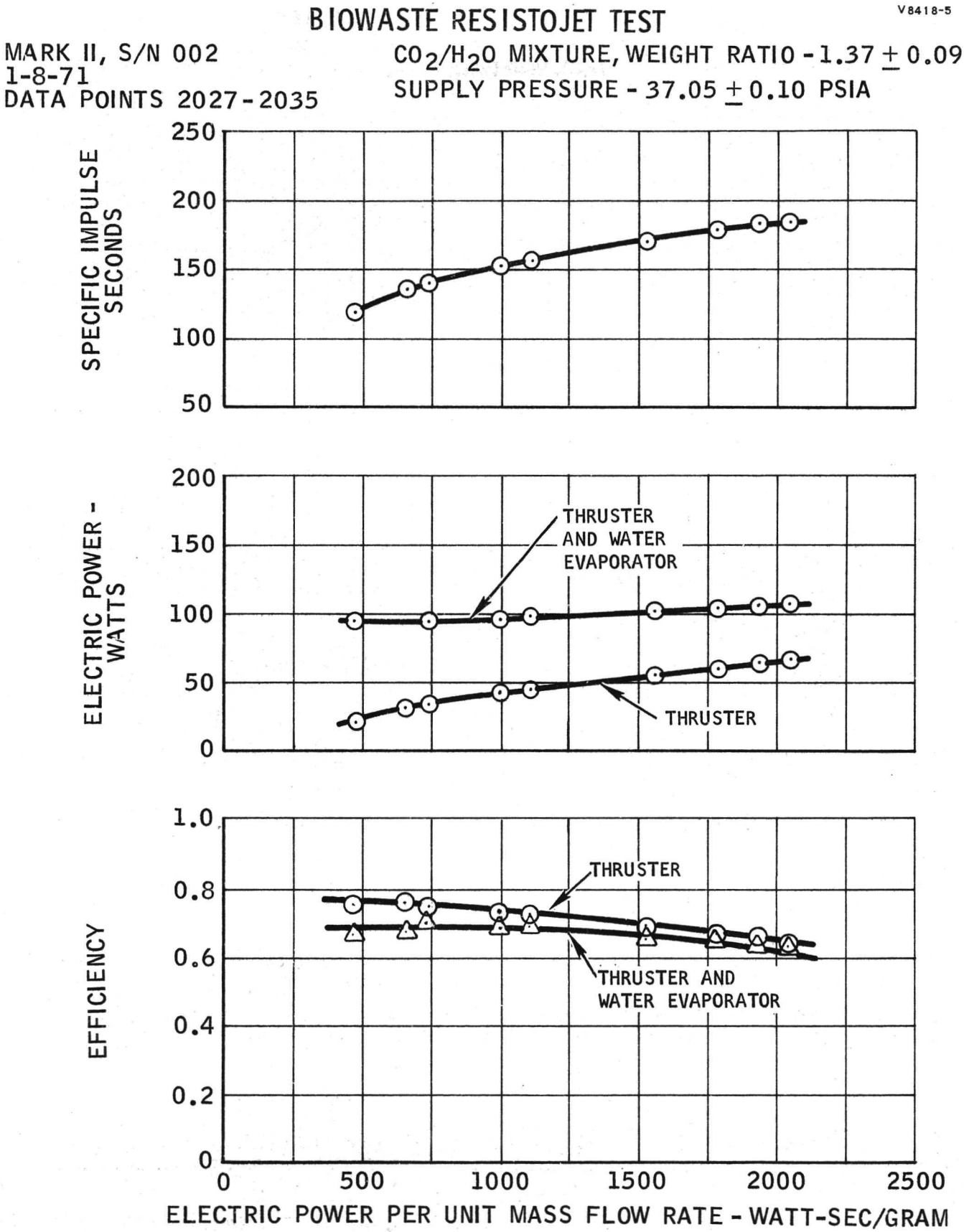
BIOWASTE RESISTOJET TEST
V8418-5
MARK II, S/N 002
1-8-71
DATA POINTS 2027-2035
CO_2/H_2O MIXTURE, WEIGHT RATIO - 1.37 ± 0.09
SUPPLY PRESSURE - 37.05 ± 0.10 PSIA
SPECIFIC IMPULSE SECONDS
250
200
150
100
50
ELECTRIC POWER - WATTS
200
150
100
50
0
THRUSTER AND WATER EVAPORATOR
THRUSTER
EFFICIENCY
1.0
0.8
0.6
0.4
0.2
0
THRUSTER
THRUSTER AND WATER EVAPORATOR
0
500
1000
1500
2000
2500
ELECTRIC POWER PER UNIT MASS FLOW RATE - WATT-SEC/GRAM

Figure 40

BIOWASTE RESISTOJET TEST

MARK II, S/N 002
1-8-71
DATA POINTS 2027-2035

CO_2/H_2O MIXTURE, WEIGHT RATIO - 1.37 ± 0.09
SUPPLY PRESSURE - 37.05 ± 0.10 PSIA

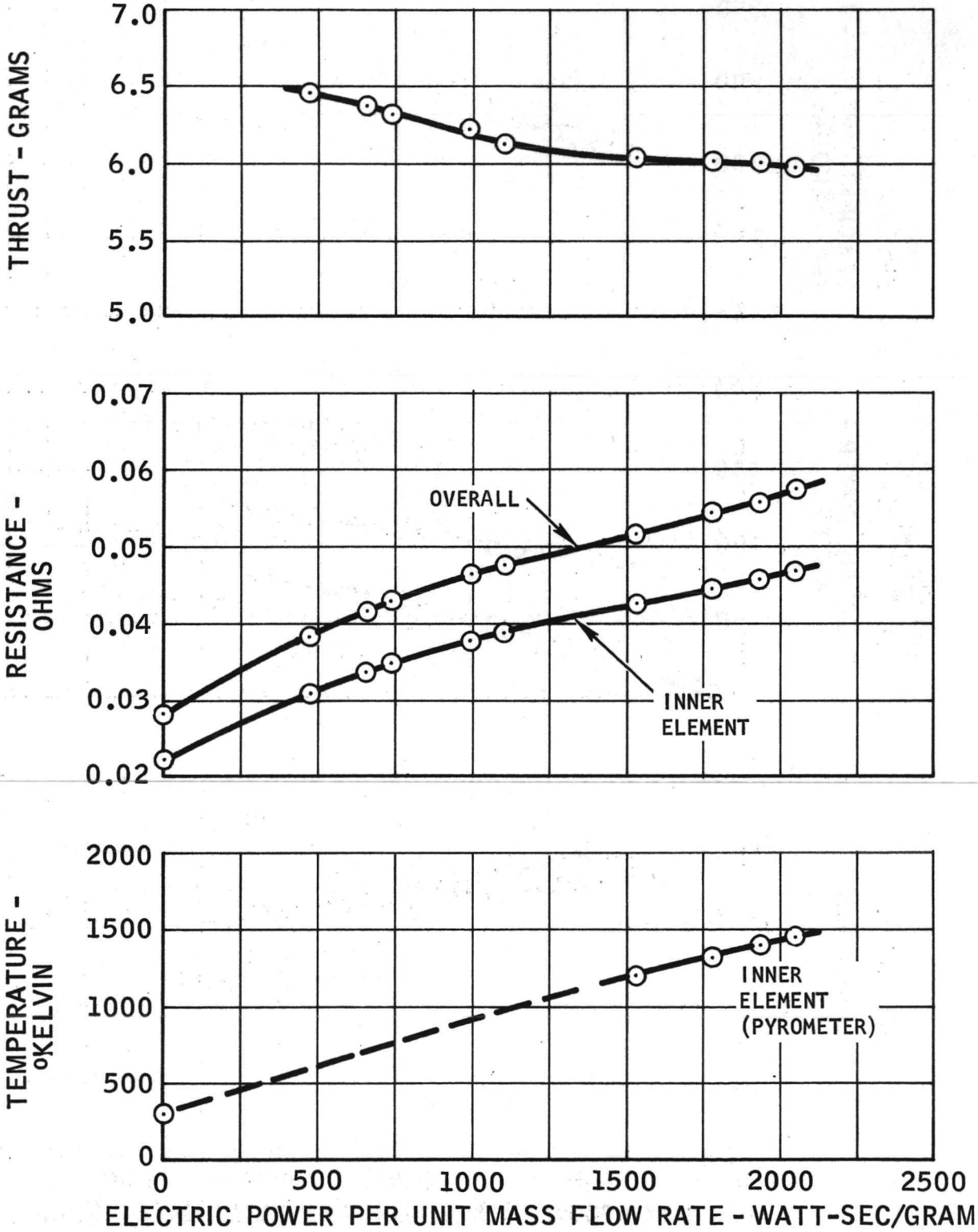

Figure 41

V8418-7

BIOWASTE RESISTOJET TEST

MARK II, S/N 002
1-14-71
DATA POINTS 2043-2056

CH_4/H_2O MIXTURE WEIGHT RATIO-1.01 ± 0.05
SUPPLY PRESSURE-37.05 ± 0.15 PSIA

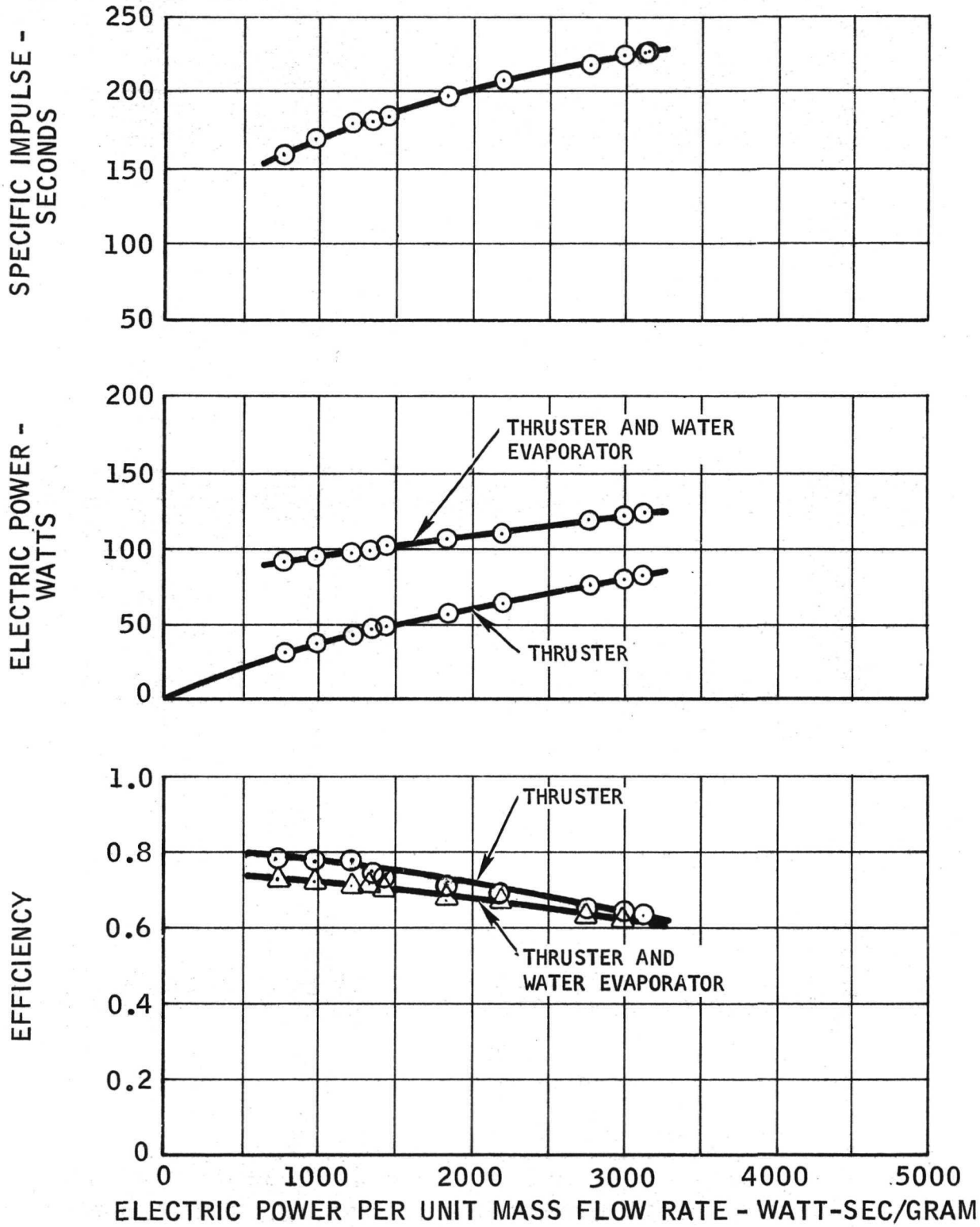

Figure 42

V8418-2

BIOWASTE RESISTOJET TEST

MARK II, S/N 002
1/14/71
DATA POINTS 2043 - 2056

CH_4/H_2O MIXTURE WEIGHT RATIO - 1.01 ± 0.05
SUPPLY PRESSURE - 37.05 ± 0.15 PSIA

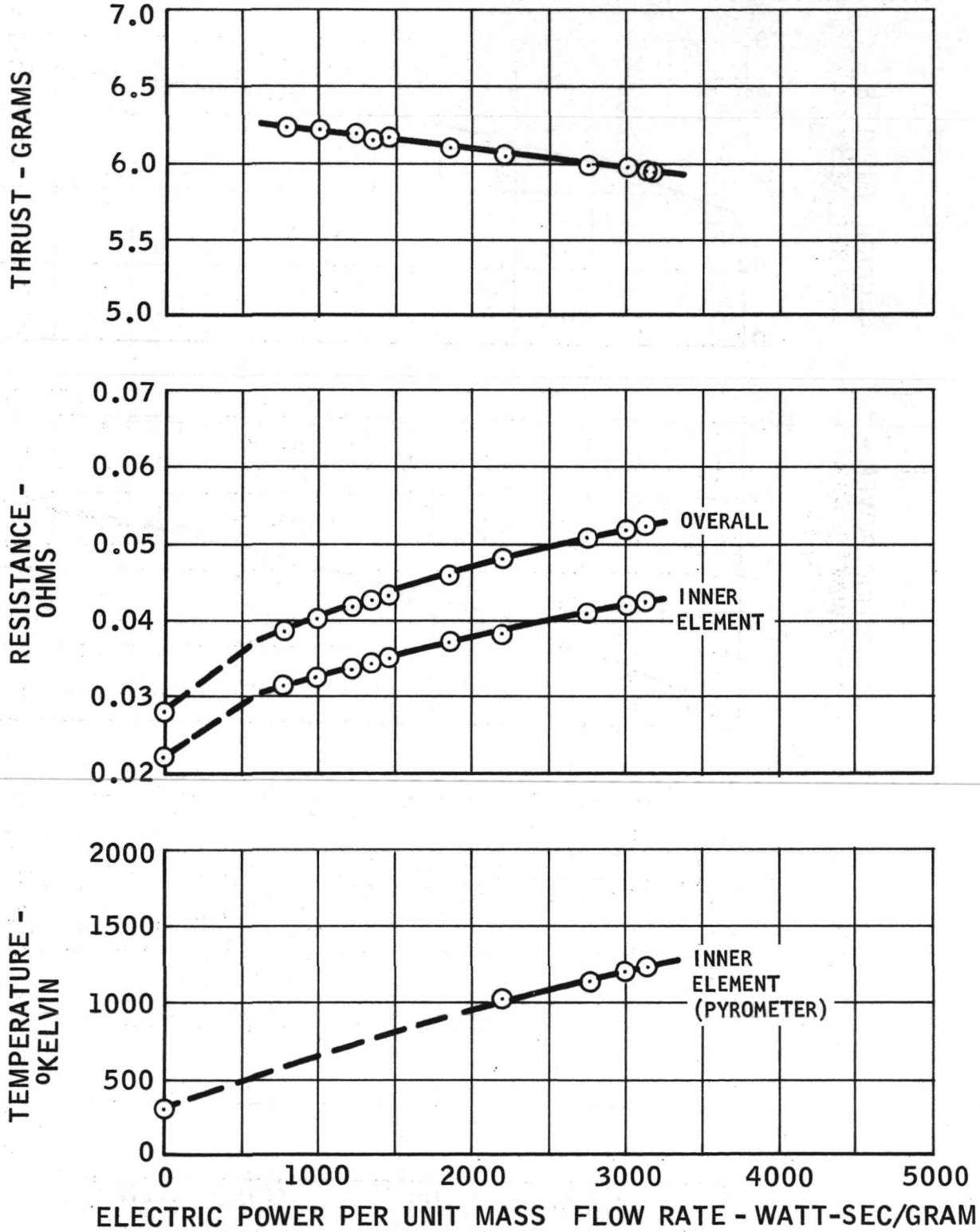

Figure 43

BIOWASTE RESISTOJET TEST

A71-5-012-2

MARK II, S/N 002
5/4/71
DATA POINTS 2060 - 2066

CO_2/CH_4 MIXTURE WEIGHT RATIO 0.985 ± 0.025
SUPPLY PRESSURE - 37.00 ± 0.02 PSIA

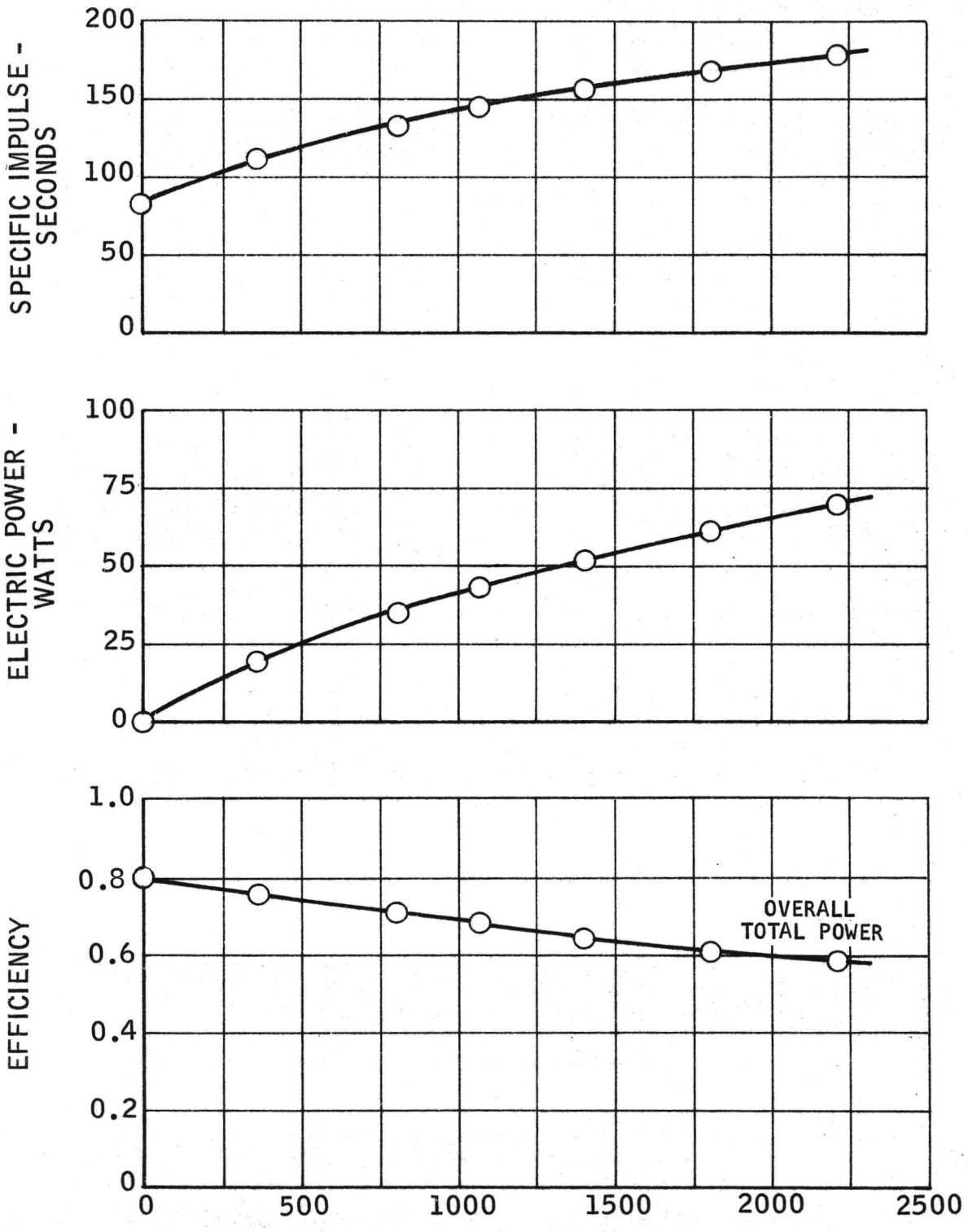

Figure 44

A71-5-012-1

BIOWASTE RESISTOJET TEST

MARK II, S/N 002
5/4/71
DATA POINTS 2060 - 2066

CO_2/CH_4 MIXTURE WEIGHT RATIO 0.985 ± 0.025
SUPPLY PRESSURE 37.00 ± 0.02 PSIA

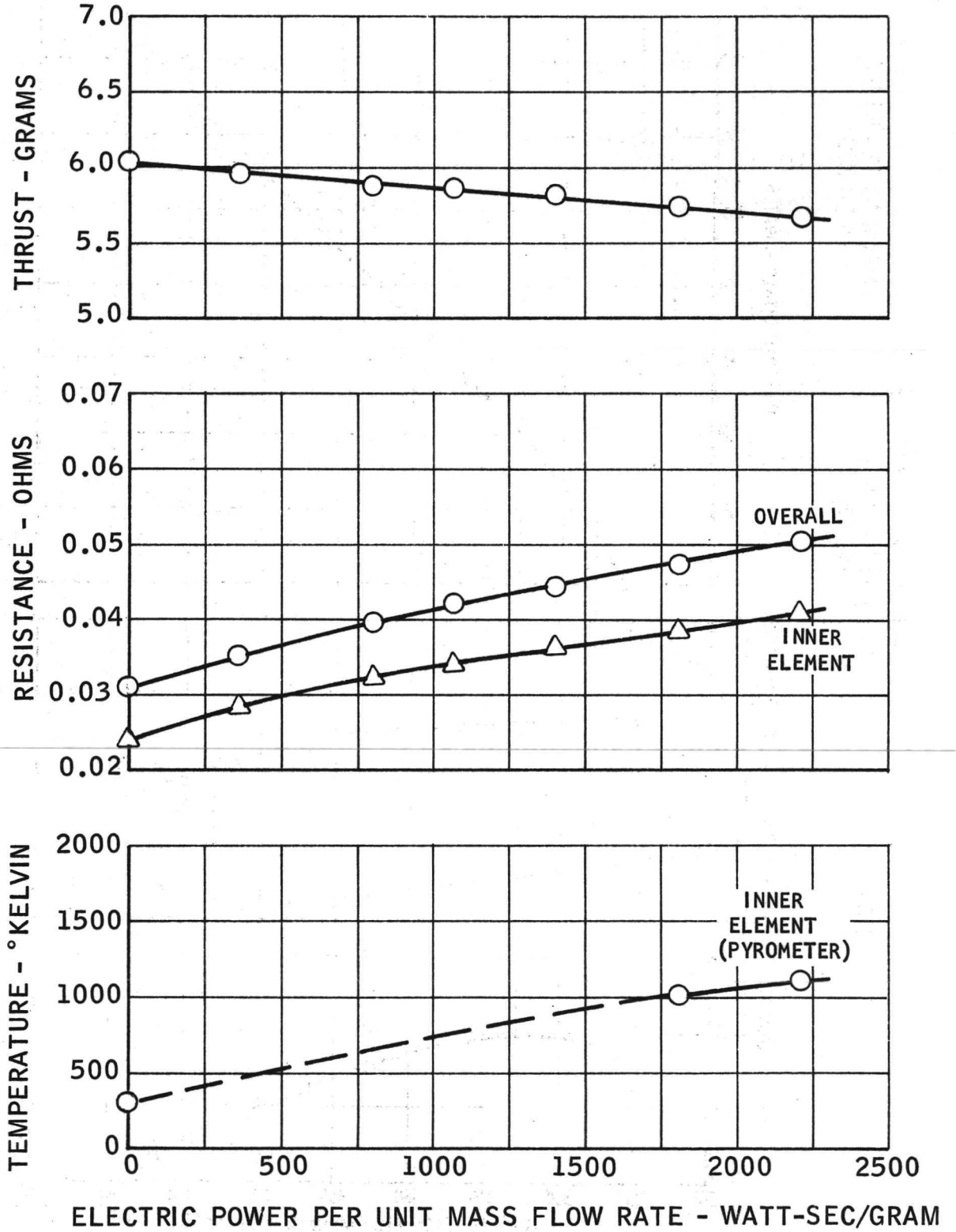

Figure 45

A71-6-020-2A

BIOWASTE RESISTOJET PERFORMANCE WITH HYDROGEN

MARK II - S/N 003 THRUSTER
SUPPLY PRESSURE 37.0 PSIA

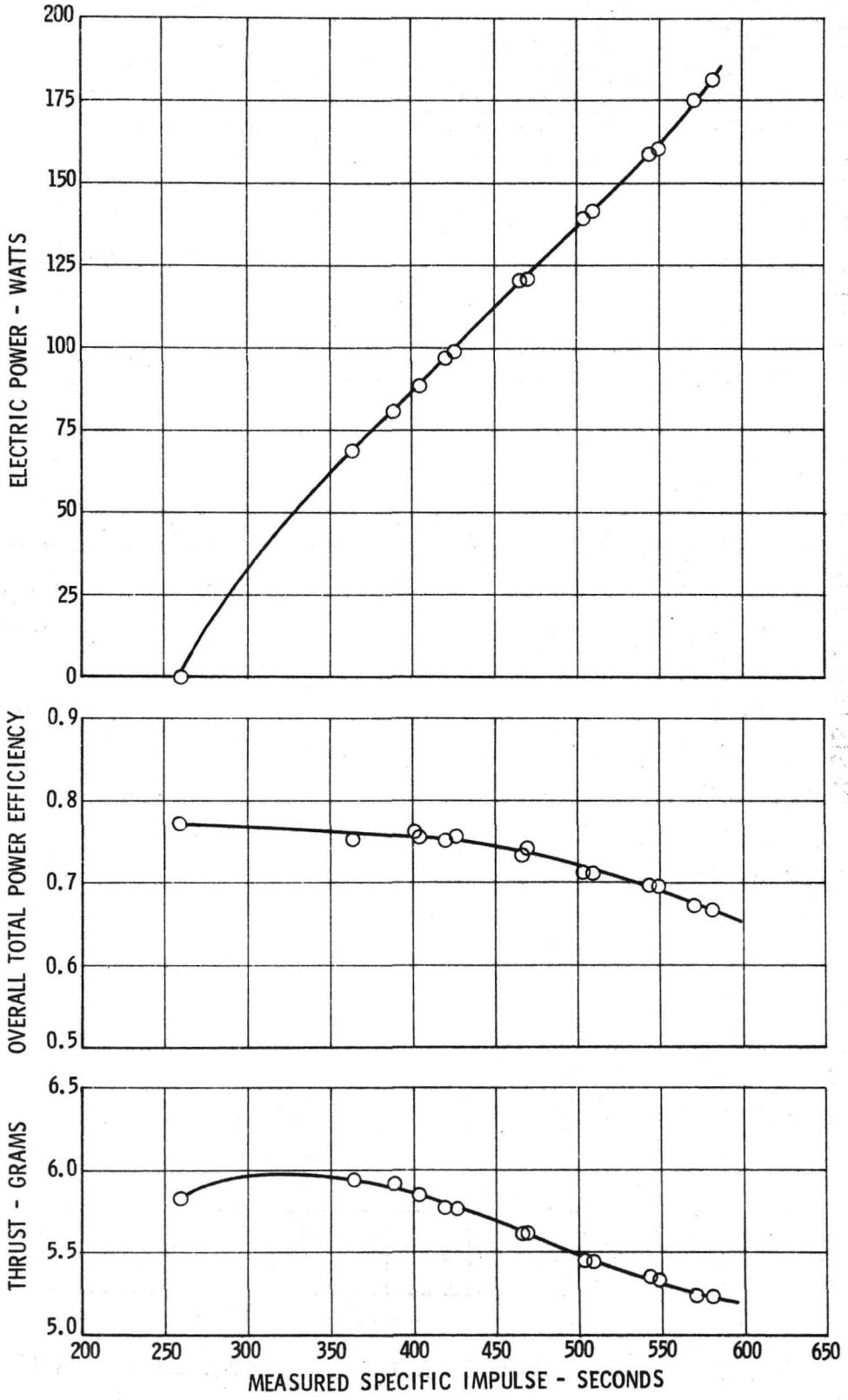

Figure 46

BIOWASTE RESISTOJET PERFORMANCE WITH TYPICAL PROPELLANTS

MARK II - S/N 001 AND 002 THRUSTERS

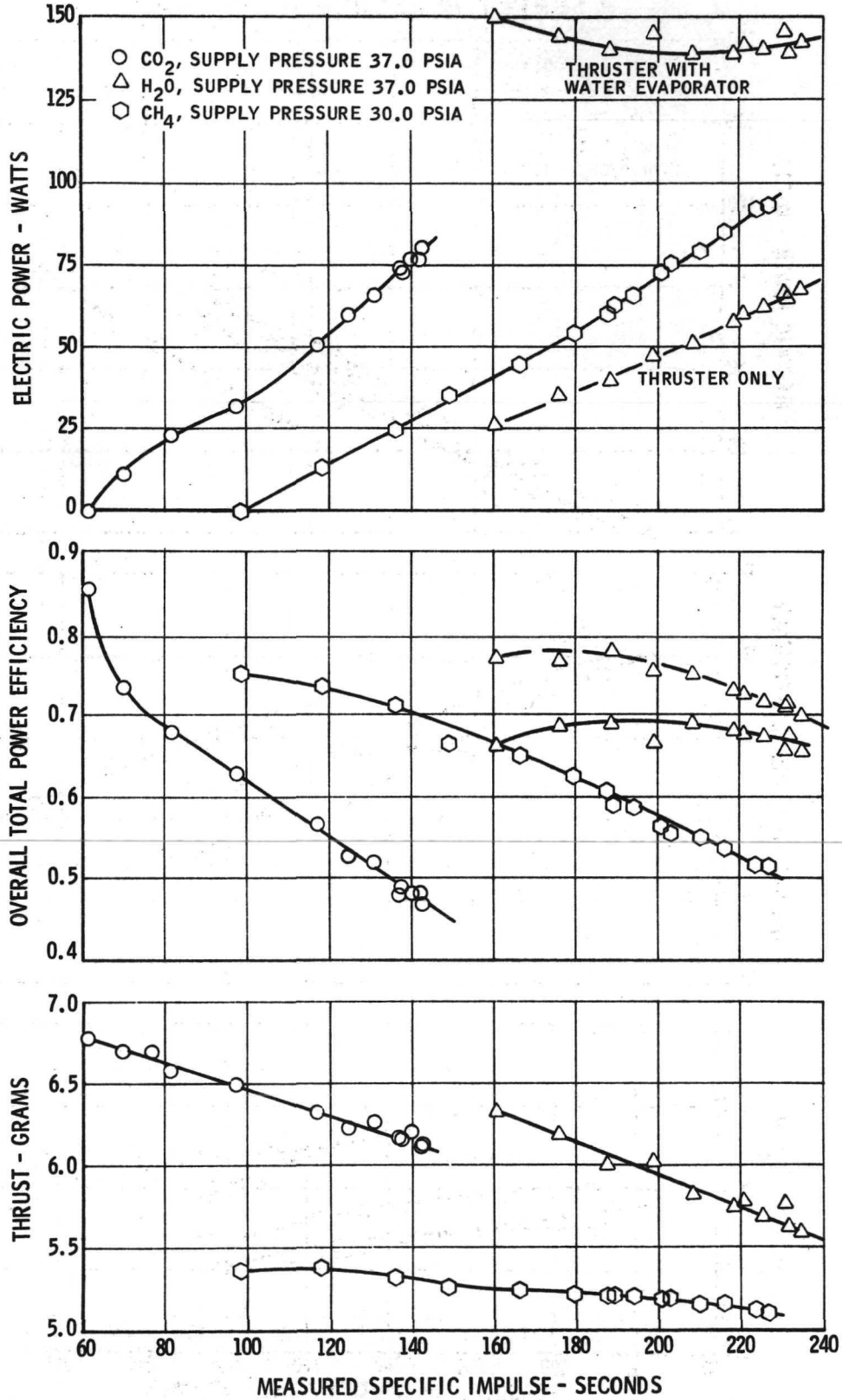

Figure 47

A71-6-020-1A

BIOWASTE RESISTOJET PERFORMANCE WITH TYPICAL PROPELLANT MIXTURES

MARK II - S/N 002 THRUSTER
SUPPLY PRESSURE 37.0 PSIA

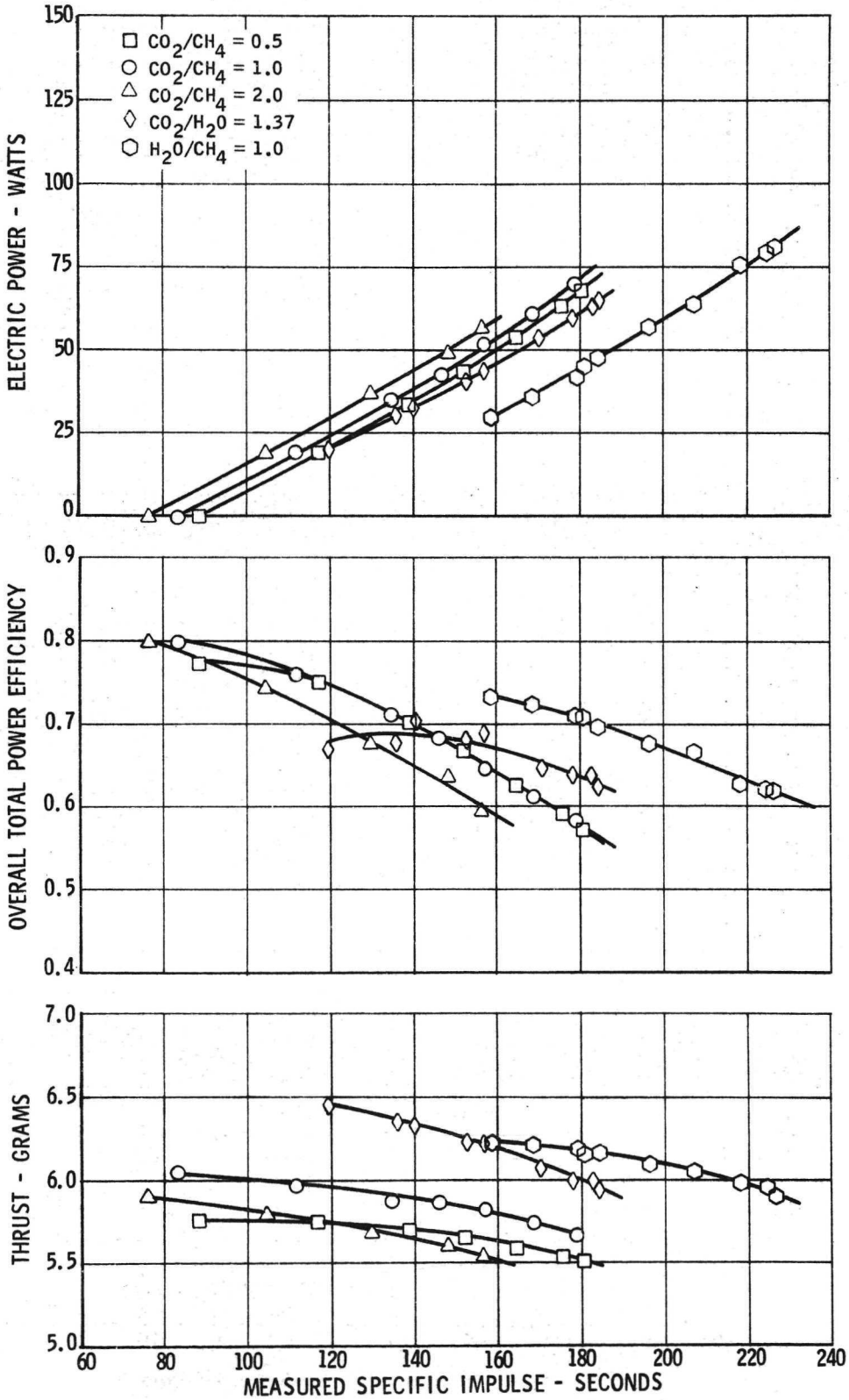

Figure 48

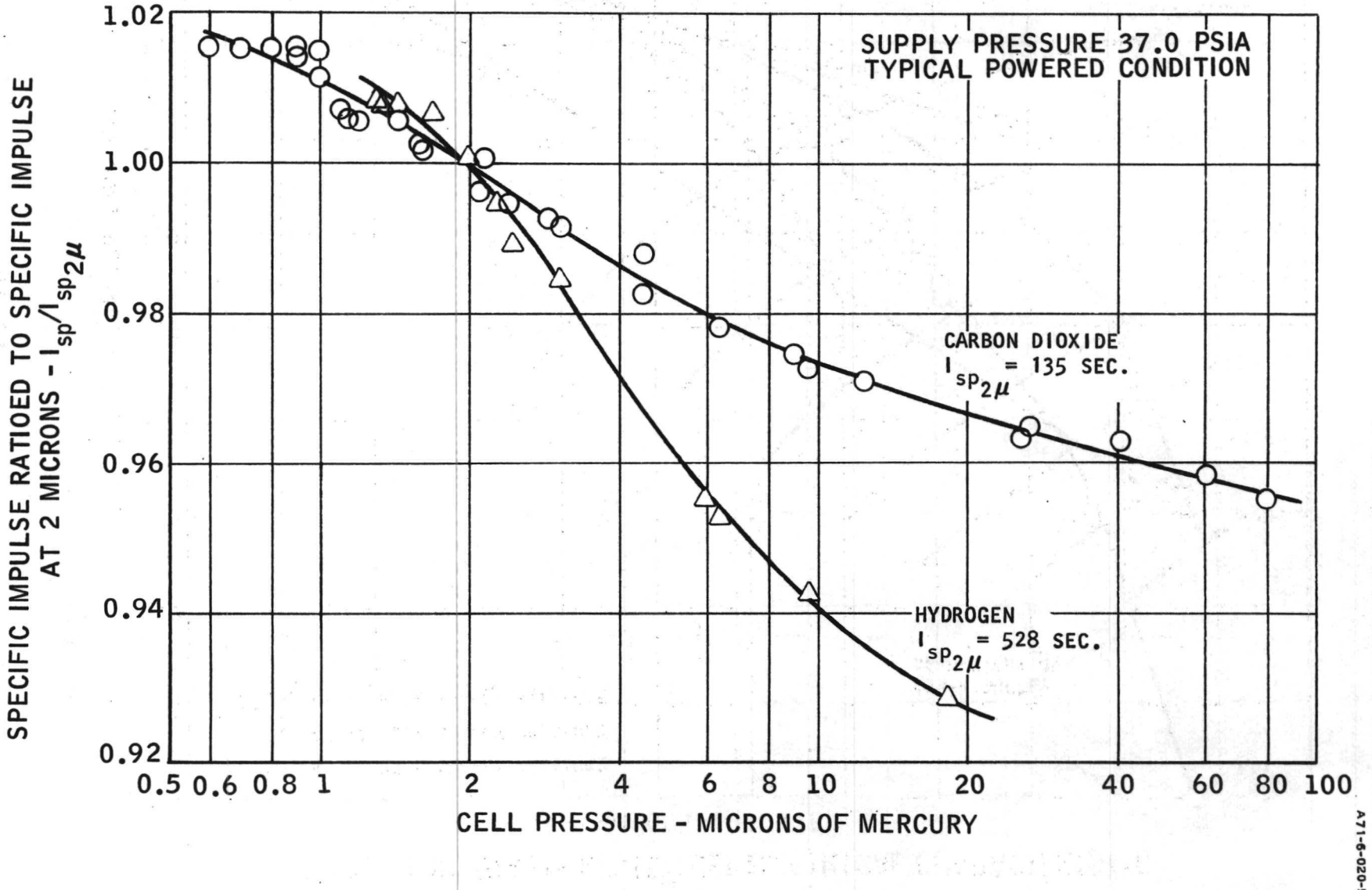
CELL PRESSURE EFFECT ON BIOWASTE RESISTOJET PERFORMANCE
SUPPLY PRESSURE 37.0 PSIA
TYPICAL POWERED CONDITION
CARBON DIOXIDE
$I_{sp_{2\mu}}$ = 135 SEC.
HYDROGEN
$I_{sp_{2\mu}}$ = 528 SEC.
SPECIFIC IMPULSE RATIOED TO SPECIFIC IMPULSE AT 2 MICRONS - $I_{sp}/I_{sp_{2\mu}}$
1.02
1.00
0.98
0.96
0.94
0.92
0.5 0.6 0.8 1 2 4 6 8 10 20 40 60 80 100
CELL PRESSURE - MICRONS OF MERCURY
A71-6-020-5A

Figure 49

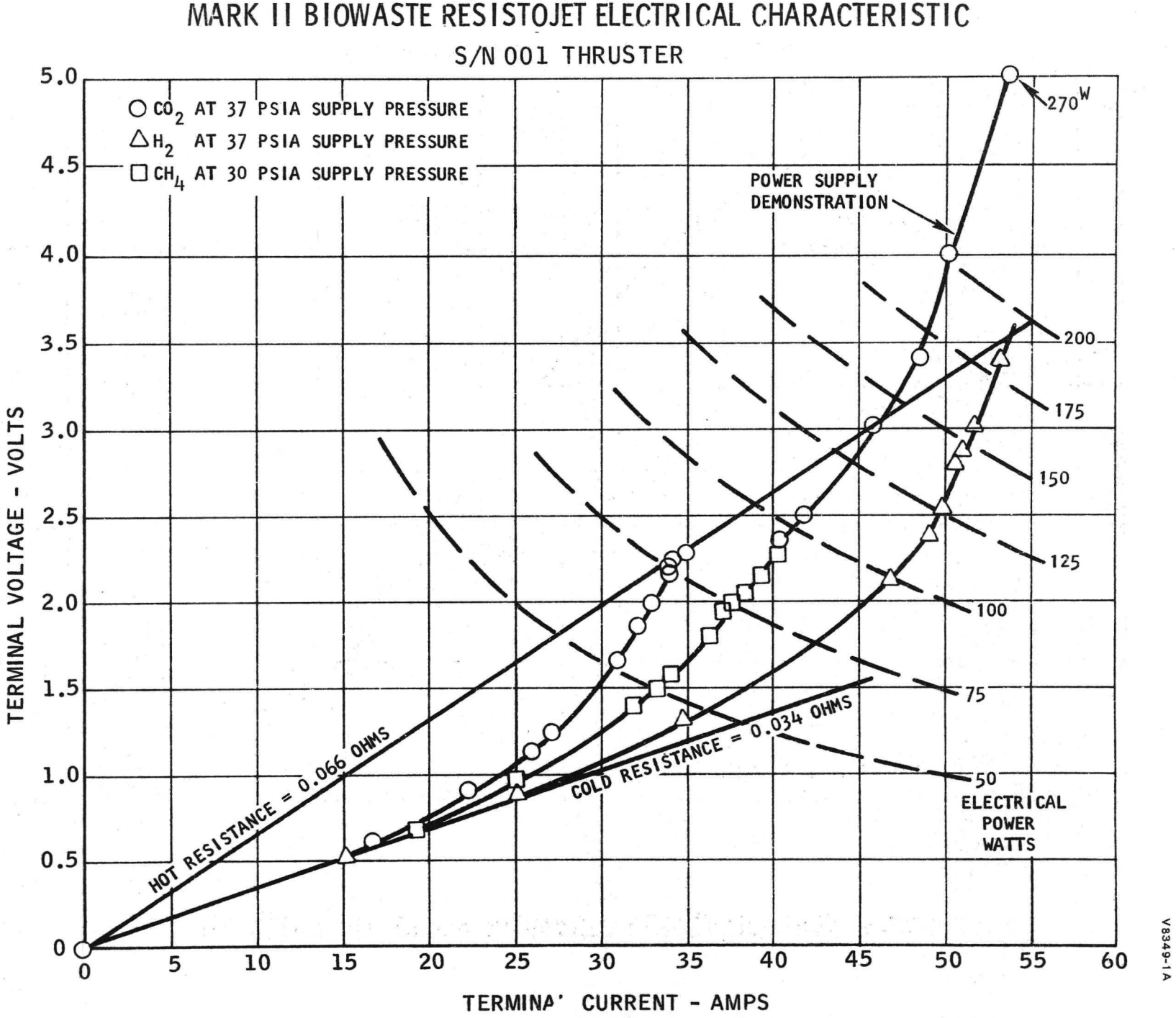
MARK II BIOWASTE RESISTOJET ELECTRICAL CHARACTERISTIC
S/N 001 THRUSTER
○ CO_2 AT 37 PSIA SUPPLY PRESSURE
△ H_2 AT 37 PSIA SUPPLY PRESSURE
□ CH_4 AT 30 PSIA SUPPLY PRESSURE
POWER SUPPLY DEMONSTRATION
270W
200
175
150
125
100
75
50
ELECTRICAL POWER WATTS
HOT RESISTANCE = 0.066 OHMS
COLD RESISTANCE = 0.034 OHMS
TERMINAL VOLTAGE - VOLTS
TERMINAL CURRENT - AMPS
0
0.5
1.0
1.5
2.0
2.5
3.0
3.5
4.0
4.5
5.0
5
10
15
20
25
30
35
40
45
50
55
60
V8349-1A

Figure 50

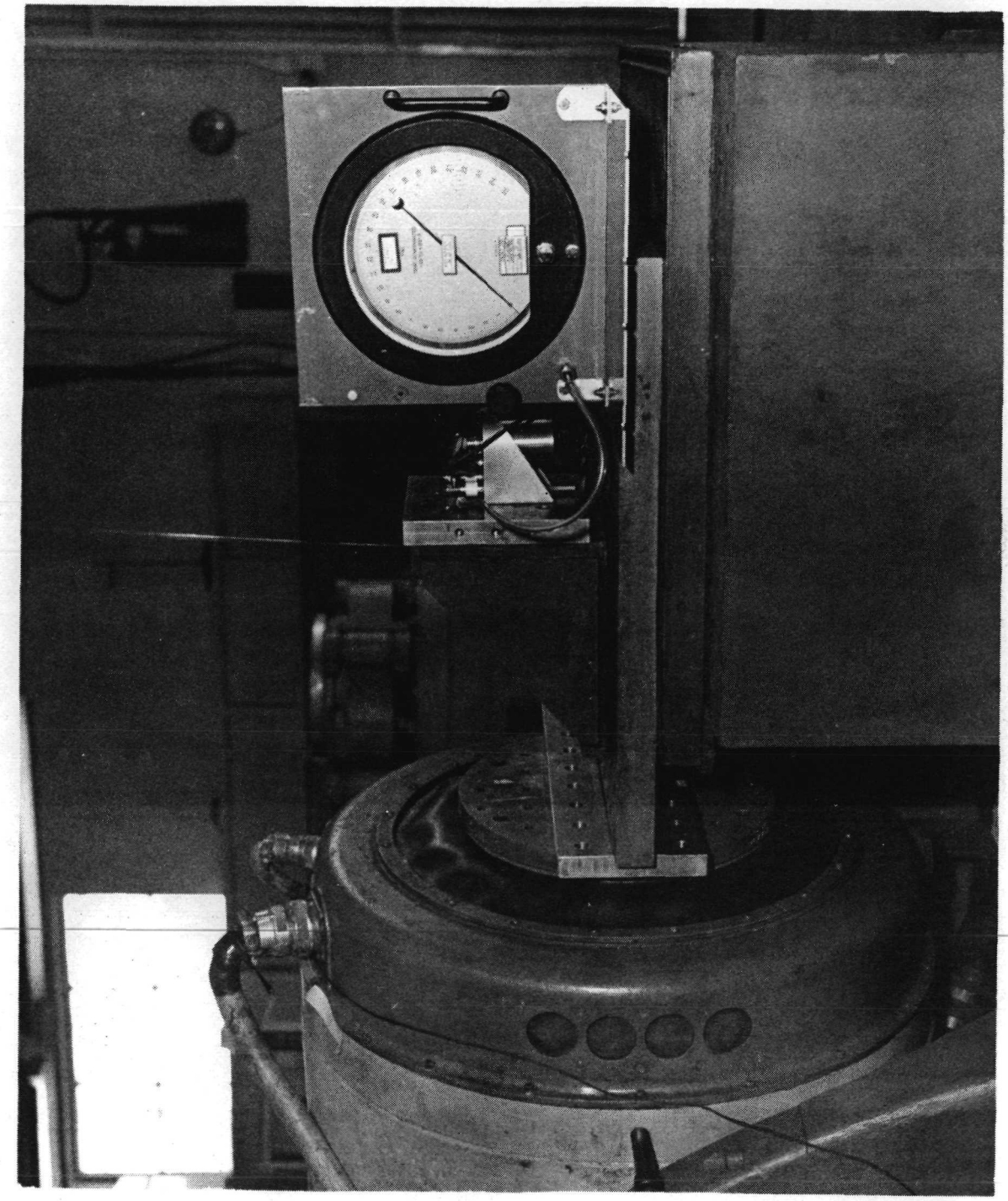

VIBRATION TEST SETUP

Figure 51

MARK II BIOWASTE RESISTOJET AFTER VIBRATION TESTS

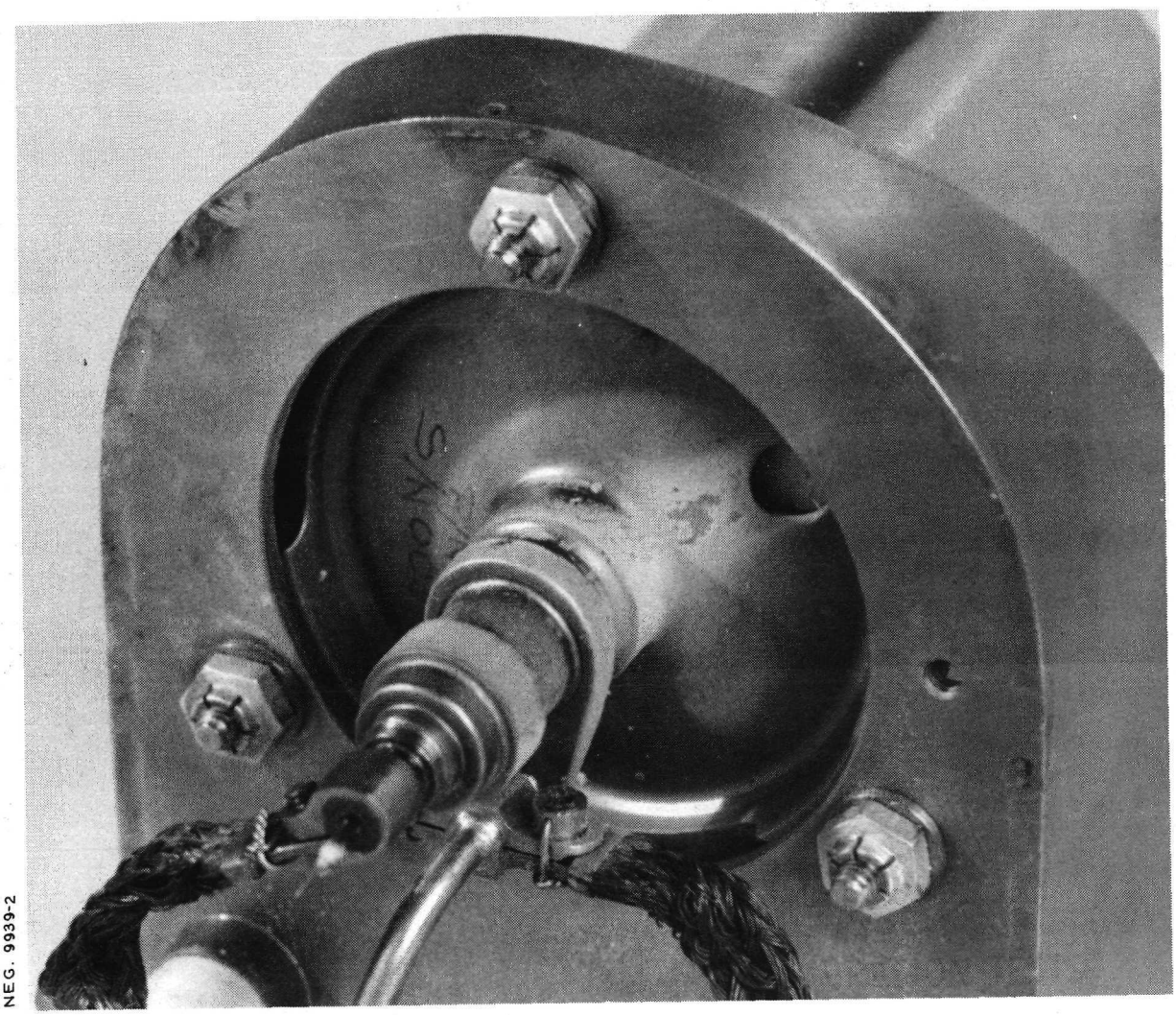

NEG. 9939-2

Figure 52

BIOWASTE RESISTOJET-DISASSEMBLED

MARK II S/N 001

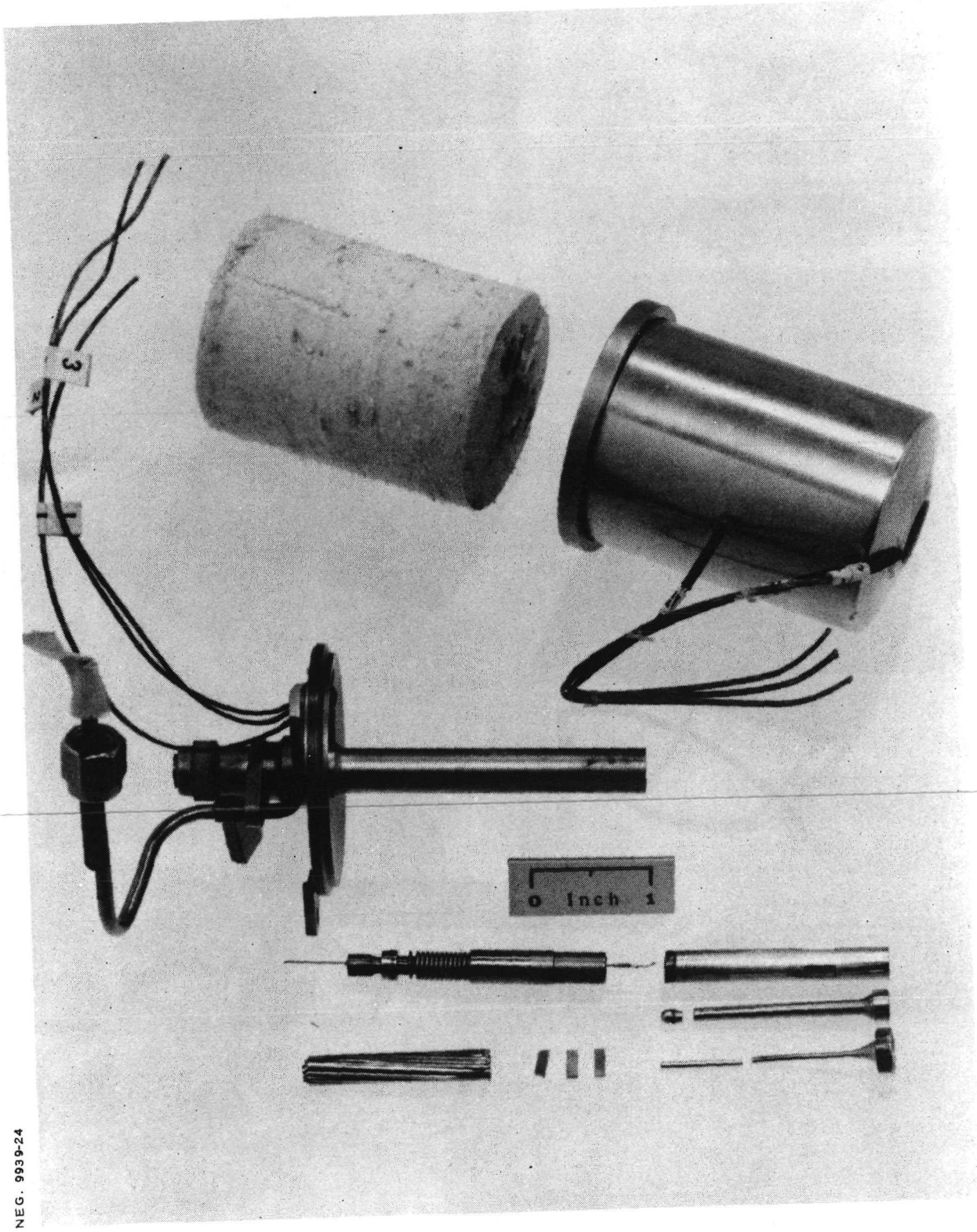

NEG. 9939-24

Figure 53

BIOWASTE RESISTOJET BELLOWS, INNERCASE AND RADIATION SHIELD

MARK II S/N 001

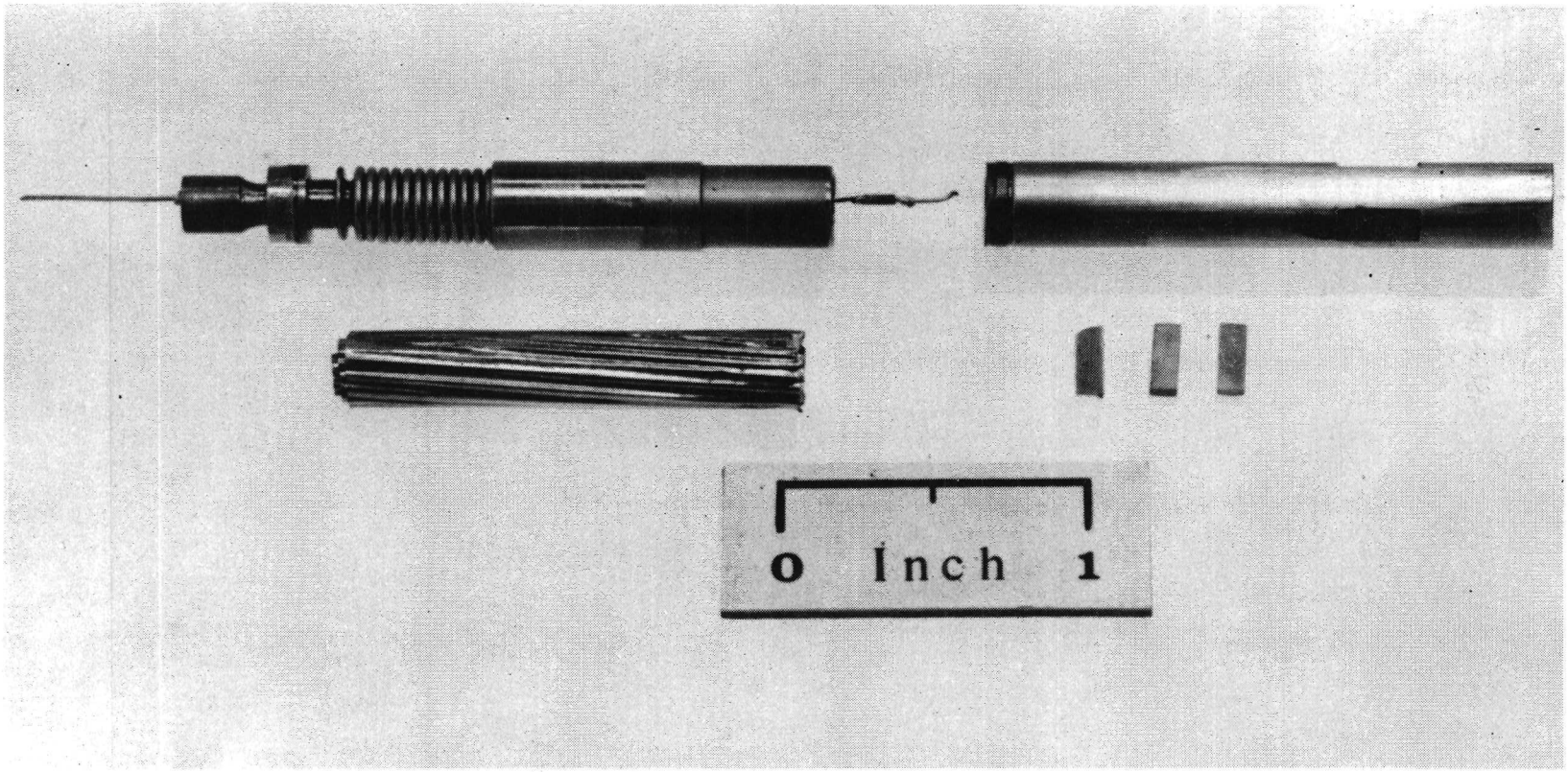

NEG. 9939-25

Figure 54

A71-8-070-1

BIOWASTE RESISTOJET HEATER PARTS AND NOZZLE

MARK II - S/N 001

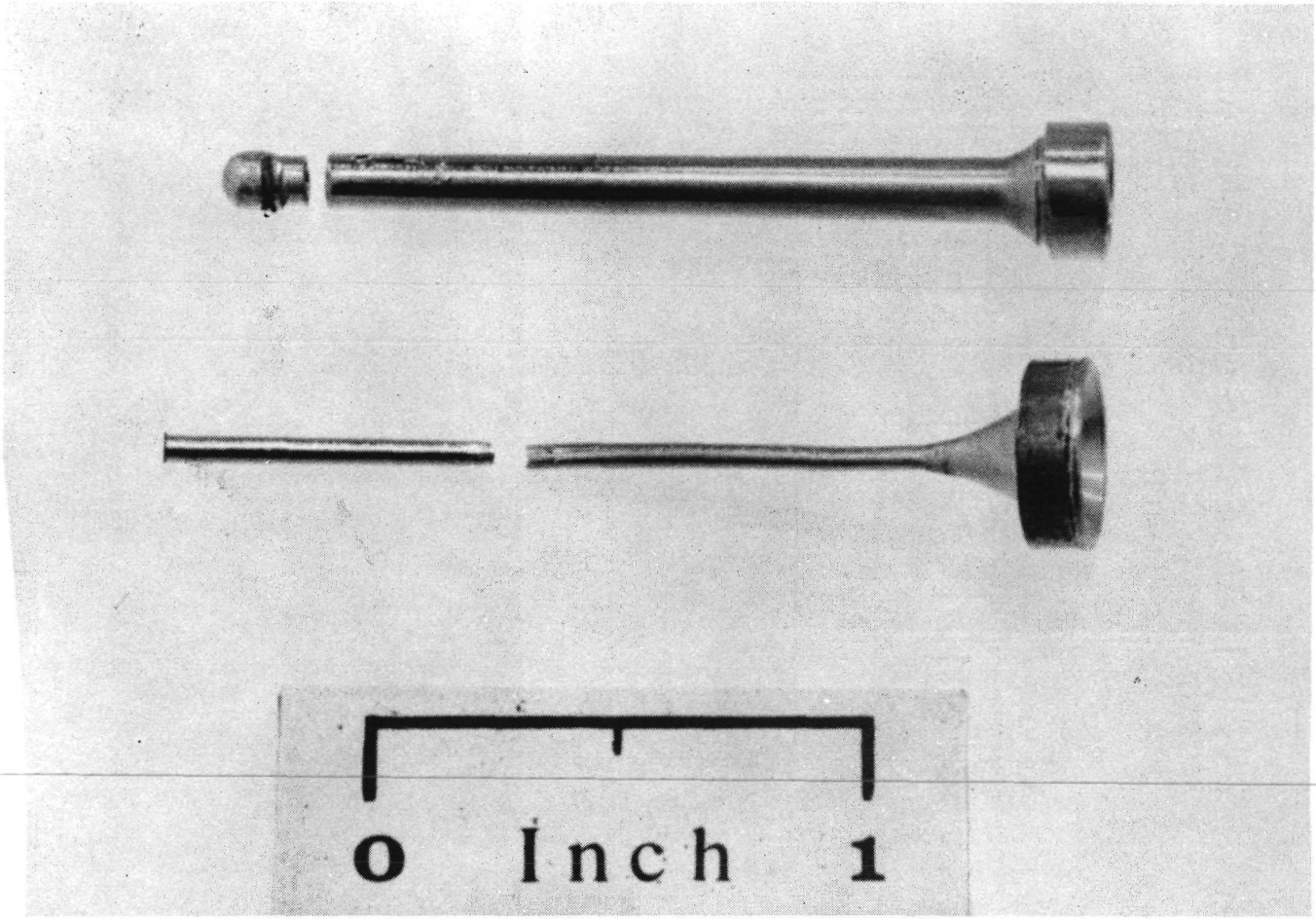

NEG. 9939-26

Figure 55

MARK II S/N 001 INNER HEATING ELEMENT AND NOZZLE
LONGITUDINAL CROSS SECTIONS
Pt-20Ir

X50

SECTION D ETCHED

X50

SECTION E ETCHED

A71-10-106-17

Figure 56

MARK II S/N 001 INNER HEATING ELEMENT
Pt-20Ir

X2

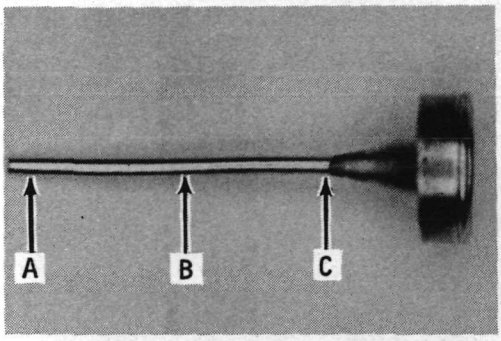

HEATING ELEMENT AND NOZZLE

X25

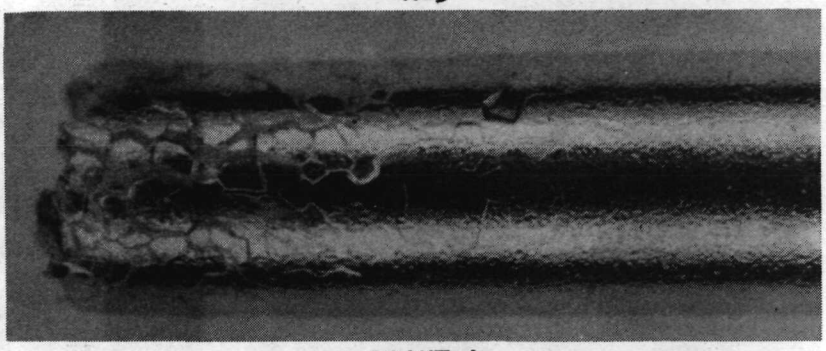

POINT A

X50

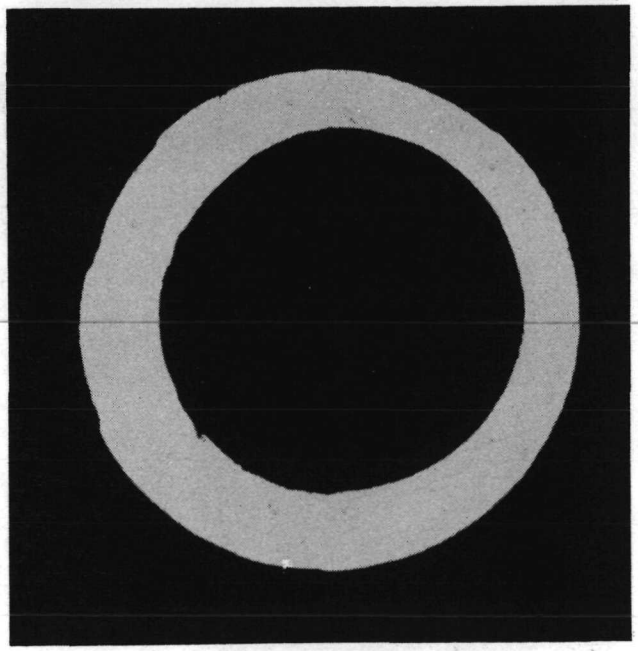

SECTION A

X50

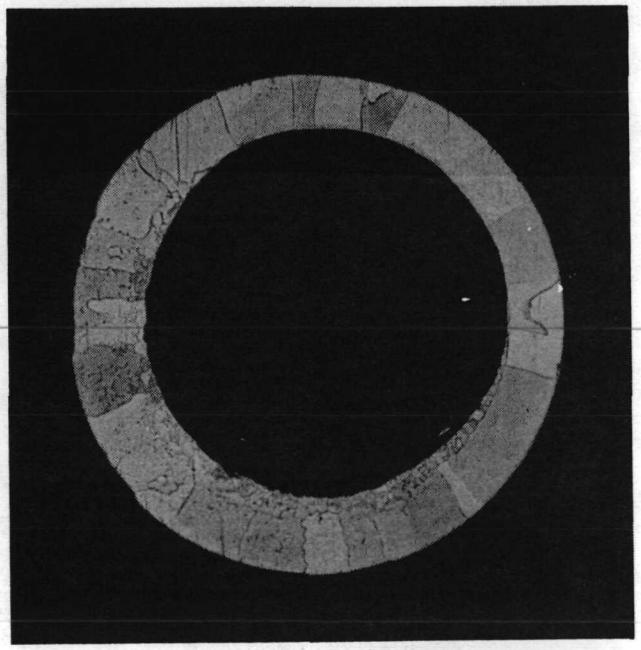

SECTION A ETCHED

Figure 57

MARK II S/N 001 INNER HEATING ELEMENT
Pt-20Ir
X50

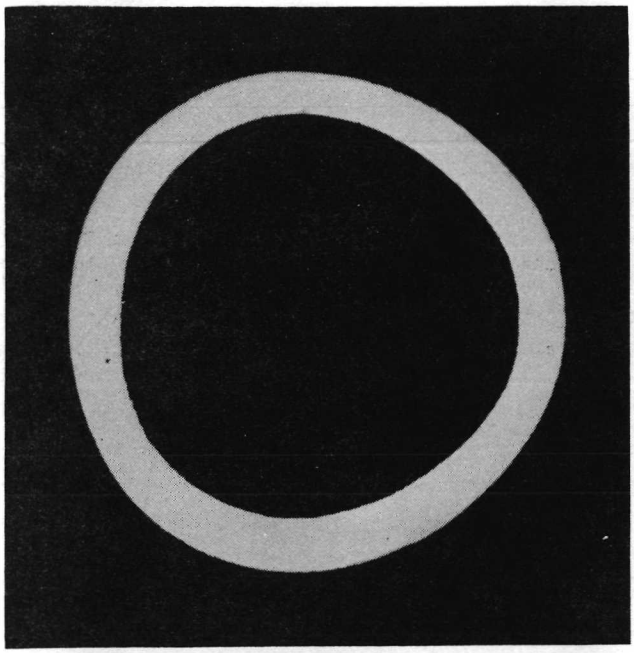

SECTION B

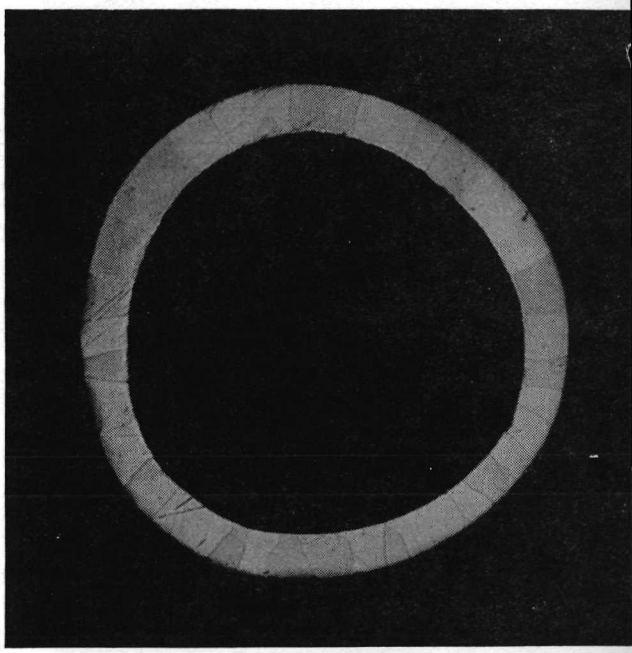

SECTION B ETCHED

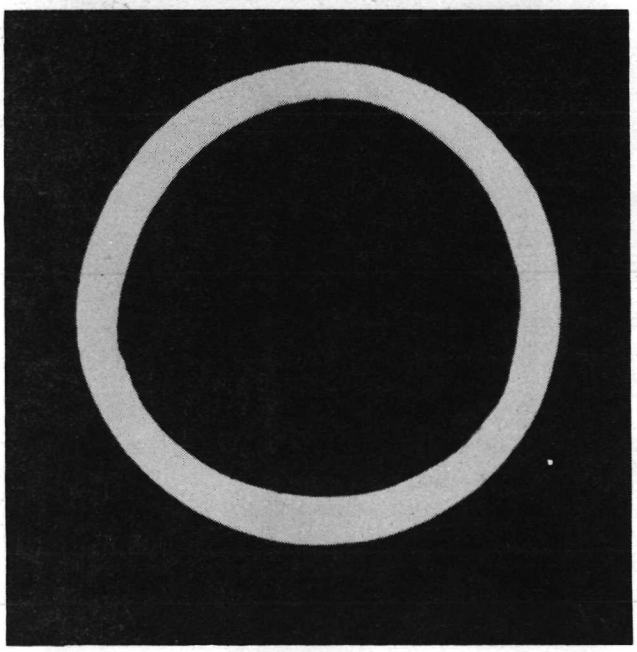

SECTION C

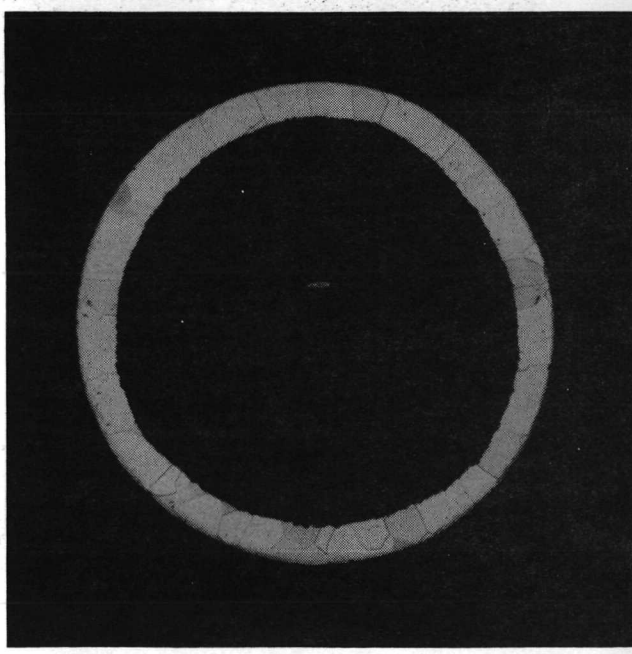

SECTION C ETCHED

Figure 58

DESIGN VERIFICATION TEST HISTORY
MARK II - S/N 002 CARBURIZING PROPELLANT
THRUSTER SUPPLY PRESSURE = 37.0 PSIA

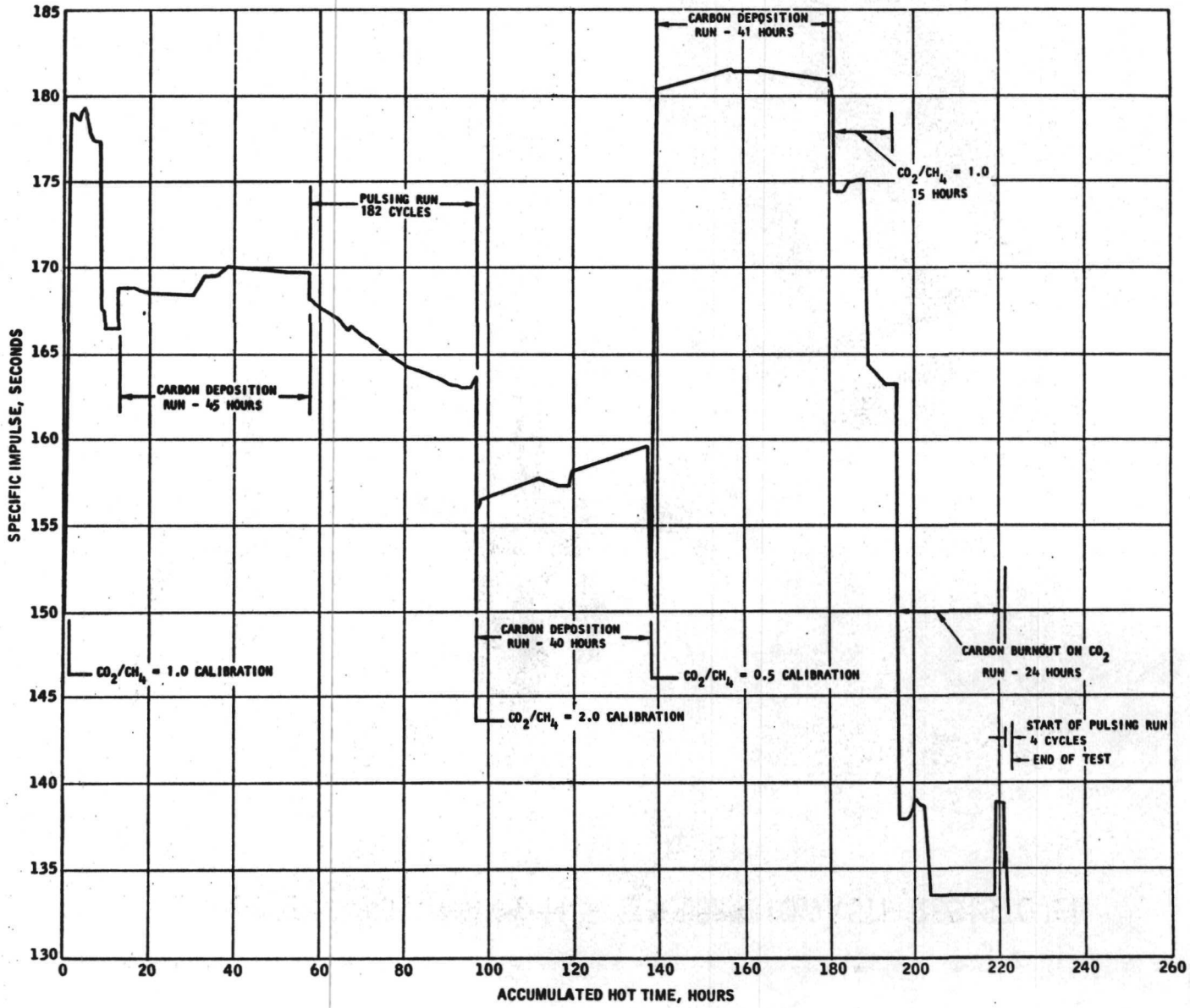

Figure 59

A71-7-055-4A

DISASSEMBLED MARK II - S/N 002 BIOWASTE RESISTOJET

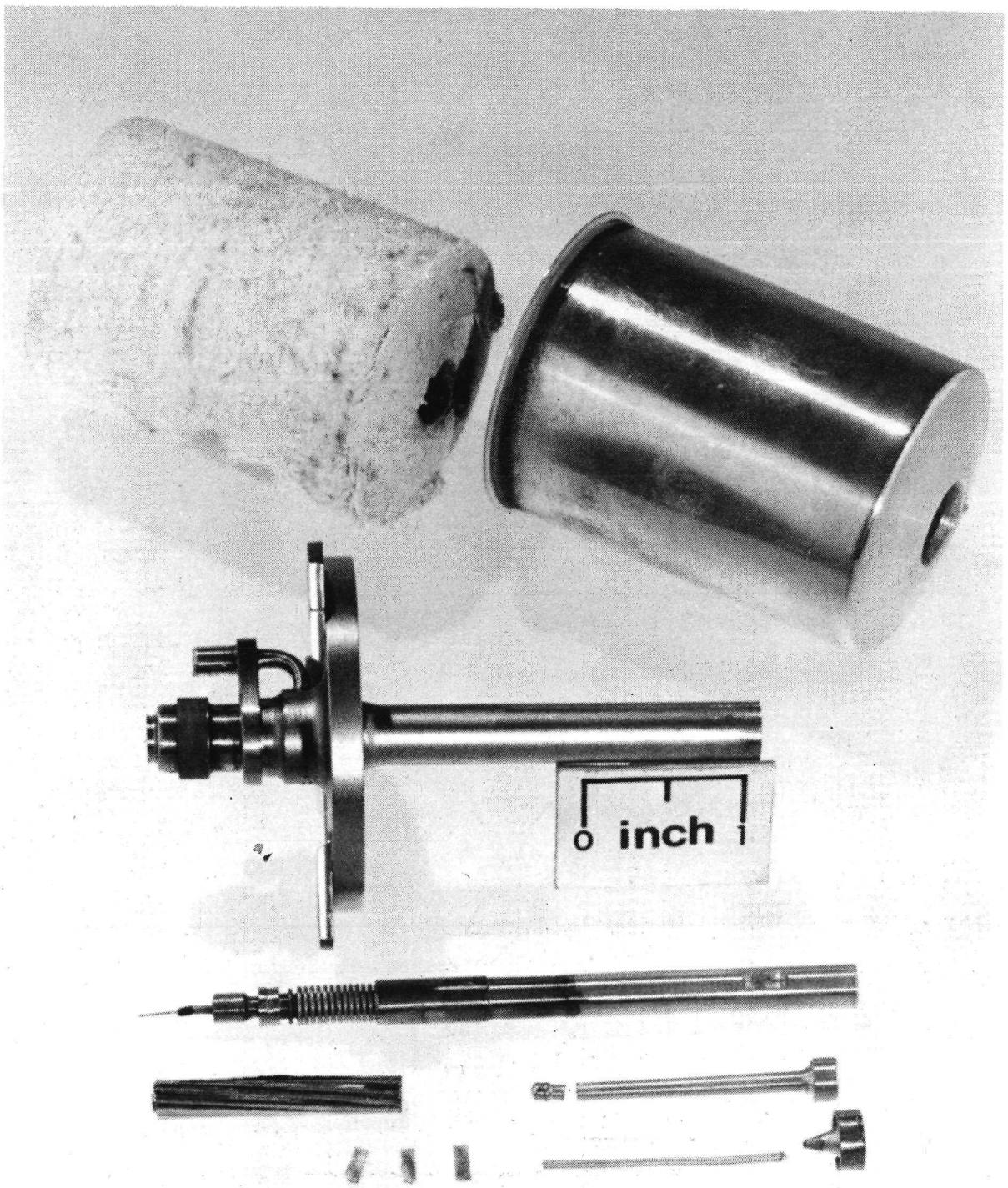

NEG. 71-141-1

Figure 60

MARK II S/N 002 BIOWASTE RESISTOJET HEATER PARTS AND NOZZLE

Figure 61

NEG. 71-141-2

A71-7-055-2

MARK II S/N 002 EXIT NOZZLE

X8

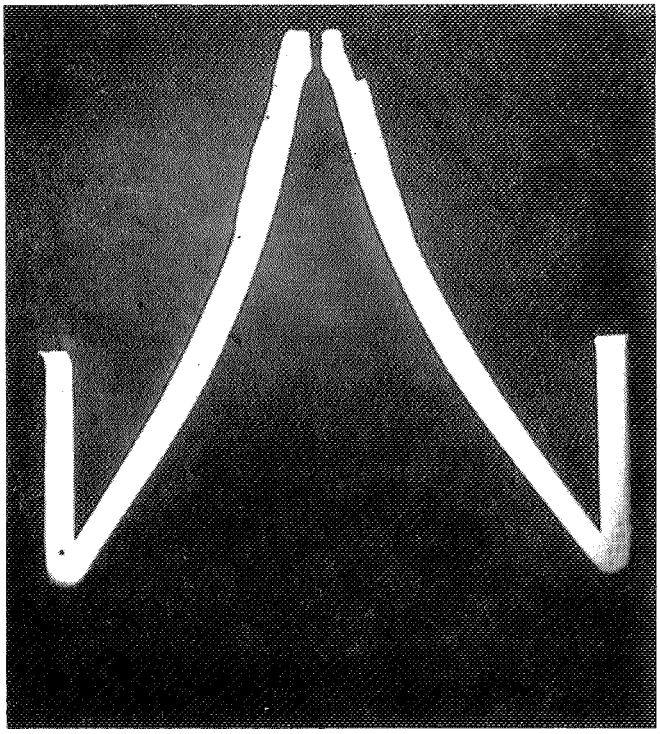

X50

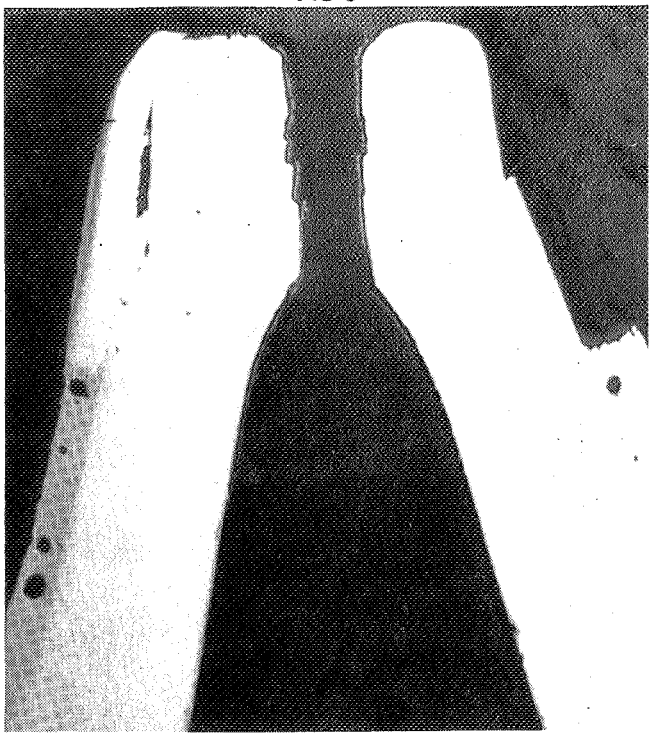

X500

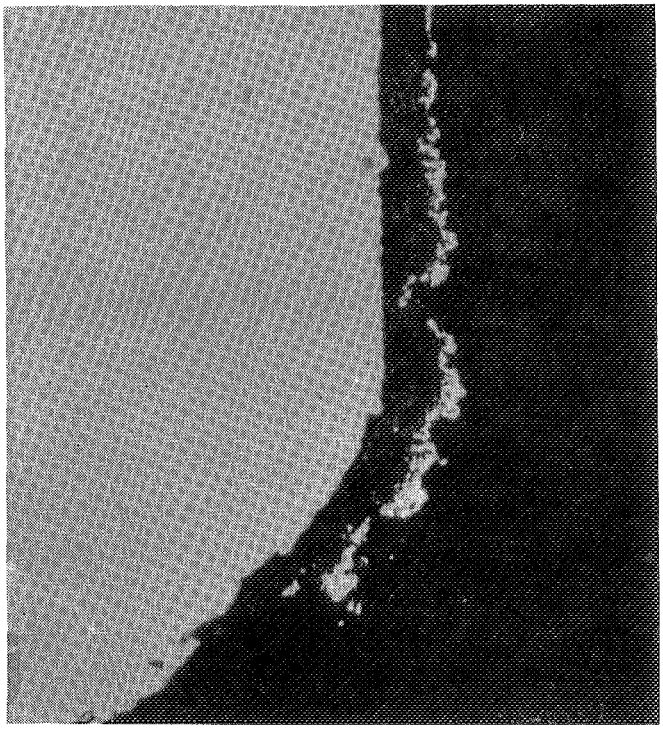

X50 ETCHED

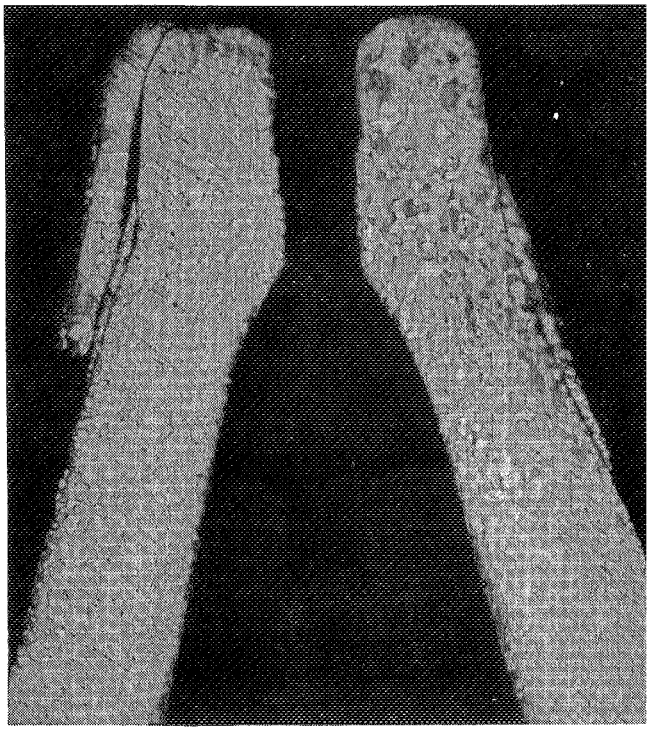

Figure 62

MARK II S/N 002 INNER HEATING ELEMENT

Pt-20 Ir X50

SECTION A

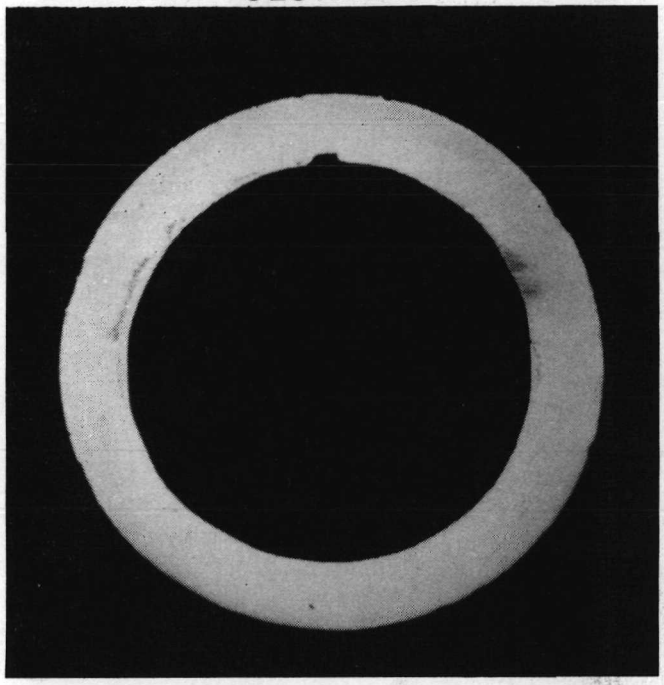

SECTION A ETCHED

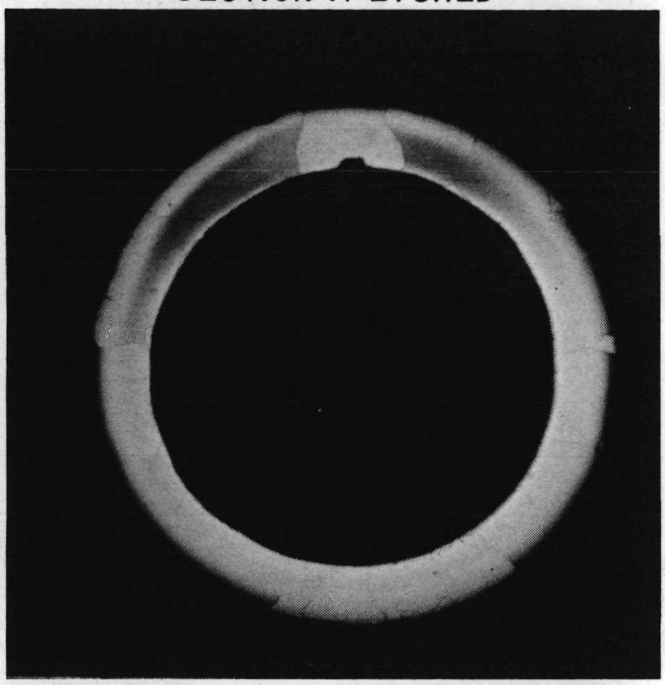

SECTION C

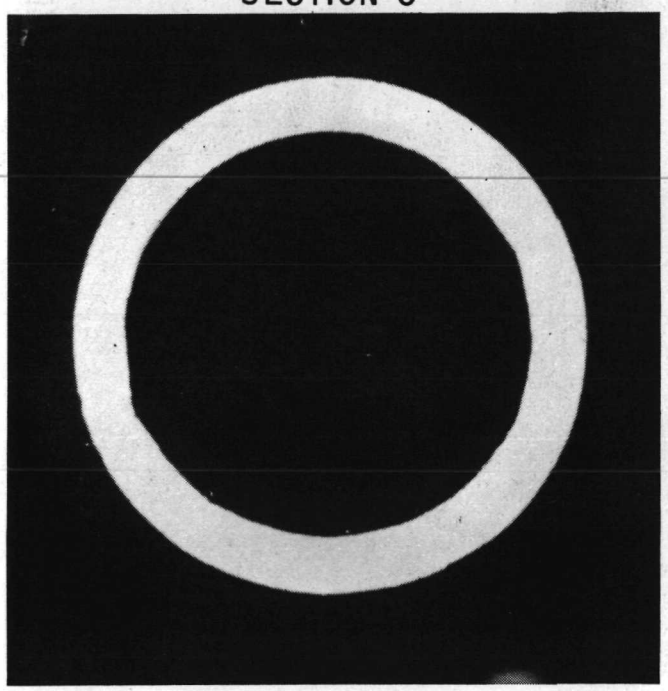

SECTION C ETCHED

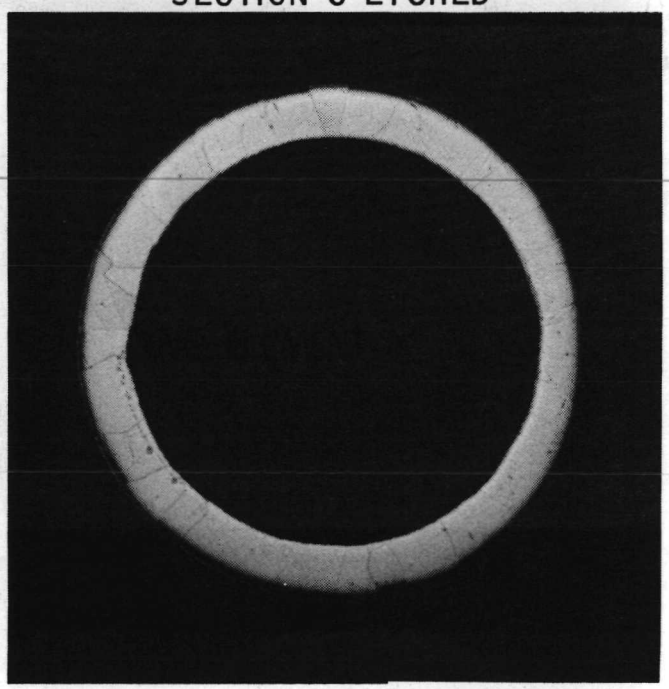

Figure 63

A71-8-070-4

MARK II S/N 002 OUTER HEATING ELEMENT

X50

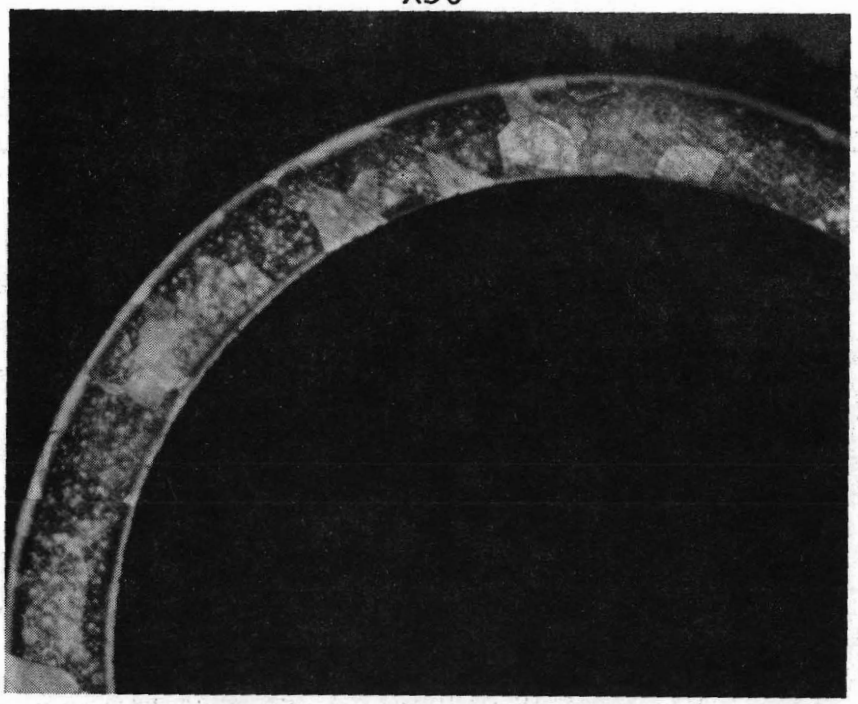

X50 ETCHED

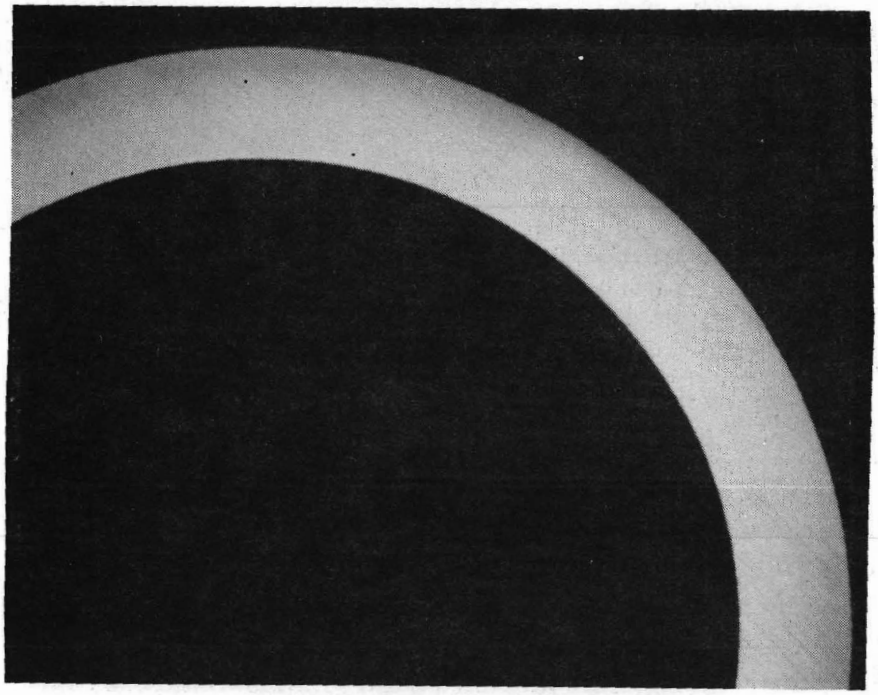

Figure 64

RANDOM VIBRATION SPECTRUM COMPARISON

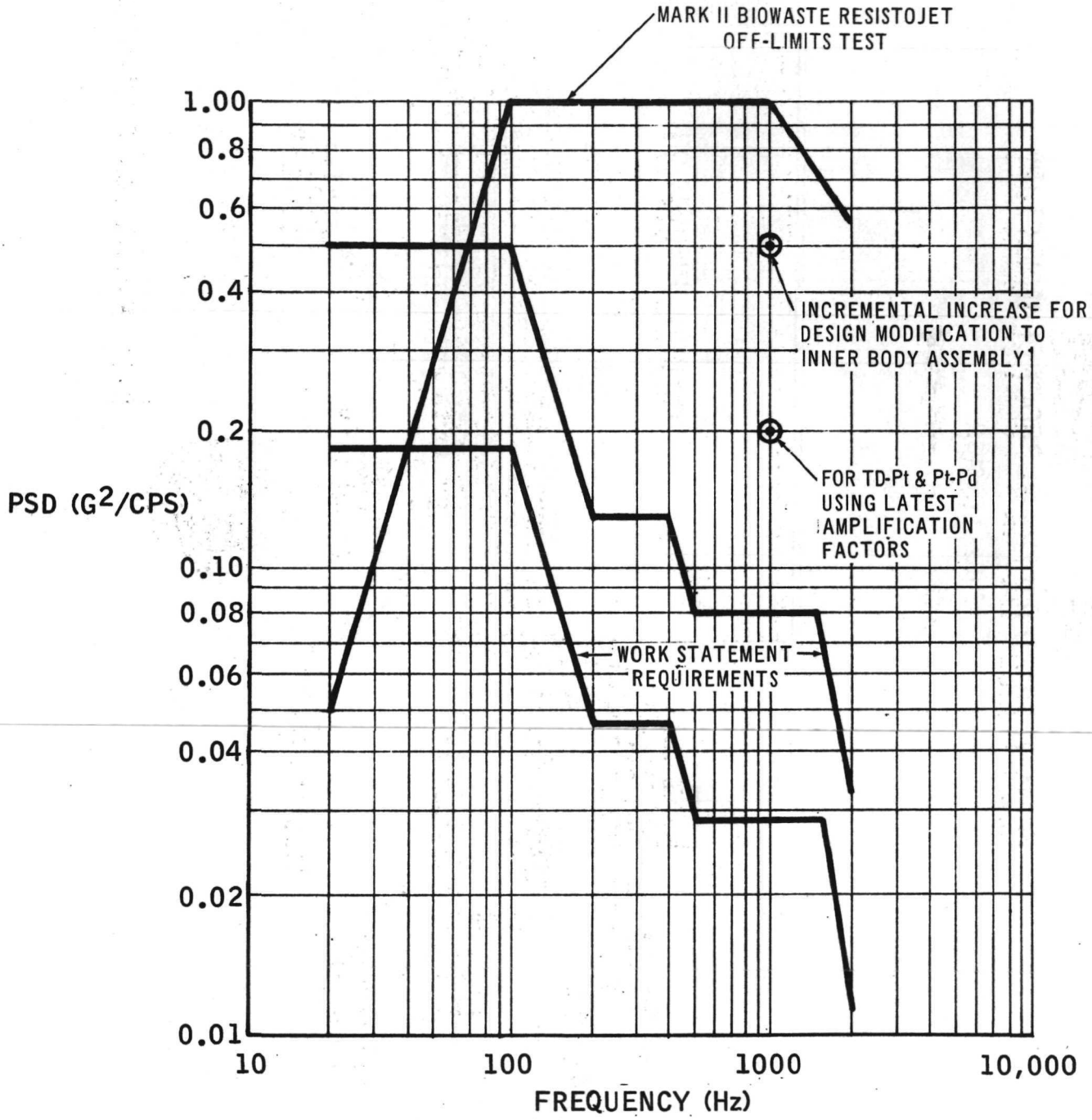

Figure 65

MARK II MODIFIED FOR SUPPORT OF INNER TUBE

RD - 1 DESIGN

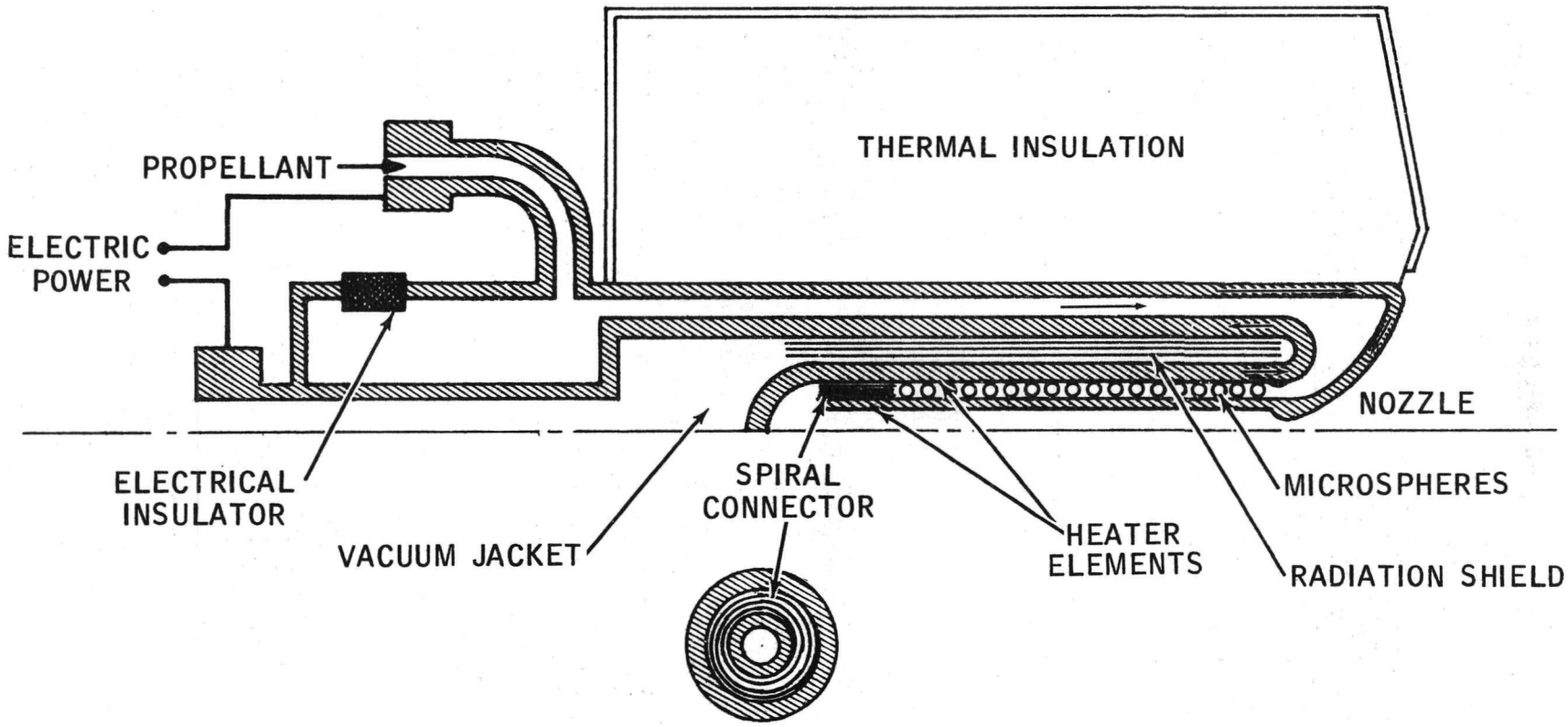

NOTE: RADIAL SCALE EXAGGERATED

Figure 66

V8294-1A

A71-12-142-7

BIOWASTE RESISTOJET COMPONENT ENGINE

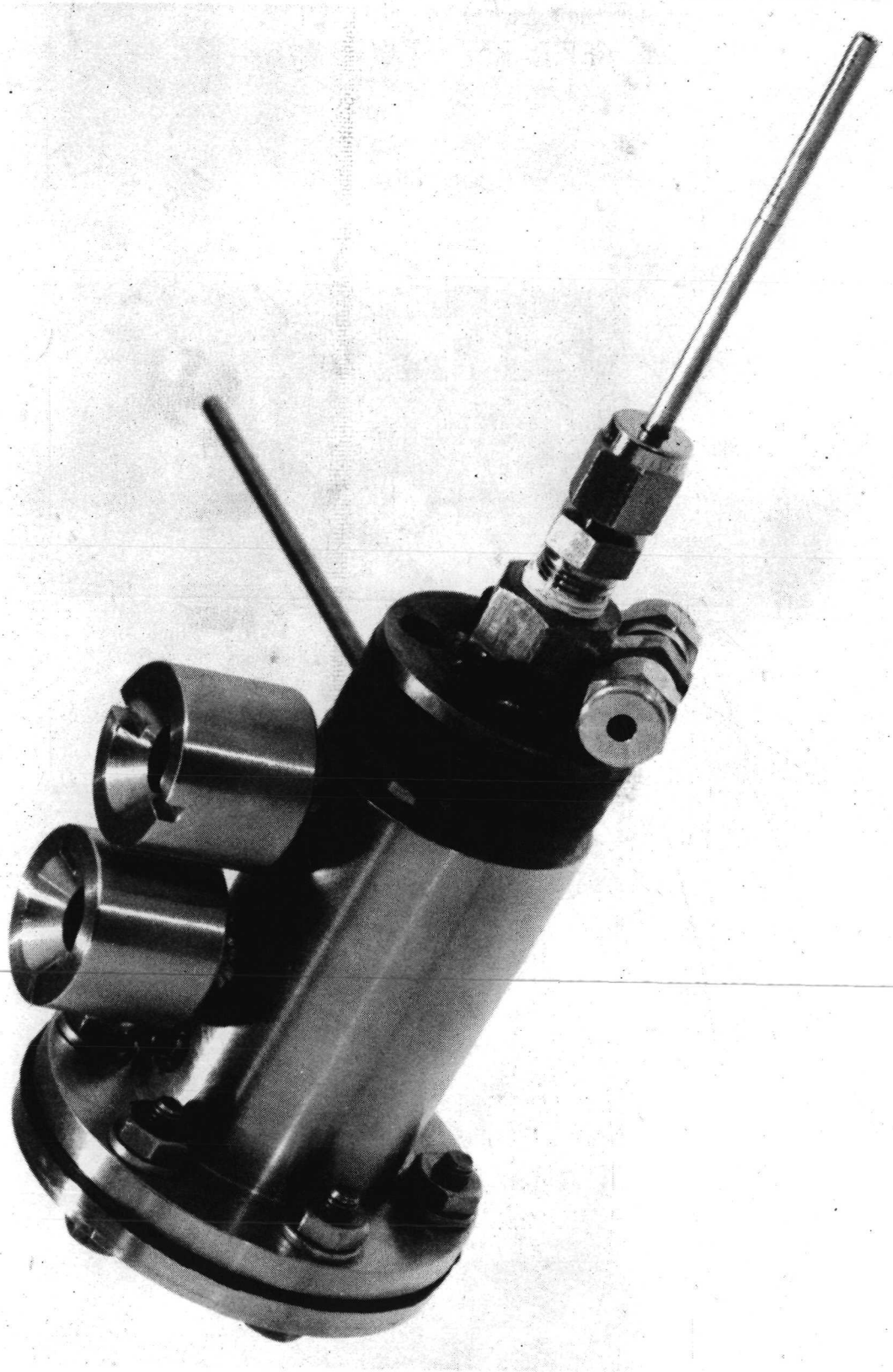

NEG. 71-174-3

Figure 67

CARBON DEPOSITION IN COMPONENT ENGINE AFTER 113 HOURS OPERATION ON CH_4

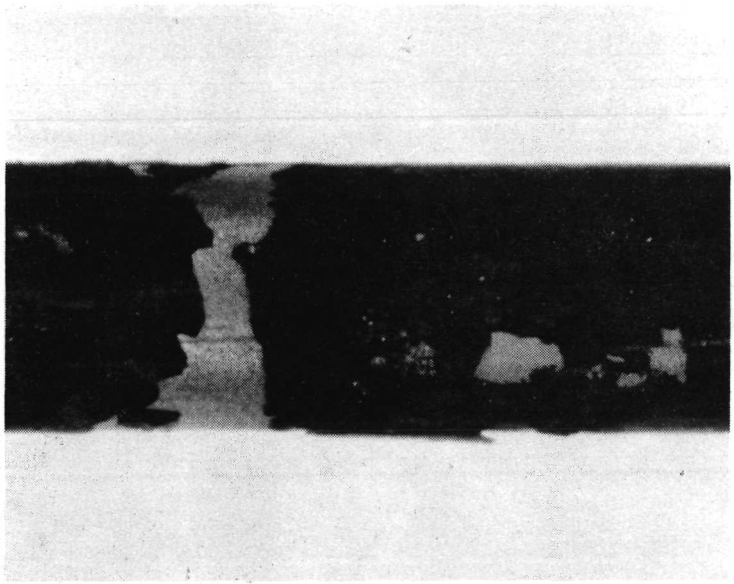

CENTER TUBE X25
Temperature 1050 °K

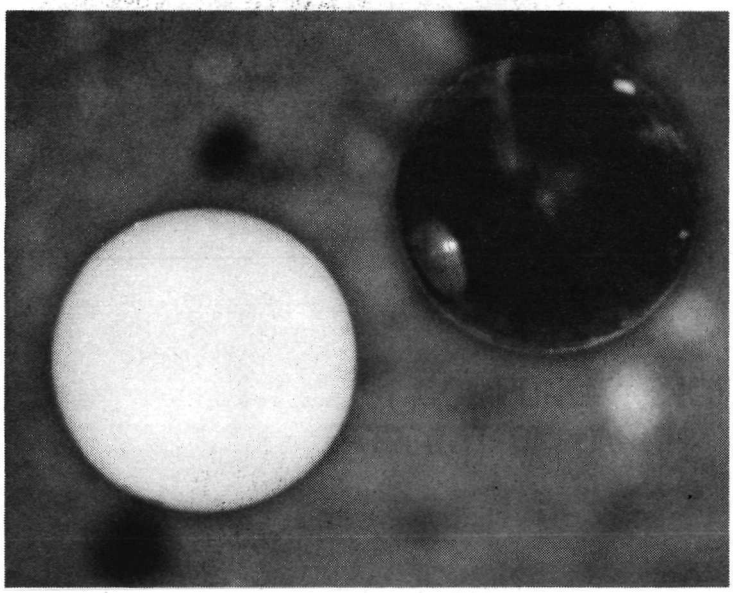

MICROSPHERES X50
Temperature 980 °K

Figure 68

A71-12-142-8

R&D BIOWASTE RESISTOJET

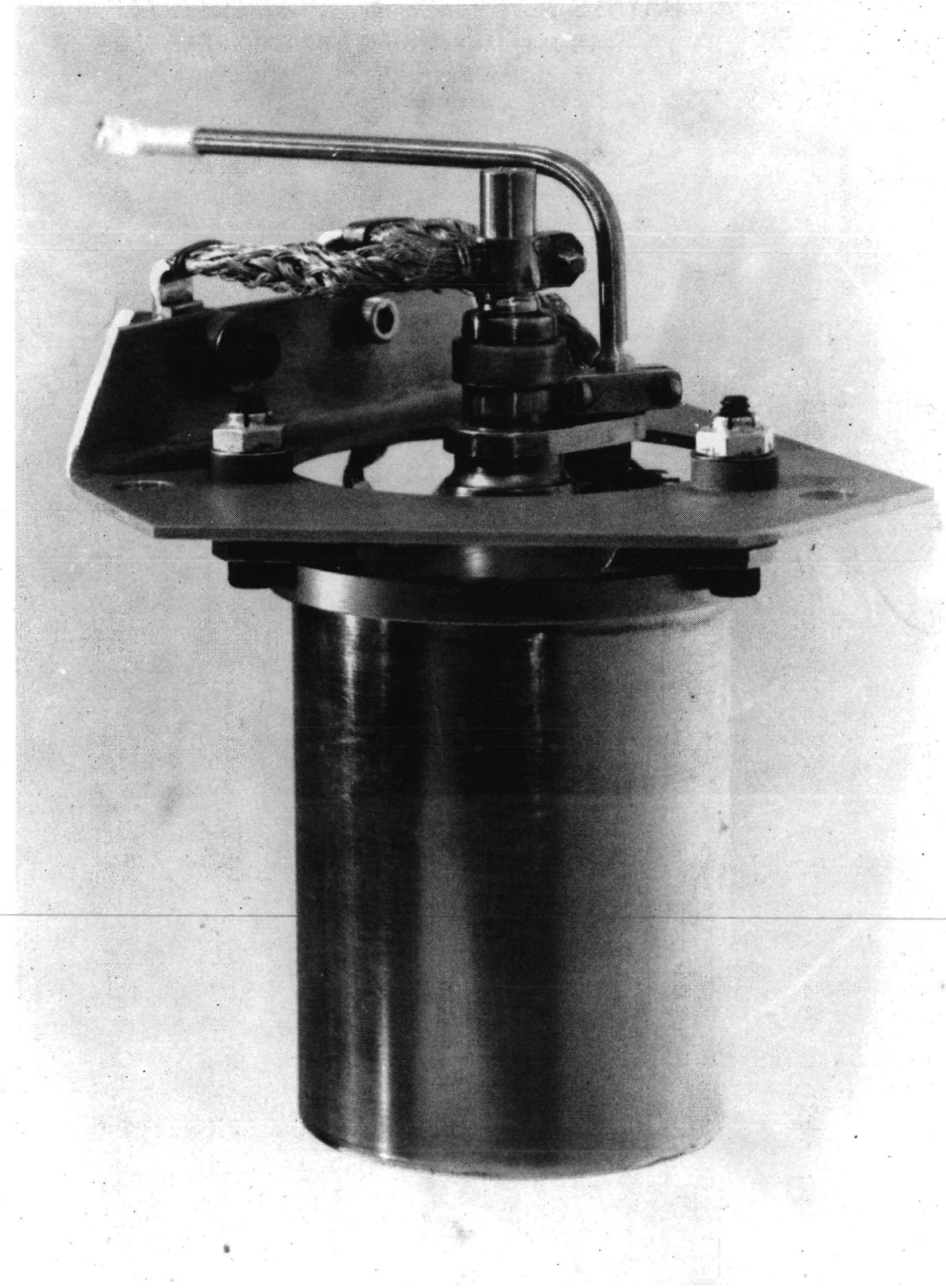

NEG. 71-174-2

Figure 69

HAYNES ALLOY NO. 188 AFTER BELL JAR TEST
1480°K MAXIMUM TUBE TEMPERATURE
89.9 HOURS TEST DURATION

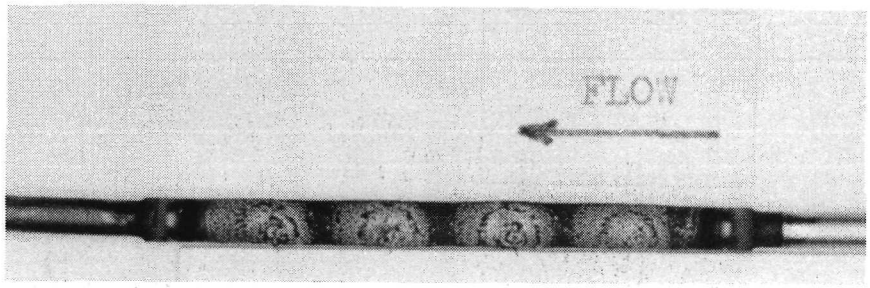

X 1.5

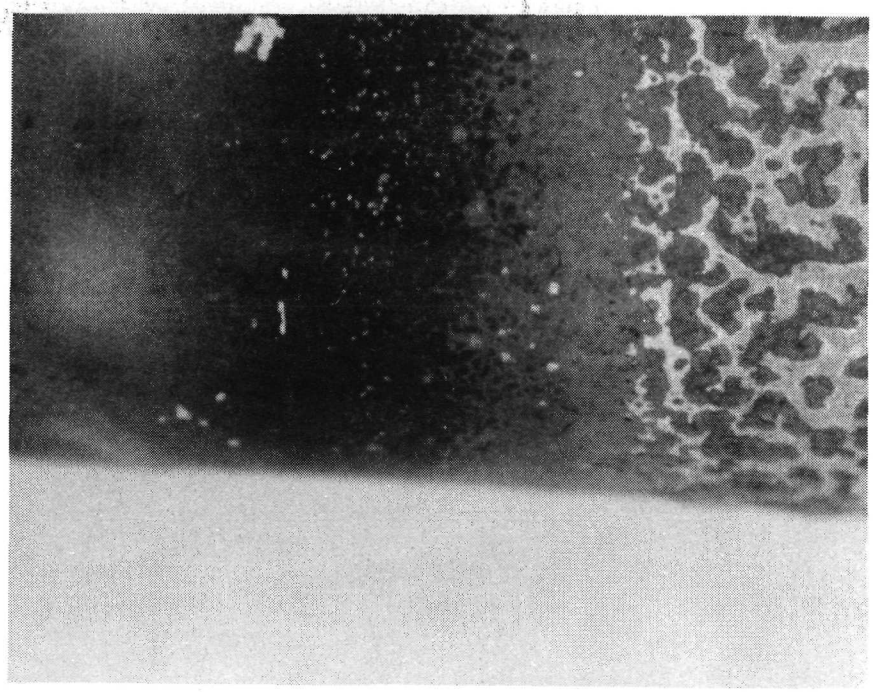

X 25 0.2 INCHES FROM DOWNSTREAM END

Figure 70

HAYNES ALLOY NO. 188 AFTER BELL JAR TEST
1480°K TUBE TEMPERATURE
89.9 HOURS TEST DURATION

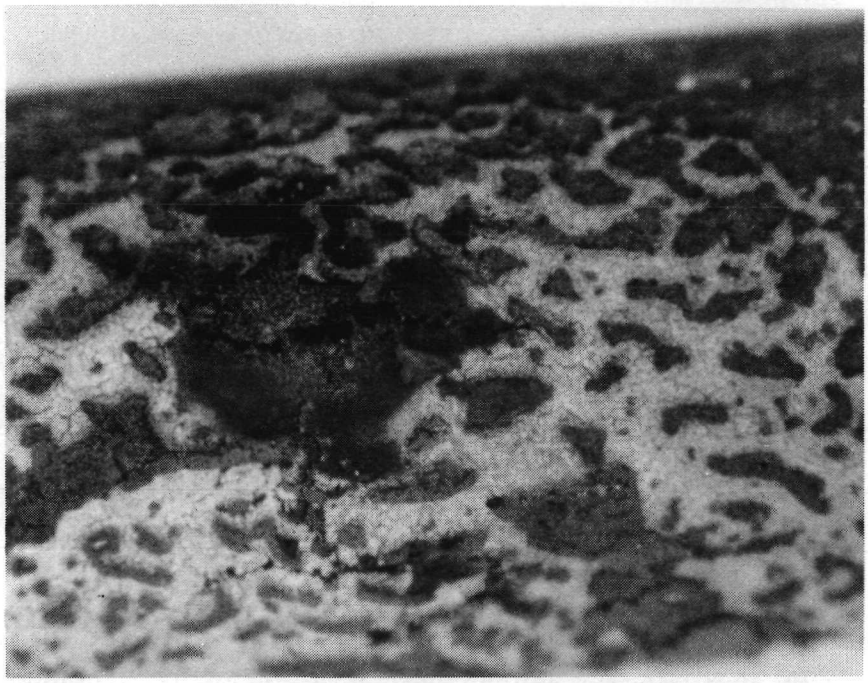

X 25 POINT OF FAILURE

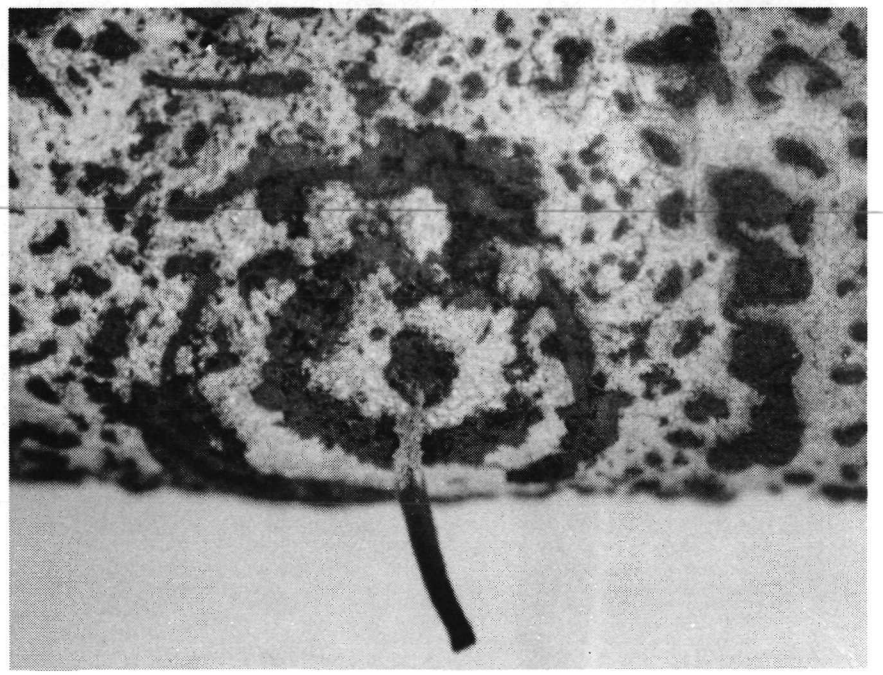

X 25 Pt INDICATOR WIRE

Figure 71

HAYNES ALLOY NO. 188 AFTER BELL JAR TEST

TEST DURATION 89.9 HOURS

TUBE TEMPERATURE 1400°K X 50

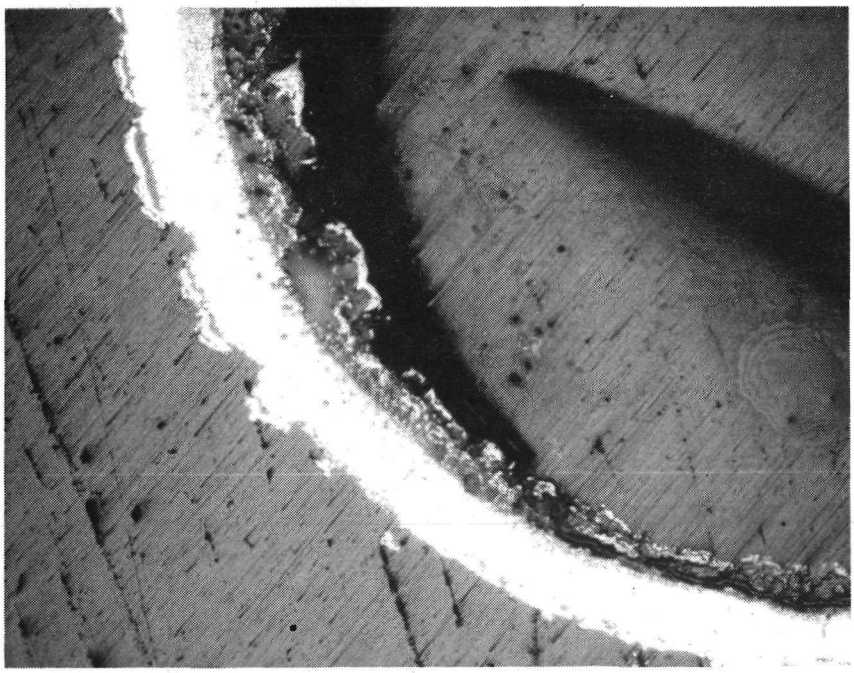

TUBE TEMPERATURE 1480°K X 50

Figure 72

TABLE I

SUMMARY OF HIGH TEMPERATURE MATERIALS TEST RESULTS

Material	Remarks
Pt-20Rh	Material is relatively oxidation resistant but suffers from carbonyl reactions when subjected to pure CO_2 at high temperature. Tubes began leaking after 500 hours at 1500°K (2700°R) temperature.
Pt-10Rh	The presence of 1.5% oxygen added to the CO_2 is effective in suppressing carbonyl reactions with 10% rhodium. Some oxidation and metal vaporization results. At 1700°K, a 16% reduction in wall thickness occurred in 500 hours. With only 0.25% oxygen added to CO_2, grain boundary attack still occurred, producing voids. However, the tube was still intact after 1500 hours at 1700°K.
Pt-5Rh	Results indicate that the 5% rhodium alloy did not suffer from carbonyl reactions with pure CO_2. No measurable reduction in wall thickness occurred after 1500 hours at 1700°K (3060 °R). There was considerable grain growth but no grain boundary attack. The effect of oxygen addition to the CO_2 was not evaluated because of insufficient time.
Pt-20Ir	Results indicate no carbonyl reactions with CO_2. After exposure to CO_2 for 700 hours at 1550°K, large grain growth was evident but no corrosion effects. Additional tests with a mixture of H_2, CO_2 and 5% water indicated no reaction after 734 hours at 1690°K (3040°R). When oxygen was added (1-1.5%) to the CO_2 mixture, tube failure occurred in about 160 hours. Apparently, the iridium oxidizes and vaporizes rapidly when oxygen is present at temperatures above 1400°K.
Pt-20Pd	No evidence of carbonyl reactions were found in the literature. However, excessive vaporization of the Pt-Pd tube occurred at temperatures above 1500°K. Analysis indicated vaporized material was mostly palladium. Using a test gas mixture of CO_2 plus 1.5% O_2, the reduction in tube wall thickness was about 13% after 500 hours at 1600°K (2880°R).

TABLE I - Continued

SUMMARY OF HIGH TEMPERATURE MATERIALS TEST RESULTS

Material	Remarks
Platinum	At temperatures above 1500°K (2700°R) platinum is subject to oxidation in a CO_2 mixture containing 1.5% oxygen. The attack generally occurs on the surface but also can occur in the grain boundaries.
TD-Pt	Thoriated platinum containing 0.5% thoria offers the best promise of operation with all currently projected biowaste gases. In pure CO_2, a sample tube was maintained at 1700°K (3060°R) for 1500 hours with no evidence of attack or measurable reduction in wall thickness. Carbon deposition in the tubes, due to operating with CH_4, did not result in reduction of the thorium oxide. When 1.5% oxygen was added to the CO_2, the reduction in tube wall thickness was only about 5% after 1000 hours at 1600°K (2880°R). Very little, if any, reduction in wall thickness resulted from exposure to CO_2 with 0.25% oxygen for 1500 hours at 1700°K. The test results indicate that the finely dispersed thoria is not only effective in improving high temperature strength properties by inhibiting grain growth, but it also appears to suppress oxidation and vaporization of the platinum.

TABLE II

MARK I

BIOWASTE RESISTOJET PERFORMANCE SUMMARY

Propellant	CO_2	H_2O
Thrust*, grams (mlb)	6.48 (14.3)	5.45 (12)
Mass Flow*, grams/sec	0.0487	0.0257
Specific Impulse**, sec	133	212
Electric Power*, watts	87	94.5
Heater Efficiency	0.82	0.81
Overall Efficiency	0.43	0.45
Supply Pressure, atm	2.9	3.0
Cell Pressure, microns	52	51

*Note that high thrust levels resulted in proportionately higher mass flow and electric power.

**Specific impulse is uncorrected for space vacuum

TABLE III

MARK I VERSUS MARK II THRUSTER PERFORMANCE

FOR CARBON DIOXIDE PROPELLANT AND 0.7 MICRON CELL PRESSURE

THRUSTER	MARK I	MARK II
Data Point	7027	1023
Thrust, grams	6.86	6.11
Specific Impulse, Seconds	142	142
Mass Flow Rate, grams/second	.0487	.0430
Electric Power, Watts	87	77
Power per unit Mass Flow Rate, $\frac{\text{watt-sec}}{\text{gram}}$	1790	1790
Overall Total Power Efficiency	0.480	0.485

TABLE IV

ESTIMATED PERFORMANCE FOR THRESHOLD CARBON DEPOSITION

MARK II RESISTOJET

Propellant	Chamber Gas Temperature, ^{o}K (^{o}R)	Specific Impulse, Seconds	Overall Total Power Efficiency
CH_4	890 (1600)	205	0.67
$CO_2/CH_4 = 0.5$	970 (1750)	185	0.66
$CO_2/CH_4 = 1.0$	970 (1750)	175	0.65
$CO_2/CH_4 = 2.0$	970 (1750)	160	0.64
$H_2O/CH_4 = 0.5$	1030 (1850)	225	0.69
$H_2O/CH_4 = 1.0$	1030 (1850)	215	0.70
$H_2/CH_4 = 0.1$	1030 (1850)	270	0.68

TABLE V

ESTIMATED PERFORMANCE FOR 10 MLB BIOWASTE RESISTOJET

Propellant	Chamber Gas Temperature, ^{o}K (^{o}R)	Specific Impulse, Seconds	Overall Total Power Efficiency
CO_2	1555 (2800)	170	0.62
H_2O	1555 (2800)	240	0.72
CH_4	890 (1600)*	205	0.67
H_2	1555 (2800)	590	0.71

*Limited by carbon deposition at high temperature.